Biexciton Gain and the Mott Transition in GaAs Quantum Wires

Yuhei Hayamizu, Masahiro Yoshita, Yasushi Takahashi, and Hidefumi Akiyama
Institute for Solid State Physics (ISSP), University of Tokyo, and CREST, JST 5-1-5 Kashiwanoha, Kashiwa, Chiba 277-8581, Japan

C. Z. Ning*
Department of Electrical Engineering, Arizona State University, Tempe, AZ 85287, USA

Loren N. Pfeiffer and Ken W. West
Bell Laboratories, Alcatel-Lucent, 600 Mountain Avenue, Murray Hill, New Jersey 07974, USA
(Received 2 October 2006; published 19 October 2007)

Optical gain and the Mott transition in GaAs quantum wires were studied via simultaneous measurements of absorption and photoluminescence (PL). We observed well-separated PL peaks assigned to excitons (X) and biexcitons (XX) even at densities where optical gain existed. A sharp optical gain first appeared when the XX peak overtook the X peak, indicating the gain origin of biexciton-exciton population inversion. The XX peak eventually changed to a broad peak of plasma, and a broad gain due to plasma was observed as the Mott transition was completed.

DOI: 10.1103/PhysRevLett.99.167403 PACS numbers: 78.67.Lt, 42.55.Px, 71.35.Lk, 78.55.Cr

The transition from a dilute exciton gas to a dense electron-hole (e-h) plasma (often called the Mott transition) in a semiconductor is one of the central unresolved issues in many-body physics [1,2]. A first-principles theory that is valid for the vast density regime from a dilute exciton gas to dense plasma to deal with the entire transition is not available. This is especially true when biexcitons are involved. Experimentally, this transition is alternatively associated with the quenching of an exciton peak in absorption, significant broadening of photoluminescence (PL), or the appearance of optical gain. The two extremes are clear: dilute nondegenerate excitons are bosons with no optical gain, whereas dense electrons and holes in a degenerate e-h plasma are fermions showing optical gain. Thus, it is often considered that optical gain signifies the Mott transition. Even though the two extremes are well understood both experimentally and theoretically, the picture of the intermediate regime is not so clear, where coexistence, spatial overlapping, and mutual conversion between different species occur.

The Mott transition becomes especially interesting in a one-dimensional (1D) system and when biexcitons are involved, but the experimental research has been scarce in these cases. PL spectroscopic studies involving excitons and biexcitons have mostly been limited to the low-density regime for both GaAs and II–VI materials, where the transition to plasma does not appear. Optical gain has been observed only at high densities for the plasma phase in GaAs, while low-density gain mechanisms with excitonic nature have been reported in II–VI materials [3–6]. In 1D systems, theoretical studies have provided conflicting pictures, with predictions ranging from no Mott transition and no optical gain at any density [7] to a plasma gain at a density of $2\text{–}3 \times 10^5$ cm^{-1} [8,9].

In this Letter, we report our systematic investigation of the density dependence of PL and absorption spectra measured *simultaneously* under continuous-wave (cw) pumping for carrier densities covering the whole Mott transition in clean intrinsic GaAs T-shaped quantum wires (T wires) [10–15]. The quenching of exciton absorption, appearance of gain, and quenching of excitonic PL were observed successively as the e-h density increased. We interpret that the gain initially originated from biexciton-exciton inversion. As the gain grew, a continuous change in gain mechanism from biexcitons to an unbound e-h plasma and completion of the Mott transition took place. Biexcitons played key roles in optical spectra in the critical intermediate-density region.

The samples used in this study were fabricated by the cleaved-edge overgrowth method using molecular beam epitaxy [10]. We used two types of T-wire-laser structures, a single-wire laser [11,12], and a 20-wire laser [13,14], where each wire was formed at the T intersection of a 14-nm (001) $Al_{0.07}Ga_{0.93}As$ quantum well (stem well) and a 6-nm (110) GaAs quantum well (arm well). The cavity length ℓ of the lasers was 500 μm, and their cavity-mirror facets were left uncoated. The structures and fabrication methods of the samples are described in detail in our previous reports [11–14]. We used a cw Ti-sapphire laser with a photon energy $E_{ex} = 1.631$ eV to achieve a point [12,14] or uniform [10,11,13] excitation from the top surface of the laser samples (inset of Fig. 1). In the uniform excitation, we formed a filamentlike excitation profile within $\pm 10\%$ uniformity along the 500-μm-long T wires via cylindrical and 0.4-numerical-aperture objective lenses. The waveguide-emission spectrum emitted through one of the cavity mirrors was measured at 5 K with a spectral resolution of 0.04 meV using a spectrometer after a polarizer set parallel to the arm well. Simultaneously, the PL spectrum emitted perpendicular to the waveguide was measured in the backscattering geometry.

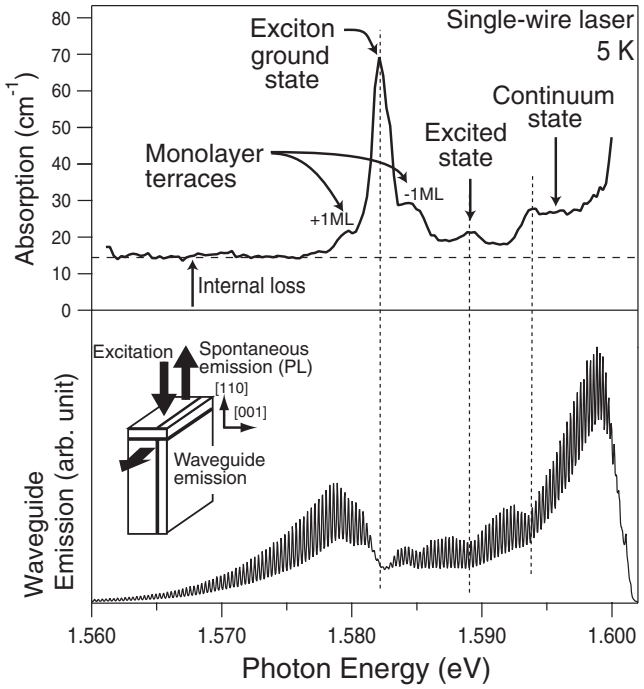

FIG. 1. Waveguide-emission spectrum (lower panel) from a single T wire and the derived absorption spectrum (upper panel).

The bottom panel of Fig. 1 shows the waveguide-emission spectrum under point excitation, where the oscillation depth of the Fabry-Perot fringes varied with the photon energy. For each oscillation, we evaluated the ratio p of the average intensity over a period to the valley intensity. Then we derived the absorption coefficient α using the equation $\alpha = (1/\ell)\ln[R(p+1)/(p-1)]$ with cavity-mirror reflectivity $R = 31\%$ according to Cassidy's method [16]. Since absorption occurs everywhere in the T-wire except the 1-μm excitation spot, the derived absorption spectrum in the top panel of Fig. 1 represents the linear absorption spectrum in the low e-h density limit. Flat background absorption is due to the internal optical scattering loss in the cavity, which is subtracted in the data below. This absorption spectrum agrees very well with those obtained independently in the waveguide transmission experiment [15] and in the PL excitation spectrum experiment [14]. Spectral assignments have already been studied there showing agreement with theoretical calculations [14]: the sharp absorption peak with a 1.3-meV width at 1.582 eV shows the ground-state exciton. A small peak at 1.589 eV shows the first excited-state exciton, and a step edge at 1.594 eV shows the onset of higher exciton states and 1D continuum states. The energy separation between the onset and the exciton ground state was 12 meV, which is close to the calculated exciton binding energy of 14 meV for this T wire [14]. The additional small peaks on both sides of the ground exciton peak are from regions of the T wire with one-monolayer (± 1 ML) variation in the arm-well thickness.

Figure 2(b)–2(g) shows the absorption (solid curves) and PL (dashed curves) spectra measured simultaneously under uniform excitation for various e-h densities. Figure 2(a) represents the spectra in the low e-h density limit, where PL was measured for uniform excitation with minimum power and absorption was measured for point excitation as in Fig. 1. We first explain the PL spectra in Fig. 2(a)–2(g), which very well reproduce our previous results of a more detailed micro-PL study [12,17]: At the lowest density Fig. 2(a), a PL peak marked as X was observed at 1.582 eV showing a small Stokes shift of 0.3 meV from the absorption peak. As the excitation increased [Fig. 2(c)–2(e)], another PL peak marked as XX appeared 3 meV below the X PL peak showing a similar width and grew without shift. The XX intensity scaled quadratically with the X intensity as pumping increased. Then, the XX intensity overtook the X intensity, and the two PL peaks broadened and eventually changed to a broad

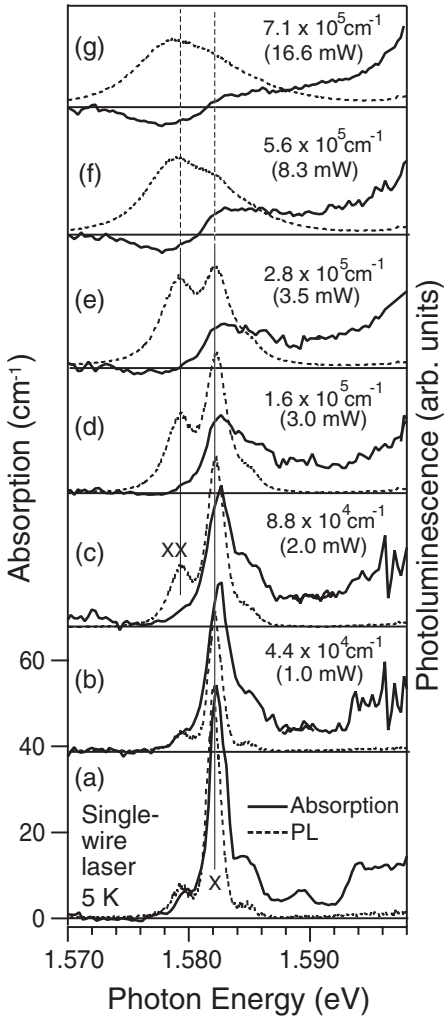

FIG. 2. Absorption (solid curves) and PL (dashed curves) spectra from a single T wire at 5 K for various excitation densities (powers) from (a) nearly zero to (g) 7.1×10^5 cm^{-1} (16.6 mW). Large fluctuations around 1.596–1.598 eV in (b), (c) are noise exaggerated in the Cassidy's analysis for weak signals.

PL band [Fig. 2(f) and 2(g)]. Our previous micro-PL scan study [12] showed that two small PL peaks on both sides of the X PL peak in the lowest density [Fig. 2(a)] were position-dependent PL peaks located at certain locations along the wire corresponding to the ± 1 ML terrace. However, all the PL features at higher densities [Fig. 2(c)–2(g)] and the XX PL peak did not have any position dependence [18] or localization-induced asymmetric tails [19]. Interpretation of the X and XX peaks will be discussed later. The total PL intensity of the wire increased with the excitation power and then saturated when the wire states were fully occupied by excited carriers. On the basis of the PL intensity as well as a saturation density of 1.2×10^6 cm^{-1} for a 21-meV energy separation between the wire and arm well, we estimated [12,17] the e-h densities, as shown in the figure. The e-h density where the well-defined X PL peak became invisible was about 5×10^5 cm^{-1}, whereas at much smaller density of 3×10^5 cm^{-1} the XX PL peak overtook the X PL peak. Detailed density characterization, quadratic intensity dependence, and PL spectra in fine density steps are given elsewhere [12,17].

The absorption spectra in the low e-h density regime [Fig. 2(a)–2(d)] show intriguing quenching of excitonic absorption. As the density increased, the absorption peak height of the ground-state exciton decreased without a peak shift and an asymmetric broadening developed. The gap between the ground-state exciton and the 1D continuum states was gradually filled. The continuum edge at 1.594 eV also broadened, but showed no shift, at least up to 1.6×10^5 cm^{-1}. It should be noted that quenching of exciton absorption and formation of the continuous absorption band did not result from a redshift of the continuum band edge toward the exciton level, or diminishing of exciton binding energy, but from the asymmetric broadening of the exciton peak. It is also noteworthy that the quenching of excitonic absorption occurred at low e-h densities of about 1–2×10^5 cm^{-1}. In Fig. 2(d) at 1.6×10^5 cm^{-1} density, the discrete exciton peak was quenched almost completely and the continuous band was formed in the absorption spectrum. The density of 1.6×10^5 cm^{-1} corresponds to an electron Fermi energy of only 0.36 meV or to a mean interexciton distance of 63 nm. Such a sensitive quenching of exciton absorption might be a unique inherent property of 1D systems. In the high-density regime [Fig. 2(f) and 2(g)], where e-h densities were estimated as 5.6×10^5 and 7.1×10^5 cm^{-1}, the absorption spectra showed gain. The gain and absorption existed in the low- and high-energy regions, respectively. The spectral shape of the gain showed no similarity to the 1D density of states.

To investigate the intermediate-density regime near Fig. 2(e) with density of about 3×10^5 cm^{-1}, or the gain threshold, we switched the sample from the single-wire laser to the 20-wire laser to increase the signal-to-noise ratio. Figure 3 shows six absorption spectra (solid curves) and three PL spectra (dashed curves) for e-h densities (powers) from 2.3×10^5 cm^{-1} (32 mW) to 3.8×10^5 cm^{-1} (52 mW), covering the density range around Fig. 2(e). Though higher excitation powers were used in the 20-wire laser to obtain the same e-h densities per wire as in a single-wire laser, the same e-h density calibration [12] was performed, so direct comparison between Figs. 2 and 3 is possible. The vertical lines at 1.5829, 1.5844, and 1.5874 eV in Fig. 3 indicate the energies of the gain peak, the XX and X PL peaks, respectively.

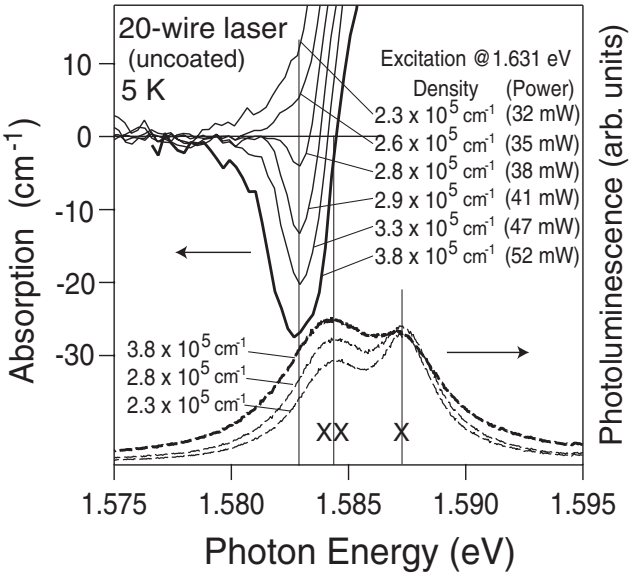

FIG. 3. Absorption spectra (solid curves) of a 20-wire laser for various e-h densities from 2.3 to 3.8×10^5 cm^{-1} and PL spectra (dashed curves) for e-h densities of 2.3, 2.8, and 3.8×10^5 cm^{-1}. The vertical lines indicate the energies of the gain peak, the XX and X PL peaks.

As shown in Fig. 3, a sharp gain peak with a width of 0.8 meV appeared at 1.583 eV when an e-h density reached 2.8×10^5 cm^{-1}, corresponding to the same level of excitation as in Fig. 2(e). This gain peak energy was 1.5 meV below the XX PL peak. At this density, the X and XX PL peaks were both clearly observed with almost the same height. As the e-h density increased up to 3.8×10^5 cm^{-1}, the gain peaks became larger and broader showing almost no shift. At the beginning, the gain peak was symmetric, and it then showed a tail in the low-energy region. Simultaneously the X PL peak was gradually quenched relatively to the increased and broadened XX PL peak. At higher density, both the gain and PL spectra became closer to those in Fig. 2(f) and 2(g).

We now interpret and discuss the above experimental observations. We ascribe the X PL peak to excitons because it overlaps almost completely with the exciton ground-state absorption peak except for the 0.3-meV Stokes shift in Fig. 2(a). We assigned the XX PL peak to biexcitons. This assignment is based on the intrinsic features displayed in Fig. 2(a)–2(g) such as no position dependence, 3 meV stabilization energy form excitons, PL width similar to excitons, and most importantly the quadratic intensity dependence shown more in detail sepa-

rately [12,13]. We comment that a microscopic luminescence theory [20] was reported and is debated in the community, which argues that a PL peak at the exciton resonance frequency originates not necessarily from an incoherent exciton population but may well result from a Coulomb correlation process in an *e-h* plasma. Similar arguments could in principle be made for a PL peak at biexciton resonance, but such a theory including biexcitons does not exist currently. Therefore, hereafter, we follow the conventional PL picture of excitons and biexcitons in semiconductors [1–9,21,22], and we relate the intensities of the X and XX PL peaks to their respective populations.

We saw in Figs. 2 and 3 that optical gain occurred at the critical density of about 3×10^5 cm^{-1} when the XX peak was about to overtake the X peak. The simultaneous appearance of gain with the crossover of X and XX indicated that the system still contained significant exciton and biexciton populations and that the Mott transition had not completed. The 0.8-meV gain bandwidth corresponds to a homogeneous dephasing time of 5 ps, which seems to be too long to be associated with the dephasing process in an unbound plasma, typically of the order of 100 fs [23]. All these evidences suggest that the origin of optical gain near the gain threshold was from biexciton-to-exciton transition (biexciton $\Leftrightarrow$ exciton + photon) when the system contained more biexcitons than excitons. We can rule out the possibility of exciton-exciton scattering gain, which has been discussed in wide-gap materials [4], because the gain appeared 4.5 meV below the exciton ground-state peak, while the first excited state of the exciton is 7 meV above the gain peak [14]. Phonon-assisted gain can be ruled out since there is no optical phonon or confined acoustic phonon that matches the 4.5 meV energy.

At high densities above 5×10^5 cm^{-1} in Fig. 2(f) and 2(g), the X PL peak was quenched and a broad PL band was formed at the position of the XX peak. These indicated that an unbound *e-h* plasma was formed instead of excitons and biexcitons, completing the Mott transition. Gain was thus ascribed to a plasma. The low- and high-energy edges of the gain region were regarded as the positions of the band edge and Fermi edge, respectively. Continuous evolution of the broad plasma gain from the sharp biexciton gain without peak shift suggested a gradual change in the origin of gain from biexcitons to a plasma.

To conclude, our results of absorption or gain and PL spectra measured simultaneously at various *e-h* densities in clean intrinsic GaAs T wires at 5 K shed light on the long-standing issue of the Mott transition in an optically excited semiconductor. While the coexistence of excitons with plasma [1] and biexcitons [21,22] have been discussed in connection with Si, Ge, or GaAs quantum wells, our results here provide richer experimental evidence that excitons, biexcitons, and plasma all participate in the Mott transition. From Figs. 2 and 3, we can clearly distinguish four stages of the system as the total *e-h* density is increased: stage one involves purely exciton as shown in Fig. 2(a) and 2(b). Stage two involves coexistence of excitons and biexcitons represented by Fig. 2(c) and 2(d) with the exciton feature dominating. Stage three starts when the biexciton feature overtakes the exciton feature [Figs. 2(e) and 3] and ends when the exciton disappears [Fig. 2(f)] and the Mott transition is completed. During this stage, we observe gain, which starts as a sharp gain due to biexciton-exciton inversion and grows with broadening but without a shift. The 1D-continuum absorption edge seen in Figs. 1 and 2(a)–2(c), or the bare band edge, is not observable anymore, but continuous absorption extends to an edge just above the gain region [Fig. 2(e) and 2(f)]. In this stage, excitons, biexcitons, and possibly plasma coexist, though exciton and biexciton features become less and less well defined with greater spatial overlapping and more scattering events as the *e-h* density increases. Finally stage four involves a pure high-density plasma. It appears that the unbound plasma phase evolves continuously from dense biexcitons. We believe that such a complete sequence of stages during the Mott transition provides a more complete set of experimental evidence for the coexistence of various species.

This work was financially supported partly by a Grant in Aid from MEXT, Japan.

*A visiting professor at ISSP University of Tokyo in 2006.

[1] R. Zimmermann, *Many-Particle Theory of Highly Excited Semiconductors* (Teubner, Leipzig, 1988).
[2] H. Haug and S. W. Koch, *Quantum Theory of the Optical and Electronic Properties of Semiconductors* (World Scientific, Singapore, 2004).
[3] J. Ding *et al.*, Phys. Rev. Lett. **69**, 1707 (1992).
[4] Z. K. Tang *et al.*, J. Cryst. Growth **287**, 169 (2006).
[5] F. Kreller *et al.*, Phys. Rev. Lett. **75**, 2420 (1995).
[6] O. Homburg *et al.*, Phys. Rev. B **60**, 5743 (1999).
[7] D. W. Wang and S. Das Sarma, Phys. Rev. B **64**, 195313 (2001).
[8] S. Das Sarma and D. W. Wang, Phys. Rev. Lett. **84**, 2010 (2000).
[9] C. Piermarocchi and F. Tassone, Phys. Rev. B **63**, 245308 (2001).
[10] W. Wegscheider *et al.*, Phys. Rev. Lett. **71**, 4071 (1993).
[11] Y. Hayamizu *et al.*, Appl. Phys. Lett. **81**, 4937 (2002).
[12] M. Yoshita *et al.*, Phys. Rev. B **74**, 165332 (2006).
[13] H. Akiyama *et al.*, Phys. Rev. B **67**, 041302 (2003).
[14] H. Itoh *et al.*, Appl. Phys. Lett. **83**, 2043 (2003); H. Akiyama *et al.*, Appl. Phys. Lett. **82**, 379 (2003).
[15] Y. Takahashi *et al.*, Appl. Phys. Lett. **86**, 243101 (2005).
[16] D. T. Cassidy, J. Appl. Phys. **56**, 3096 (1984); B. W. Hakki and T. L. Paoli, J. Appl. Phys. **46**, 1299 (1975).
[17] M. Yoshita *et al.*, J. Phys. Condens. Matter **19**, 295217 (2007).
[18] A. Feltrin *et al.*, Phys. Rev. Lett. **95**, 177404 (2005).
[19] R. F. Schnabel *et al.*, Phys. Rev. B **46**, 9873 (1992).
[20] M. Kira, F. Jahnke, and S. W. Koch, Phys. Rev. Lett. **81**, 3263 (1998).
[21] M. Combescot, Phys. Rev. Lett. **32**, 15 (1974).
[22] J. C. Kim, D. R. Wake, and J. P. Wolfe, Phys. Rev. B **50**, 15 099 (1994).
[23] R. Binder *et al.*, Phys. Rev. B **45**, 1107 (1992).

One-Dimensional Band-Edge Absorption in a Doped Quantum Wire

Toshiyuki Ihara,* Yuhei Hayamizu, Masahiro Yoshita, and Hidefumi Akiyama
Institute for Solid State Physics (ISSP), University of Tokyo, and CREST, JST, 5-1-5, Kashiwanoha, Kashiwa, 277-8581 Chiba, Japan

Loren N. Pfeiffer and Ken W. West
Bell Laboratories, Lucent Technologies, Murray Hill, New Jersey 07974, USA
(Received 17 November 2006; published 20 September 2007)

Low-temperature photoluminescence-excitation spectra are studied in an n-type modulation-doped T-shaped single quantum wire with a gate to tune electron densities. With a nondegenerate one-dimensional (1D) electron gas, the band-edge absorption exhibits a sharp peak structure induced by the 1D density of states. When the dense 1D electron gas is degenerate at a low temperature, we observe a Fermi-edge absorption onset without many-body modifications.

DOI: 10.1103/PhysRevLett.99.126803 PACS numbers: 73.21.Hb, 73.20.At, 78.55.Cr, 78.67.−n

Optical spectroscopy of the one-dimensional (1D) electron gas formed in n-type doped semiconductor quantum wires has been an exciting challenge in the past two decades [1,2]. Theories have pointed out some interesting phenomena inherent in the 1D electron gas, such as the appearance or disappearance of band-edge singularity induced by inverse square root 1D density of states (DOS) divergence, and also strong 1D many-body interaction effects [3–5]. Experimental investigations of Fermi-edge singularity (FES) effects [6–8] and 1D band-gap renormalization (BGR) effects [9–11] have been reported. However, no experiment has shown band-edge singularity induced by 1D-DOS divergence. Thus the question of whether the 1D band-edge singularity appears in optical spectra still remains unanswered.

To clarify such fundamental properties by optical spectroscopy, we need to measure both emission and absorption spectra at various temperatures and electron densities. This is because emission and absorption in doped systems selectively occur for occupied and unoccupied conduction-band states, respectively. However, it is difficult to measure absorption spectra of a quantum wire because of its small volume. Thus, there have been no systematic experimental studies of temperature-dependent absorption spectra of 1D electron systems at various densities. To investigate this unexplored subject, we developed a photoluminescence-excitation (PLE) measurement system that provides complete and clear line shapes of absorption spectra even for a single quantum wire.

This Letter reports the first observation of the sharp band-edge absorption peak structure induced by 1D DOS probed by low-temperature PLE measurements on an n-type doped single quantum wire with a gate to tune electron densities. The sharp band-edge absorption peaks appear in the PLE spectra when the 1D electron gas is not degenerate at high temperature, or at low electron density. In the presence of a dense electron gas at low temperature (5 K), we observe absorption onset at the Fermi edge of the degenerate 1D electron gas. Sharp excitonic peaks appear in the spectra at very low densities of less than 1×10^5 cm^{-1}, while no strong many-body effects appear in spectra at high densities.

The structure of the sample of n-type doped GaAs quantum wire is illustrated in Fig. 1. A single T-shaped quantum wire was formed in the cross section of a 14 nm-thick $Al_{0.07}Ga_{0.93}As/Al_{0.33}Ga_{0.67}As$ quantum well (stem well) and 6 nm-thick $GaAs/Al_{0.45}Ga_{0.55}As$ quantum well (arm well). Delta doping of Si at a distance of 100 nm from the stem well induced 2D electron gas with a density of 1×10^{11} cm^{-2} in the stem well. By applying dc gate voltage (V_g) to a gate layer on the top of the arm well relative to the 2D electron gas in the stem well, we tuned the electron densities (n_e) in the 1D wire. The 1D electron density n_e for each V_g was determined via our model fitting of optical spectra shown later in this Letter. A more detailed description of the sample preparation is given elsewhere [9].

In our micro-PL and PLE measurements, excitation light from a continuous-wave titanium-sapphire laser with polarization parallel to the [001] direction (perpendicular to the wire axis) was focused into a 1-μm spot by a 0.5 numerical aperture objective lens on the top (110) surface of the sample. The photoluminescence (PL) emission in the [001] direction was detected via a 0.5 numerical aperture

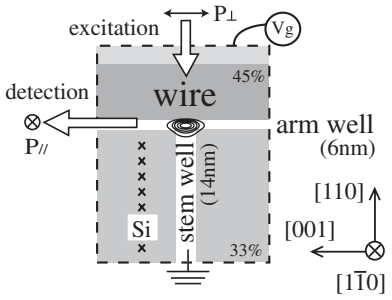

FIG. 1. Schematic view of n-type doped T-shaped quantum wire sample.

objective lens and a polarizer set in the $[1\bar{1}0]$ polarization direction to reduce intense laser scattering.

Normalized PLE spectra at various temperatures in the presence of a dense 1D electron gas are shown by solid curves in Fig. 2(a). The gate voltage was fixed to 0.7 V, which corresponds to an electron density of about 6×10^5 cm^{-1} in the quantum wire. At low temperature (5 K), we observed a single absorption onset at 1.575 eV with a long low-energy tail. We assigned this onset (FE) as the Fermi edge, which separates the occupied and unoccupied states in the conduction band. A large absorption by the arm well showed its low-energy tail at around 1.578 eV. As the temperature was increased, the FE onset became smeared and the low-energy tail increased in intensity. At 30 K, another absorption onset was formed at 1.565 eV. At higher temperatures, this onset increased in intensity and formed a sharp peak structure at 50 K. We assigned this structure to the 1D band-edge (BE) absorption peak induced by the inverse square root 1D DOS.

Dotted curves in Fig. 2(a) indicate PL spectra. We set photon energy of the laser between 1.57 and 1.575 eV so that excited carriers are formed only in the wire. At 5 K, we observed an asymmetrical PL peak at 1.565 eV. We assigned this PL peak to the band-edge emission. We observed a large energy gap of 10 meV between this peak and PLE onset at FE. As the temperature was increased, the PL peak shifted to lower energy without any remarkable change in its line shape. This redshift with increasing temperature also appears in bulk GaAs and is known as the Varshni shift [12]. At 50 K, we found that the PL and PLE peaks appeared at exactly the same energy of band edge, denoted by BE.

We calculated optical spectra with a free-particle model. This model includes the 1D joint DOS with the energy dependence of $1/\sqrt{E}$, Fermi distribution functions for electrons and holes, and a broadening function of Gaussian line shape, but does not take into account many-body Coulomb interactions. Figure 2(b) shows normalized emission (dotted curves) and absorption (solid curves) spectra calculated for various temperatures for electrons and holes, T_e ($= T_h$), with the following parameters: broadening (Γ) of 1.0 meV, the effective masses for electrons and holes of $0.067m_0$ and $0.105m_0$, respectively [13], where m_0 is electron mass in vacuum, and electron density (n_e) of 6×10^5 cm^{-1}. The band-gap energies with shifts at various temperatures, $E_g(T)$, were estimated from those for bulk GaAs [12,14]. The absorption spectrum at 5 K, shown as the bottom solid line in Fig. 2(b), exhibits an onset at the energy of $E_g + 10$ meV, which corresponds to the Fermi edge of the degenerate 1D electron gas. The emission spectrum exhibits a peak at the energy of E_g, which corresponds to the band edge. At higher temperature, the Fermi-edge absorption onset disappears while another low-energy absorption onset of the band edge appears at the same energy as the emission peak (E_g). At 40 or 50 K, the absorption spectra exhibit a sharp asymmetrical peak at the band edge of the nondegenerate 1D electron gas. This peak originates from the 1D-DOS divergence with broadening of 1.0 meV. We found that the experimental results agree well with these free-particle-model calculations. This supports our assignment that the sharp PLE peak at 50 K originates from the 1D band-edge singularity induced by 1D DOS.

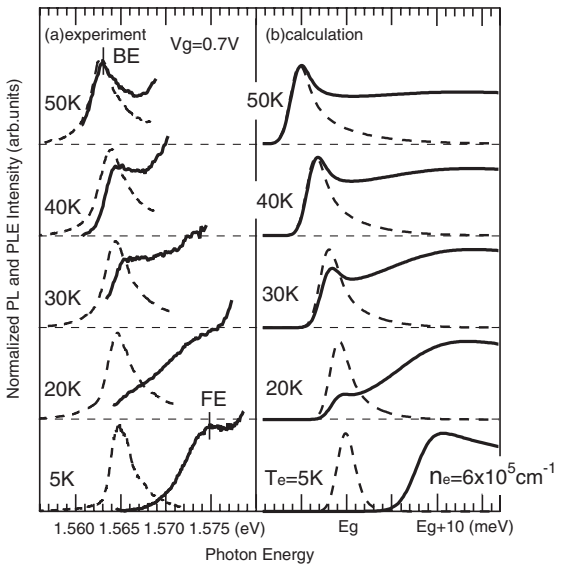

FIG. 2. Experimental (a) and calculated (b) spectra of PL (dotted line) and PLE (solid line) for 1D wire at various temperatures.

We also studied the electron density dependence of PLE spectra at low temperature (5 K) using the same sample of doped quantum wire. The solid curves in Fig. 3(a) indicate the normalized PLE spectra at various V_g. The top line at $V_g = 0.7$ V shows the single Fermi-edge absorption onset (FE), which is the same as the bottom line in Fig. 2(a). As the density was decreased, the FE onset shifted to lower energy. The photon energies of the FE onset are plotted by filled inverted triangles in Fig. 4(a). At $V_g = 0.4$ V, band-edge absorption onset appeared at the low-energy side (1.566 eV). At $V_g = 0.35$ V, this onset increased in intensity, and a characteristic double peak structure was formed.

As the density was further decreased, the Fermi-edge peak merged into the tail of the low-energy peak and formed a single asymmetrical absorption peak structure at $V_g = 0.2$ V. This asymmetrical peak became a symmetrical peak (X^-) at $V_g = 0.15$ V. This X^- peak lost its intensity as the density approached zero. Instead, another peak appeared at higher energy (1.569 eV), which became a sharp symmetrical peak (X) at 1.5685 eV at $V_g = 0$ V. The full width at half maximum (FWHM) of the X peak was 0.9 meV. The splitting of the X peak is probably due to monolayer thickness fluctuations in the stem well. In Fig. 4(a), we plot peak energies of X^- (filled triangles) and X (filled circles).

Dotted curves in Fig. 3(a) indicate PL spectra, which are almost the same as those we reported in detail in a previous

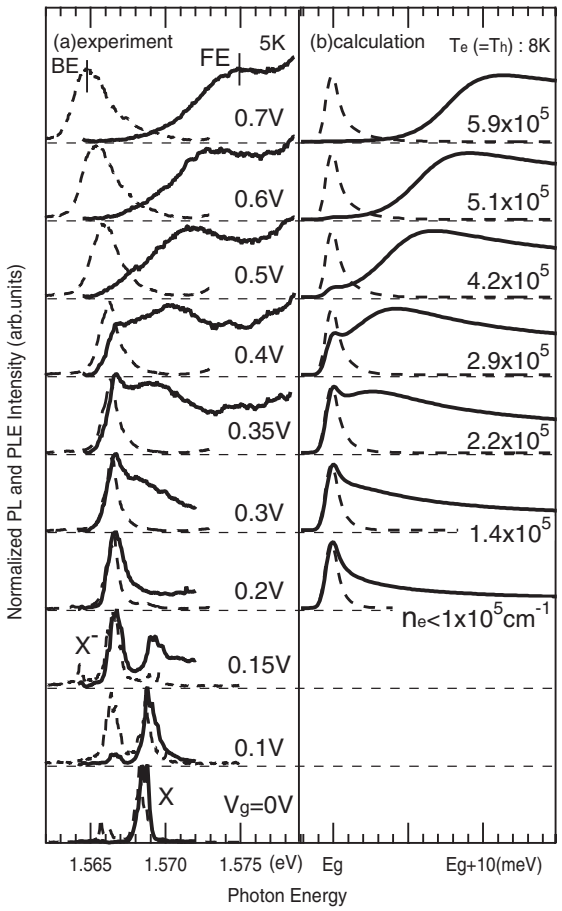

FIG. 3. Normalized experimental (a) and theoretical (b) spectra of PL (dotted lines) and PLE (solid lines) for 1D quantum wire at various electron densities. X was assigned to excitons and X^- to trions.

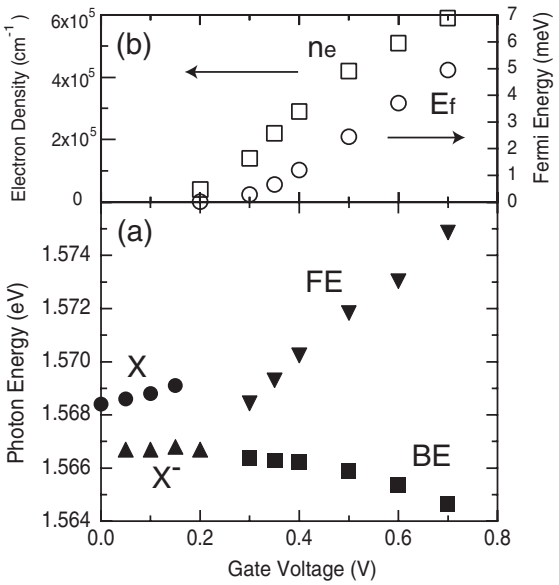

FIG. 4. (a) Peak positions and (b) estimated electron density and corresponding Fermi energy plotted as a function of gate voltage.

Letter [9]. We set the photon energy of the laser between 1.568 and 1.575 eV to form carriers in the wire. At V_g from 0.7 to 0.2 V, we observed a broad PL peak that shifted to higher energy with decreasing electron density, which represents the BGR shift. The energies of the PL peak at BE are plotted by filled squares in Fig. 4(a). At 0–0.15 V, PL spectra also showed sharp peaks of X^- and X.

In 2D systems, very similar crossover from band-to-band transition to X^- and X with decreasing electron density has been well studied experimentally [15,16] and theoretically [17,18]. Thus, we analogously assigned [9] the present X^- and X peaks to trions (a bound state of two electrons and a hole) and neutral excitons (a bound state of an electron and a hole), respectively. Furthermore, we confirmed the assignment of X by additionally measuring PLE features near and above the X peak at 0 V that were the same as those of excitons and continuum states identified in nondoped quantum wires [19,20].

Figure 3(b) shows calculated normalized emission (dotted curves) and absorption (solid curves) spectra with the free-particle model assuming various electron densities (n_e). We assumed a slightly high carrier temperature of T_e ($= T_h$) $= 8$ K and a broadening of $\Gamma = 0.4$ meV to obtain the best fit to the PLE spectra. The assumed electron density (n_e) in the calculations and corresponding Fermi energy, $E_f = \frac{\pi^2\hbar^2 n_e^2}{8m_e}$, are plotted as a function of V_g in Fig. 4(b) as open squares and open circles, respectively.

The calculated absorption spectra for $n_e > 1 \times 10^5$ cm^{-1} show good agreement with the experimental PLE spectra at $V_g > 0.2$ V. In particular, the characteristic double peak structures of the band-edge and Fermi-edge absorptions at $V_g = 0.35$–0.4 V are almost completely reproduced by the calculations. The sharp band-edge absorption originates from 1D DOS, and it appears in the PLE spectra when the 1D electron gas is not degenerate at low density. We have already demonstrated, in Fig. 2(a), the appearance of 1D band-edge absorption peak in the PLE spectra at high temperature (50 K). These results prove that the singularity of 1D DOS appears in the PLE spectra in the presence of nondegenerate electron gas at low density, or at high temperature.

The characteristic double peak structures in the PLE spectra at $V_g = 0.35$–0.4 V is unique to 1D systems, which have never been observed for 2D systems [15,16]. In previous studies of FES including microscopic theories [17,18], the effect of Coulomb interaction, or Coulomb enhancement, appeared at the Fermi edge while the band edge reflected the shape of single particle DOS. Following these studies, we ascribed the origin of the sharp band-edge peak in the double peak at $V_g = 0.35$–0.4 V to the 1D-DOS singularity instead of Coulomb interaction. As for the single asymmetric PLE peak in the crossover region of $V_g = 0.2$–0.3 V, it is difficult to distinguish the two contributions of 1D-DOS singularity and Coulomb interaction. The sharp symmetrical absorption peaks at $V_g =$ 0–0.15 V, where very low densities below 1×10^5 cm^{-1}

are estimated from extrapolation in Fig. 4(b), are caused by trions and excitons, which originate from the Coulomb interaction.

We remark here that nondoped quantum wires [19–22] show absorption spectra without 1D band-edge singularity due to strong 1D Coulomb interaction. Thus, doping was essential in the present first observation of 1D band-edge singularity. Moreover, PLE measurements were also indispensable, because PL spectra at low temperature are dominated by the lowest energy transitions and by themselves do not represent 1D DOS [9].

Let us now discuss the 1D many-body effects in PL and PLE spectra at high electron densities. As we have mentioned, previous reports predicted theoretically or investigated experimentally several interesting many-body effects, such as the FES and BGR effects. The theories of FES [3–5] predicted a sharp FES peak, or a power-law singularity, at a low-energy (high-energy) shoulder in absorption (emission) spectra. This effect results from multiple scattering processes involving electrons near the Fermi level. The theories of BGR [1,23,24] predicted a redshift of the band-edge emission peak with increasing electron density, which results from the electronic correlation effects. In our experiments, as shown in Fig. 3(a) or Fig. 4(a), the BGR effect was observed as redshifts of the band-edge PL peak (BE) with increasing density.

However, the FES effect in the PLE spectra was negligible. No sharp peak nor power-law singularity was observed at the Fermi edge of the PLE spectra. Note that the wire size was small (14 nm $\times$ 6 nm), the inhomogeneous broadening was small (0.9 meV), and the temperature was low (5 K), which are favorable conditions for studying 1D FES effects. Even under these conditions, the FES effect was found to be weak.

Similar experimental results [6] were reported by Oberli *et al.* They observed weak FES effects in PLE spectra for 1D electron systems formed in *V*-groove quantum wires. They pointed out that the existence of a strong FES effect is related to the hole localization effect and a resonance with a partially empty higher subband. In other words, the strong FES effect was not attributed to the character of the 1D electron gas formed in a high-quality 1D limit quantum wire. In fact, the quantum wires used in the earlier experiments showing strong FES effects [7,8] had large sizes and large wire width fluctuations, and the electrons and holes were not in the same positions in the structure.

Theories have shown that optical spectra exhibit a strong peak at the Fermi edge with extrinsic origins, such as impurities [3], Fano resonance [25], empty higher subband near the Fermi edge, and a type II structure [4]. These calculations indeed explain the earlier experimental results [6–8].

As for intrinsic FES effects in clean 1D systems, theoretical calculations have been used to investigate the values and characteristics of the power-law critical exponents as a function of electronic correlation and finite effective mass of the valence hole [5,26]. However, the strength and robustness of intrinsic FES under finite temperature and damping due to scatterings with phonons and carriers remain to be investigated. We hope that our experimental results will inspire further theoretical investigations of the optical responses of 1D electron systems at various densities including the effect of finite temperature and finite damping.

In conclusion, we performed low-temperature PLE measurements on an *n*-type doped quantum wire and achieved the first observation of sharp band-edge absorption peaks induced by 1D DOS. In the presence of a dense electron gas at low temperature (5 K), the PLE spectra showed a Fermi-edge absorption onset without FES enhancements.

We wish to thank Professor T. Ogawa, Dr. M. Takagiwa, and Dr. K. Bando for valuable discussions. This work was partly supported by a Grant-in-Aid from the Ministry of Education, Culture, Sports, Science, and Technology (MEXT), Japan.

*ihara@issp.u-tokyo.ac.jp

[1] H. Haug and S. W. Koch, *Quantum Theory of the Optical and Electronic Properties of Semiconductors* (World Scientific, Singapore, 2004), 4th ed.
[2] C. Klingshirn, *Semiconductor Optics* (Springer, Berlin, 2004), 2nd ed.
[3] P. Hawrylak, Solid State Commun. **81**, 525 (1992).
[4] F. J. Rodríguez and C. Tejedor, Phys. Rev. B **47**, 13 015 (1993).
[5] T. Ogawa *et al.*, Phys. Rev. Lett. **68**, 3638 (1992).
[6] D. Y. Oberli *et al.*, Physica (Amsterdam) **11E**, 224 (2001).
[7] J. M. Calleja *et al.*, Solid State Commun. **79**, 911 (1991).
[8] M. Fritze *et al.*, Phys. Rev. B **48**, 4960 (1993).
[9] H. Akiyama *et al.*, Solid State Commun. **122**, 169 (2002).
[10] R. Rinaldi *et al.*, Phys. Rev. B **59**, 2230 (1999).
[11] S. Sedlmaier *et al.*, Phys. Rev. B **65**, 201304(R) (2002).
[12] Y. P. Varshni, Physica (Amsterdam) **34**, 149 (1967).
[13] A. Yamaguchi *et al.*, Jpn. J. Appl. Phys. **33**, L912 (1994).
[14] The calculated redshift of the band edge with increasing temperature is larger than that of the experimental one, which is probably due to decrease of band-gap renormalization effect in the experiment.
[15] V. Huard *et al.*, Phys. Rev. Lett. **84**, 187 (2000).
[16] R. Kaur *et al.*, Phys. Status Solidi B **178**, 465 (2000).
[17] P. Hawrylak, Phys. Rev. B **44**, 3821 (1991).
[18] T. Ogawa and M. Takagiwa, Nonlinear Opt. **29**, 465 (2002).
[19] H. Akiyama *et al.*, Appl. Phys. Lett. **82**, 379 (2003).
[20] H. Itoh *et al.*, Appl. Phys. Lett. **83**, 2043 (2003).
[21] Y. Takahashi *et al.*, Appl. Phys. Lett. **86**, 243101 (2005).
[22] Y. Takahashi *et al.*, Appl. Phys. Lett. **87**, 223119 (2005).
[23] M. Stopa, Phys. Rev. B **63**, 195312 (2001).
[24] Ben Yu-Kuang Hu and S. Das Sarma, Phys. Rev. Lett. **68**, 1750 (1992).
[25] T. Mélin and F. Laruelle, Phys. Rev. B **65**, 195303 (2002).
[26] Y. Tsukamoto *et al.*, Phys. Rev. B **58**, 3633 (1998).

Japanese Journal of Applied Physics
Vol. 46, No. 14, 2007, pp. L330–L332

Low-Threshold Current-Injection Single-Mode Lasing in T-shaped GaAs/AlGaAs Quantum Wires

Shu-man LIU, Masahiro YOSHITA, Makoto OKANO, Toshiyuki IHARA, Hirotake ITOH, Hidefumi AKIYAMA, Loren PFEIFFER[1], Ken WEST[1], and Kirk BALDWIN[1]

Institute for Solid State Physics, University of Tokyo, and CREST, Japan Science and Technology Agency, Kashiwa, Chiba 277-8581, Japan
[1]*Bell Laboratories, Alcatel-Lucent, 600 Mountain Avenue, Murray Hill, New Jersey 07974, U.S.A.*

(Received January 26, 2007; accepted February 21, 2007; published online March 30, 2007)

A one-dimensional active region consisting of 20-period T-shaped GaAs/AlGaAs quantum wires of $14 \times 6\,\mathrm{nm}^2$ combined with a well-defined current-confinement scheme has been utilized to obtain a low-threshold-current high-efficiency laser. A threshold current as low as 0.27 mA, a single-mode cw output power of 0.13 mW at 1 mA injection current, and a differential quantum efficiency of 12% were achieved at 30 K using a quantum-wire laser with a 500-μm-long Fabry–Perot cavity coated by high-reflectivity thin metals. [DOI: 10.1143/JJAP.46.L330]

KEYWORDS: low threshold, single mode, quantum-wire laser, cleaved-edge overgrowth, current injection

Ideal one-dimensional (1D) quantum-wire lasers are predicted to operate efficiently with low injection currents in the μA regime due to the small volume of the active region and the large density of states at the subband edges.[1,2] Intensive experimental efforts have been made to obtain such low-threshold and high-efficiency 1D lasers. Most of the research has been based on V-groove wires with dimensions of 2–5 nm thickness and 10–30 nm width and a limited wire array density,[3–5] among which the lowest threshold current of 0.19 mA and output power of 50 μW under cw multimode operation were reported by Tiwari *et al.* in 3-period $10 \times 35\,\mathrm{nm}^2$ strained InGaAs V-groove wire lasers grown by molecular-beam epitaxy (MBE).[4] In addition, a smaller size for strong quantum confinement and a higher array density were realized in T-shaped quantum wires (T-wires) fabricated by a cleaved-edge-overgrowth (CEO) method with MBE, and laser diodes incorporating such T-wires as an active region were reported by Wegscheider *et al.*[6] Therein, 0.4–0.7 mA threshold currents for cw multimode emission were measured in 15-period $7 \times 7\,\mathrm{nm}^2$ GaAs T-wire lasers at 4 K, although neither output power nor efficiency was measured. Recently MBE-grown T-wires with atomically flat interfaces have been demonstrated by introducing a growth-interrupt annealing technique in CEO,[7] and T-wire lasers have been studied intensively by optical pumping.[8,9] More recently, Yagi *et al.* reported a low threshold current of 2.7 mA and a high differential quantum efficiency of 19%/facet for 1.5-μm-wavelength cw single-mode operation at room temperature in GaInAsP/InP distributed-feedback quantum-wire lasers.[10] To establish the fundamental device properties of quantum-wire lasers on the basis of the above progress, the achievement and quantitative study of single-mode quantum-wire lasing with an expected sub-mA low threshold current and high efficiency comparable to theoretical results[1,2] are necessary even at low temperatures.

Here, we report on cw single-mode lasing at 30–70 K from a high-quality 20-period $14 \times 6\,\mathrm{nm}^2$ GaAs/AlGaAs T-wire active material by adopting a new simple carrier-injection scheme with well-defined current confinement. A threshold current as low as 0.27 mA was achieved at 30 K under a cw operation condition, with an output power of 0.13 mW at 1 mA and an external differential quantum efficiency of 12% for a 500-μm-long laser with high-reflectivity

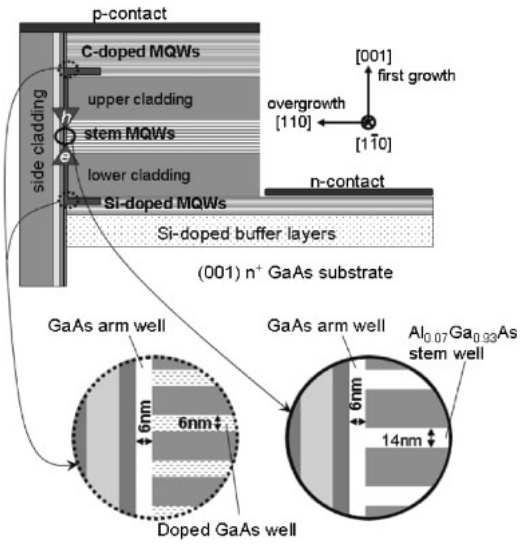

Fig. 1. Schematic structure of a T-shaped quantum-wire laser sample with 20 wires.

(HR) metal-coated Fabry–Perot cavity facets. This result gives an estimated threshold carrier density of $7 \times 10^5/\mathrm{cm}$ per wire, consistent with theoretical results and those from optically pumped laser experiments.[2,8,9]

The T-wire-laser structure, schematically shown in Fig. 1, was grown by the CEO method with MBE. On a (001)-oriented n^+-GaAs substrate we first grew a 1.0 μm n-type GaAs buffer layer, 20 periods of an n-type GaAs (6 nm)/$Al_{0.35}Ga_{0.65}As$ (9 nm) multiple-quantum-well (MQW) injection layer, a 1.5 μm lower cladding layer of 50% digital alloy $(GaAl)_4(AlAs)_4$, a MQW layer composed of 20 periods of 14 nm $Al_{0.07}Ga_{0.93}As$ quantum wells (stem wells) and 44 nm $Al_{0.35}Ga_{0.65}As$ barriers with a total thickness of 1.1 μm for the stem region, a 1.5 μm upper cladding layer of 50% digital alloy $(GaAl)_4(AlAs)_4$, 100 periods of p-type GaAs (6 nm)/$Al_{0.35}Ga_{0.65}As$ (9 nm) MQW injection layer, and a 10 nm p-type GaAs cap layer. Si and C were used as n- and p-type dopants, respectively. The nominal doping level in both p- and n-type injection layers was $1 \times 10^{18}\,\mathrm{cm}^{-3}$. Then we performed the CEO method on the *in situ* cleaved (110) edge to form a 6 nm GaAs QW (arm well) layer, an

11 nm $Al_{0.5}Ga_{0.5}As$ barrier layer, a 171 nm $Al_{0.1}Ga_{0.9}As$ core layer, a 1.0 μm side cladding layer of 50% digital alloy $(GaAs)_6(AlAs)_6$, and a 10 nm GaAs cap layer by growth-interrupt annealing.[7] After the MBE growth, the upper (001) layers were partially etched away so as to minimize leakage current and also to contact the n-type layers from the top. The width of the unetched region in the [110] direction in Fig. 1 was 0.7 mm. Evaporated metal films of AuBe/Au were used for the p-type ohmic contact. After evaporation of the metal films, the wafer was annealed at 450 °C for 30 min for contact alloying.

In the previous current-injection T-wire laser,[6] electrons and holes were injected from two perpendicular parent quantum wells, i.e., the arm well and the stem well, respectively. In this work, parallel p- and n-type doped MQW layers were electrically isolated by two undoped cladding layers and connected only via the arm well. The injection current path was thus confined in the thin arm well during laser operation, which contributes to the low threshold current and high efficiency.

Laser bars of cavity length $L = 500$ μm were cut from the wafer by cleavage with the cleaved facets perpendicular to the axis of the quantum wires. After deposition of a 70 nm SiO_2 insulating layer by plasma-assisted chemical vapor deposition, the cavity facets were HR-coated by a 50 nm Au layer on the front and a 300 nm one on the rear. The laser device was attached p-type side up to a copper block using silver-epoxy glue, and set on the cold finger in a helium-flow-type cryostat. For the measurement of lasing characteristics, light emission from the laser diode was dispersed in a 0.75 m monochromator and recorded using a charge-coupled-device detector. A Si photodiode power meter was used for the measurement of output power. Photoluminescence (PL) measurements were performed using excitation light having a photon energy of 1.67 eV from a cw titanium–sapphire laser in a backward-scattering geometry via the overgrown (110) surface. The excitation light was focused into a 0.8 μm spot using a 0.5 numerical aperture objective lens.

Figure 2(a) shows a PL spectrum of the laser diode at 30 K. An emission peak at 1.564 eV was ascribed to the free ground-exciton recombination in the T-wires.[11] The splitting of the peak was due to the monolayer thickness fluctuation of the arm well. The peak at 1.63 eV was due to the stem wells. The weak band centered at 1.582 eV originated from the arm well and the doped MQW layers according to our separate spatially resolved imaging measurements.

The spectra of electroluminescence (EL) and lasing from the front cavity facet for various current levels at 30 K are shown in Figs. 2(b)–2(d). The insets show the corresponding near-field patterns. Emission from the T-wires dominates the EL spectra. No emission from the stem wells was observed in the EL and lasing spectra at all injection currents investigated here. The absence of EL from the stem wells indicates that current leakage into the stem wells was effectively prevented, and the current was confined in the arm well, as expected. The very weak EL emission centered at 1.582 eV from the arm well and doped MQW layers indicates that only a small number of carriers passed through the T-wire active region and recombined outside under the present operation conditions.

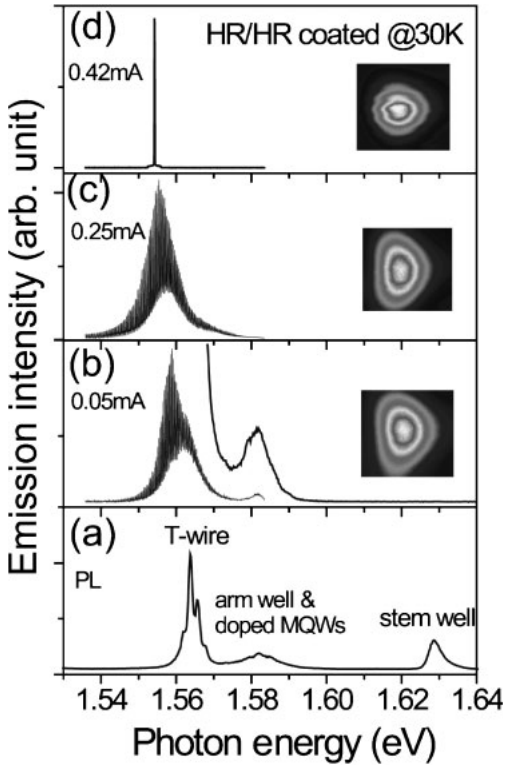

Fig. 2. (a) PL spectrum measured in the geometry of point excitation and high-resolution EL spectra of 500-μm-long T-wire laser structure at (b) 0.05, (c) 0.25, and (d) 0.42 mA. The insets show the corresponding near-field patterns. Also shown in the inset of (b) is a low-resolution EL spectrum with a magnified vertical scale between 1.568 and 1.640 eV, which shows no emission signal around 1.630 eV.

As the current increased, the contrast ratio of the oscillations grew significantly and finally became a single lasing mode at 1.554 eV after the current reached the threshold. The corresponding near-field pattern changed from a heart shape at low current levels into a circular one, indicating tight optical confinement above the threshold. Single-mode lasing was similarly observed in the cryostat at temperatures between 30 and 70 K. The lasing energy showed a red-shift of about 10 meV from the PL peak, in contrast to there being no red-shift in previous T-wire lasers with large inhomogeneity.[6] We ascribed the present 10 meV red-shift partly to a 5–7 meV red-shift of the plasma gain peak from the free exciton peak verified in our optically pumped T-wire lasers with high homogeneity,[9] and partly to the additional red-shift due to quantum-confined Stark effects and band-gap renormalization effects in the presence of external applied electric fields and internal induced space charges.[12] The apparent lack of red-shift in previous T-wire lasers with large inhomogeneity[6] was most likely due to a Stokes shift of exciton PL with localization, as has been discussed elsewhere.[8,9]

The corresponding single-facet light outputs versus current characteristics of the laser diode operating under the cw condition are shown in Fig. 3(a). We obtained a lowest threshold current (I_{th}) of 0.27 mA and a maximum external differential quantum efficiency (η_d) of 12% at 30 K. At 30–40 K, a single-mode output power of 0.13 mW was obtained for a 1 mA input current, or about $4I_{th}$. Figure 3(b) shows the current versus voltage (I–V) characteristic of the

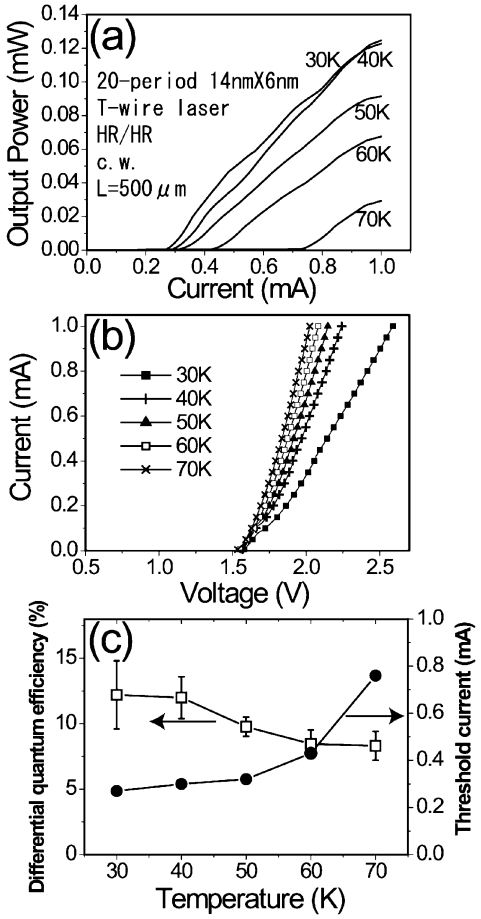

Fig. 3. (a) cw light output vs current and (b) current vs voltage characteristic curves of the 20-period $14 \times 6\,\mathrm{nm}^2$ T-wire laser operating at various temperatures. (c) Temperature dependence of the threshold current and external differential quantum efficiency of the T-wire laser. The laser has a cavity length L of 500 μm, and HR coatings of 96.8 and 98.1% estimated reflectivities for the front and rear cavity facets, respectively.

laser diode, exhibiting typical diode I–V curves. The turn-on voltages of the device at temperatures between 30 and 70 K were similar and near 1.56 V. The leakage current below 1.56 V was smaller than 1 μA. The series resistance was estimated to be 500 Ω. The soft turn-on behavior of the I–V curve, i.e., a slight rise in current with increasing voltage, at 30 K is probably due to carrier freezing in doped MQW and buffer layers.

Figure 3(c) depicts the measured threshold current as a function of the cryostat temperature. The threshold current increased slowly at first and then quickly above 60 K probably due to peak gain decrease at higher temperatures. The mean differential quantum efficiency at various temperatures is also shown in Fig. 3(c) with error bars. The efficiency was 12% at 30 K and gradually decreased to 8.3% at 70 K. These values are considered high for a laser using metal HR mirrors. For the front (rear) facet mirror with a 70-nm-thick SiO_2 dielectric film and a 50-nm (300-nm)-thick Au film on a GaAs semiconductor surface, we estimated the probabilities of reflection, transmission, and absorption at the front (rear) facet with a 50 nm (300 nm) Au coating as 96.8% (98.1%), 1.0% (0%), and 2.2% (1.9%), respectively, using the material parameters in ref. 13. If we assume an internal quantum efficiency of $\eta_i = 1$ on the basis of the high injection efficiency and the negligibly small nonradiative decay in high-quality T-wires, the measured differential quantum efficiency $\eta_d = 0.12$ gives an estimation of the internal loss $\alpha = 0.32\,\mathrm{cm}^{-1}$, or $\alpha L = 0.02$. In this structure, free-carrier absorption and scattering are minimized, because there are no dopants in the waveguide, and because all the heterointerfaces are formed by MBE growth or cleavage and have very high flatness with atomic-layer precision. This is the most likely reason for the very small estimated value of the internal loss, although it may partly originate from the estimation error in the HR coating characteristics.

The threshold current of 0.27 mA at 30 K for 20 T-wires corresponds to 0.014 mA per 500 μm-long wire. If we assume $\eta_i = 1$, and use a separately measured carrier lifetime of 0.4 ns in $14 \times 6\,\mathrm{nm}^2$ single T-wires, the threshold carrier density is estimated to be $7 \times 10^5/\mathrm{cm}$ per wire. This estimated result agrees well with the theory[2] and our separate experimental results on optically pumped T-wire lasers.[8,9]

To conclude, we have presented a low-threshold current-injection laser using 20 periods of T-shaped GaAs/AlGaAs quantum wires as the gain medium with a new current-injection scheme. We have demonstrated cw single-mode lasing at 1.554 eV with a low threshold of 0.27 mA and a high differential quantum efficiency of 12% at 30 K.

Acknowledgment

This work was partly supported by a Grant-in-Aid from the Ministry of Education, Culture, Sports, Science and Technology, Japan.

1) Y. Arakawa and H. Sasaki: Appl. Phys. Lett. **40** (1982) 939.
2) A. Yariv: Appl. Phys. Lett. **53** (1988) 1033.
3) S. Simhony, E. Kapon, E. Colas, R. Bhat, N. G. Stoffel, and D. M. Hwang: IEEE Photonics Technol. Lett. **2** (1990) 305.
4) S. Tiwari, G. Pettit, K. Milkove, F. Legoues, R. Davis, and J. Woodall: Appl. Phys. Lett. **64** (1994) 3536.
5) T. G. Kim, C. S. Son, and M. Ogura: IEEE Photonics Technol. Lett. **13** (2001) 409.
6) W. Wegscheider, L. Pfeiffer, K. West, and R. Leibenguth: Appl. Phys. Lett. **65** (1994) 2510.
7) M. Yoshita, H. Akiyama, L. Pfeiffer, and K. West: Appl. Phys. Lett. **81** (2002) 49.
8) Y. Hayamizu, M. Yoshita, S. Watanabe, H. Akiyama, L. Pfeiffer, and K. West: Appl. Phys. Lett. **81** (2002) 4937.
9) H. Akiyama, L. N. Pfeiffer, M. Yoshita, A. Pinczuk, P. B. Littlewood, K. W. West, M. J. Matthews, and J. Wynn: Phys. Rev. B **67** (2003) 041302.
10) H. Yagi, K. Miura, Y. Nishimoto, D. Plumwongrot, K. Ohira, T. Maruyama, and S. Arai: Appl. Phys. Lett. **87** (2005) 223120.
11) H. Akiyama, M. Yoshita, L. Pfeiffer, K. West, and A. Pinczuk: Appl. Phys. Lett. **82** (2003) 379.
12) N. Le Thomas, N. T. Pelekanos, Z. Hatzopoulos, and E. Aperathitis: Appl. Phys. Lett. **81** (2002) 1582.
13) K.-H. Hellwege and J. L. Olsen: *Metals: Landort-Bornstein Numerical Data and Relationships in Science and Technology* (Springer, Berlin, 1985) New Series, Group III, Vol. 15b, p. 231.

Electronic structure and efficient carrier injection in low-threshold T-shaped quantum-wire lasers with parallel *p*- and *n*-doping layers

Shu-man Liu,[a] Masahiro Yoshita, Makoto Okano, Toshiyuki Ihara, Hirotake Itoh, and Hidefumi Akiyama
Institute for Solid State Physics, University of Tokyo, and CREST, JST, Chiba 277-8581, Japan

Loren N. Pfeiffer, Ken W. West, and Kirk W. Baldwin
Bell Laboratories, Alcatel-Lucent, 600 Mountain Avenue, Murray Hill, New Jersey 07974

(Received 7 March 2007; accepted 9 July 2007; published online 27 August 2007)

We report on the electronic structure, efficient carrier injection, and quantitative lasing characteristics of T-shaped GaAs/AlGaAs quantum-wire-laser diodes with parallel *p*- and *n*-doping layers grown by a cleaved-edge-overgrowth method with molecular-beam epitaxy. Continuous single-mode lasing from the ground subband of the quantum wires was demonstrated between 30 and 70 K in laser diodes with high-reflectivity Au coating on both cavity facets. The lowest threshold of 0.27 mA and the highest differential quantum efficiency of 12% were achieved at 30 K. Micro-photoluminescence measurements demonstrated the high optical quality of the quantum wires with narrow linewidth of 0.9 meV and provided electronic structures of surrounding layers. Microscopic electroluminescence (EL) imaging measurements demonstrated the efficient carrier injection into the quantum wires at 30 K. These two factors, i.e., high material quality and efficient carrier injection, contribute to the low threshold current and high efficiency of the laser device. The result of EL imaging at 5 K indicates an inefficient carrier injection into the active region, which limits the operating temperature of the devices. © *2007 American Institute of Physics*.
[DOI: 10.1063/1.2772544]

I. INTRODUCTION

Quantum-wire lasers, in which carriers are confined in a one-dimensional (1D) active region, are predicted to exhibit low threshold currents, high modulation bandwidths, narrow spectral linewidths, and reduced temperature sensitivity.[1,2] An ultralow threshold of $2-3$ μA was predicted for a single quantum-wire laser compared with a value of 100 μA for a single quantum-well laser.[3] Thus, quantum-wire lasers are the subject of intensive research and have been studied by several groups during the past decade.[4–12] However, the expected high performance has not been verified due mainly to the difficulty of fabricating high-quality quantum wires. In fact, quantum-wire lasers have so far exhibited only inferior lasing threshold current and efficiency characteristics in comparison with the best quantum-well lasers.[13,14] They still need to be studied systematically and have their full potential developed.

The cleave-edge-overgrowth (CEO) method[15] in molecular beam epitaxy (MBE) can produce a T-shaped quantum wire (T-wire) at a T-shaped intersection of two quantum wells (QWs) with a quality comparable to that of QWs. The T-wires allow precise control of wire cross-sectional size less than the Bohr radius of the exciton with small thickness fluctuations and hence exhibit confinement in the 1D quantum limit, which makes the systems ideal for studying 1D physics.[5,9,16–20] In 1994, Wegscheider *et al.*[6] reported low threshold currents of 0.4–0.8 mA at 4 K for multimode stimulated emission from 15-period T-wire laser diodes using a T-shaped current-injection scheme, i.e., current injection from the two perpendicular parent QWs. However, there has not yet been a quantitative or in-depth microscopic investigation of output powers, quantum efficiency, current injection, or recombination behaviors in T-wire-laser diodes.

In this article, we present quantitative laser performances together with a systematic study of electronic structure and carrier injection in low-threshold T-wire-laser diodes that use a new current injection scheme. This parallel injection scheme confined current in the thin overgrown single quantum well to reduce the threshold current and enhance injection efficiency. A threshold current of 0.27 mA and a differential quantum efficiency of 12% were achieved at 30 K from 500 μm long 20-period T-wire laser diodes with high-reflectivity (HR) Au coating on both cavity facets. Samples were also investigated by microscopic photoluminescence (PL) to determine the quantum state energy of each component and by microscopic electroluminescence (EL) imaging techniques to visualize carrier recombination positions at various current-injection levels and cryostat temperatures. These microscopic investigations were used to analyze the factors contributing to the high performances of the device at 30 K, as well as the reason for no lasing at temperatures below 30 K.

II. EXPERIMENT

A schematic cross section of the T-wire-laser structure is shown in Fig. 1(a). The structure was grown by the CEO method with MBE,[15] introducing a growth-interrupt-annealing technique during the overgrowth step.[21] We first grew, on a (001)-oriented n^+-GaAs substrate at 617 °C, a

[a]Electronic mail address: lsm@issp.u-tokyo.ac.jp

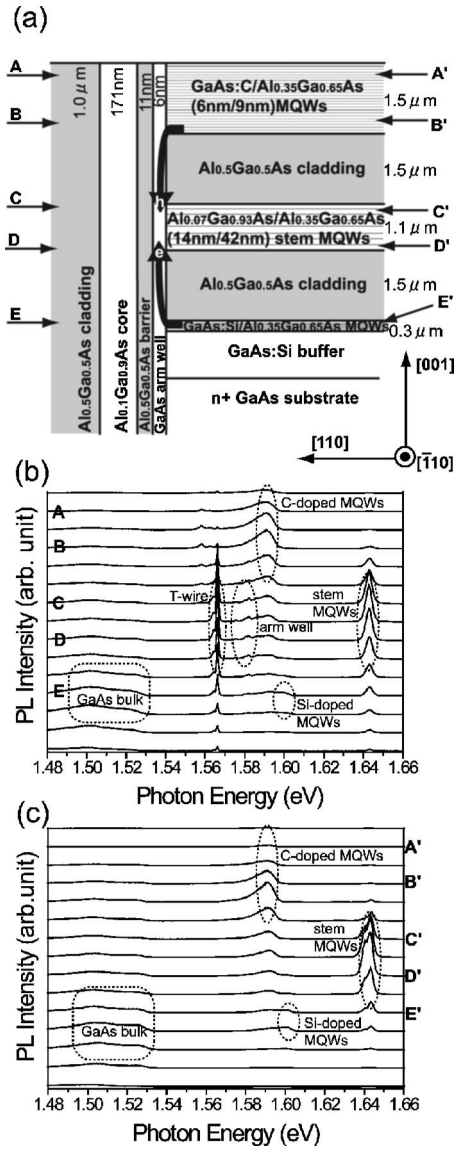

FIG. 1. (a) Schematic cross section of a T-wire laser structure, spatially resolved micro-PL spectra at 5 K when excitation light was irradiated on (b) the (110) surface and scanned along A to E and on (c) the (−110) surface and scanned along A' to E' with a step of 0.5 μm. The crude arrows in the structure indicate the carrier injection path.

1.0 μm n-type GaAs buffer layer, 20 periods of n-type GaAs(6 nm)/$Al_{0.35}Ga_{0.65}As$(9 nm) multiple-quantum-well (MQW) injection layer, a 1.5 μm cladding layer of 50% digital alloy $(GaAl)_4(AlAs)_4$, a MQW layer composed of 20 periods of 14 nm $Al_{0.07}Ga_{0.93}As$ QWs (stem wells) and 42 nm $Al_{0.35}Ga_{0.65}As$ barriers, a 1.5 μm cladding layer of 50% digital alloy $(GaAl)_4(AlAs)_4$, 100 periods of p-type GaAs(6 nm)/$Al_{0.35}Ga_{0.65}As$(9 nm) MQW injection layer, and a 10 nm p-type GaAs cap layer. Si and C were used as n- and p-type dopants, respectively. The nominal doping level in both p- and n-type injection layers was 1×10^{18} cm^{-3}.

The CEO was then performed on its *in situ* cleaved (110) edge to form a 6 nm GaAs QW (arm well) layer at the substrate temperature of 510 °C. After this arm-well growth, we interrupted the growth and annealed the sample under As_4-flux in the MBE chamber at 600 °C for 10 min and 650 °C for another 10 min.[21] Then, the substrate temperature

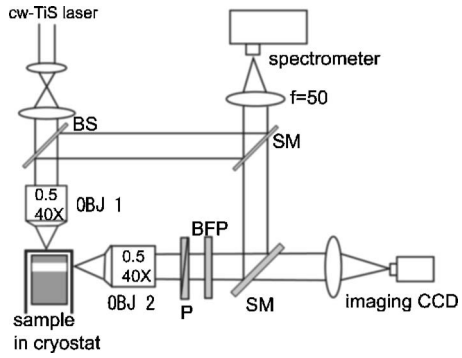

FIG. 2. Schematic layout for optical measurements. OBJ: objective lens; TiS: titanium sapphire; SM: switching mirror; BS: beam splitter; P: polarizer; and BPF: bandpass filter.

was reset to 510 °C, and an 11 nm $Al_{0.5}Ga_{0.5}As$ barrier layer, a 171 nm $Al_{0.1}Ga_{0.9}As$ core layer, a 1.0 μm cladding layer of 50% digital alloy $(GaAs)_6(AlAs)_6$, and a 10 nm GaAs cap layer were subsequently grown on the arm well.

After the MBE growth, the upper (001) layers were partially etched away so as to minimize leakage current. Evaporated metal films of 100 nm AuBe/200 nm Au were used for the p-type ohmic contact. After evaporation of these metal films, the wafer was annealed at 450 °C for 30 min for contact alloying. Laser bars with cavity length $L=500$ μm were cut from the wafer by cleavage, with the cleaved facets perpendicular to the axis of the quantum wires. The cavity mirror facets were left uncoated for micro-PL and EL imaging measurements. For lasing experiments, on the other hand, the cavity mirror facets were HR-coated with a 50 nm Au coating on the front and a 300 nm one on the rear after deposition of a 70 nm SiO_2 insulating layer by plasma-assisted chemical vapor deposition. The laser devices were attached p-type side up to copper blocks using silver-epoxy glue and set on the cold finger in a helium-flow-type cryostat.

In the previous current injection T-wire lasers,[6] electrons and holes were injected from the perpendicular arm well and stem well, respectively. In this work, we adopted two parallel p- and n-doped layers as shown in Fig. 1(a). Each doped layer was electrically isolated from the stem wells by an undoped $Al_{0.5}Ga_{0.5}As$ cladding layer. The two doped layers were connected only via the arm well. As a result, the injection current path was confined in the thin 6 nm arm well as shown by the crude arrows during laser operation, which avoided carrier losses in the totally 1.1 μm thick stem MQW and thus contributed to the low threshold current and high efficiency.

The experimental setup for the optical measurements is shown in Fig. 2. Microscopic PL measurements were performed with excitation light having photon energy of 1.67 eV from a cw titanium-sapphire laser in a backward-scattering geometry. The laser beam was focused onto a 0.8 μm spot using a 0.5 numerical aperture (NA)×40 objective lens (OBJ 1). PL emission was collected by this same objective lens, dispersed in a 0.75 m spectrometer, and recorded using a liquid-nitrogen-cooled charge-coupled-device (CCD) for spectroscopy. Spatial scans were made by moving the sample using an $x-y$ translation stage with a step size of 0.5 μm.

For the measurements of EL and lasing, the laser diode was driven by a dc-voltage-current source-monitor unit (Advantest R6240A) and studied in cw operation mode. EL emission from the front cavity facet along the [1–10] direction was collected by objective lens 2 (OBJ 2: ×40, NA: 0.5) and directed by a switching mirror to either an electrically cooled CCD camera for microscopic EL imaging measurements with spatial resolution of 0.8 μm or to the spectrometer for spectroscopy. In the microscopic EL imaging measurements, both spectrally integrated global images and spectrally resolved images were measured without and with bandpass filters being inserted, respectively. A Si photodiode power meter was inserted right next to the laser device to measure the output power.

III. RESULTS

A. Micro-photoluminescence spectra

To determine the electronic structure or the recombination energy of carriers in each constituent part of the complicated T-wire-laser-diode structure, we measured micro-PL spectra of an uncoated sample. Figure 1(b) shows the micro-PL spectra when excitation light with a 0.8 μm spot irradiated the overgrown (110) surface and scanned the entire 7 μm thickness along the [001] direction with a step of 0.5 μm. Letters *A* to *E* indicate the irradiated positions on the sample. At positions *C* and *D* around the T-wire region of the sample, the peaks at 1.566 and 1.644 eV were ascribed to 1D excitons in the T-wires and 2D excitons in the stem wells, respectively.[22] The very small peaks around 1.582 eV between these two strong peaks correspond to 2D excitons in the arm well on the 44 nm thick barrier layers separating the stem wells. The energy difference between PL from T-wires and the arm well was about 16 meV, corresponding to the confinement energy of 1D excitons. The full width at half maximum (FWHM) of the dominant 1D exciton peak was about 0.9 meV with spectral resolution of 0.2 meV. The small satellite PL peak 2.3 meV below the dominant PL peak of the T-wires resulted from lower-energy 1D excitons due to the thickness fluctuation of the overgrown arm well by a single monolayer.[20,21] The sharp PL of T-wires with a very small satellite peak demonstrates the high interface quality of the T-wires.

At positions *A* and *B* above the T-wire region, a broad PL band centered at 1.591 eV arising from the C-doped *p*-type MQWs dominates the spectrum. At position *E* below the T-wires, a very weak PL band centered at 1.600 eV from the Si-doped *n*-type MQWs is visible. The PL intensity of the 0.3 μm thick *n*-type MQW region is rather lower than that of the 1.5 μm thick *p*-type MQW region due to the smaller volume.

To confirm the above peak assignments, we also measured the PL spectra shown in Fig. 1(c) by irradiating the (−110) surface and scanning along the [001] direction with a step of 0.5 μm. The irradiated positions from A' to E' were kept far from the arm well, so no PL came from the overgrown layers. Comparing Figs. 1(b) and 1(c), one can clearly see that the emissions from the stem and from the *p*- and *n*-type MQWs are at the same energies and positions in both spectra. Therefore, the narrow peaks at 1.566 eV that appear only in Fig. 1(b) were assigned to the 1D T-wire emissions without any doubt. By using this spectrally and spatially resolved micro-PL technique, we could clearly identify each quantum state in the complicated T-wire-laser structure, which establishes the basis for further investigation of current-injection lasers.

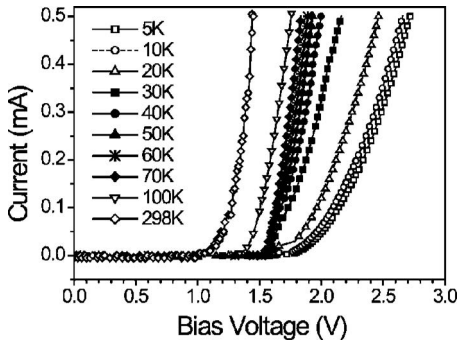

FIG. 3. Current-voltage characteristics at forward bias at temperatures from 5 K to room temperature.

B. Laser-diode current-voltage characteristics

Forward current-voltage ($I-V$) curves measured on an HR-Au-coated laser sample over temperatures ranging from 5 to 300 K are plotted in Fig. 3. The turn-on voltages between 30 and 70 K was essentially similar, around 1.6 V, which is close to the built-in potential of about 1.59 V between *p*- and *n*-type MQW layers estimated from the PL energies of 1.591 and 1.600 eV, respectively. Furthermore, the exponential nature of the $I-V$ curve at low bias voltages between 30 and 70 K is well explained in terms of the ideal diode equation for a $p-n$ junction, while at temperatures below 30 K, the current increased rather slowly with voltage. At high bias voltages, the diode current was basically limited by series resistance associated with the *p*- and *n*-doped layers. The series resistance obtained from linear fitting of the $I-V$ curve at high bias voltage[23] was about 1000 Ω at 5 K, about 500 Ω between 30 and 70 K, and about 200 Ω near room temperature. The slow turn-on behavior and high series resistance of the sample at temperatures below 30 K will be discussed below.

C. EL and single-mode lasing spectra

Figure 4 shows high-resolution EL and lasing emission spectra of the 500 μm long HR-Au-coated laser diode at 30 and 5 K in cw TE modes whose polarization direction is parallel to the arm well under various driving currents. The emissions in the spectra were from T-wires and had photon energy slightly below the T-wire PL energy of 1.566 eV.

At 30 K, EL from the T-wire showed clear Fabry-Perot (FP) longitudinal modes in the low-energy region below the current of 0.25 mA, and the FP modulation depth increased with increasing current. At and above the current of 0.31 mA, a narrow peak (<0.1 meV FWHM, limited by the spectral resolution of the detection system) developed at 1.555 eV in the center of the envelope of the longitudinal-mode spectrum, indicating single-mode lasing of the T-wire laser.

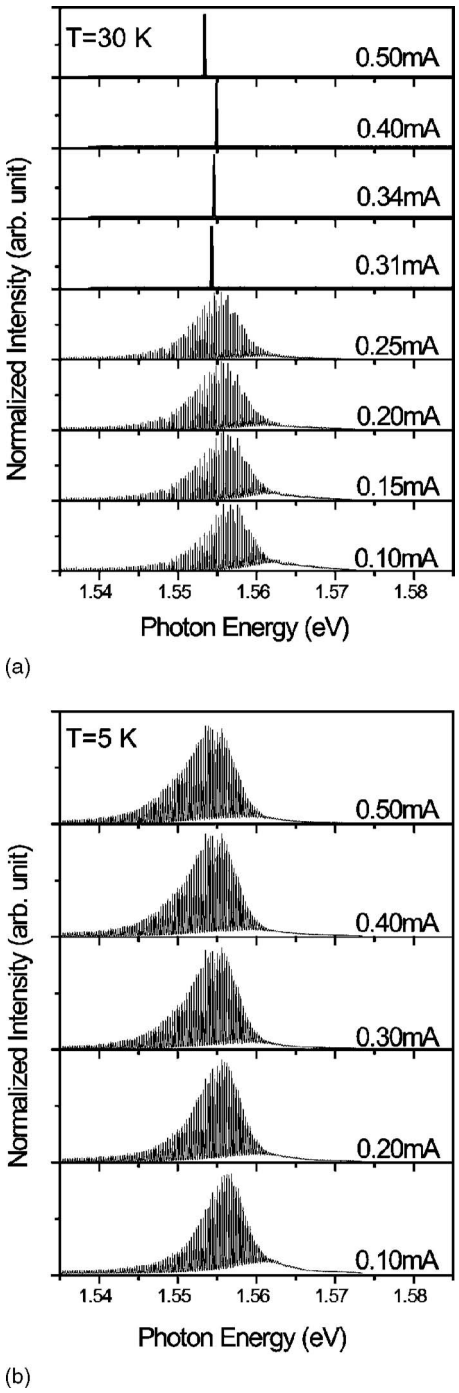

FIG. 4. High-resolution EL and lasing spectra in cw TE modes from a 500 μm long HR-Au-coated T-wire-laser diode at (a) 30 K and (b) 5 K.

Small mode hopping of the single lasing mode was observed above the threshold. Similar single-mode lasing was observed at temperatures between 30 and 70 K.

At 5 K, the EL spectra showed also the FP longitude modes but the modulation depth showed only a small increase as the current increased. The EL never switched to single-mode lasing. These observations suggest a small increase in optical gain with increasing current. The envelope peak of the modulated emission shifted about 3 meV to low energy when the current was increased from 0.1 to 0.5 mA. This redshift may be due to quantum-confined Stark effects[24] induced by the high forward bias voltage of 2.6 V and band-gap renormalization effects. At all temperatures between 5 and 100 K, no EL emission from the stem wells were observed. This indicates that no carriers were injected into the stem wells, or that all the injection current was confined in the injection path along the arm well.

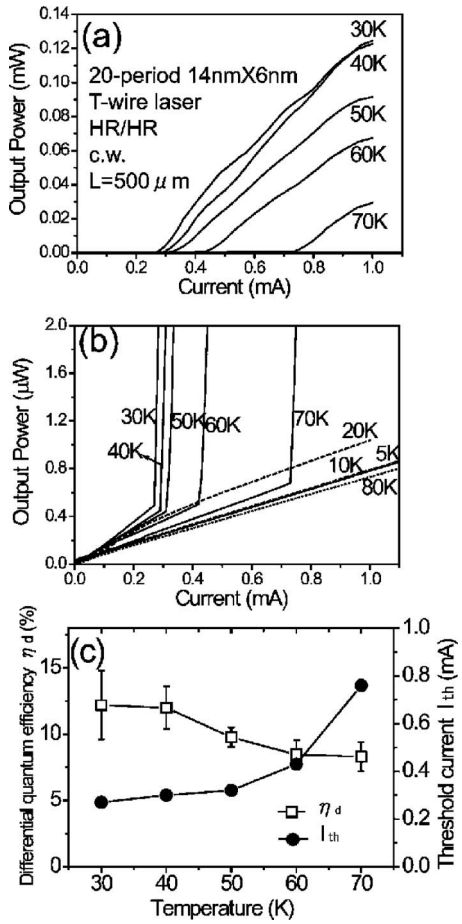

FIG. 5. Light output power vs injection current in cw TE modes from a 500 μm long HR-Au-coated T-wire-laser diode at cryostat temperatures (a) between 30 and 70 K and (b) from 5 to 80 K and (c) temperature dependence of threshold current (I_{th}) and external differential quantum efficiency (η_d).

D. Laser output power, threshold current, and differential quantum efficiency

Figure 5(a) shows the cw light output versus injection current ($I-L$) characteristics of the T-wire-laser diode with HR Au coatings at various cryostat temperatures between 30 and 70 K. There are threshold currents in the $I-L$ curves, above which the increase in output intensity became steep against the increase in injection current. Comparing with Fig. 4, one can see that the single-mode lasing started just above the threshold currents in the $I-L$ curves. The lowest threshold current was 0.27 mA at 30 K. Output power of 0.12 mW was obtained for injection current of 1 mA at 30–40 K.

Figure 5(b) shows $I-L$ curves with a magnified vertical scale of the microwatt order over a wider temperature range from 5 to 80 K. There is no turning point on $I-L$ curves below 30 K or above 70 K. The emission intensity increased

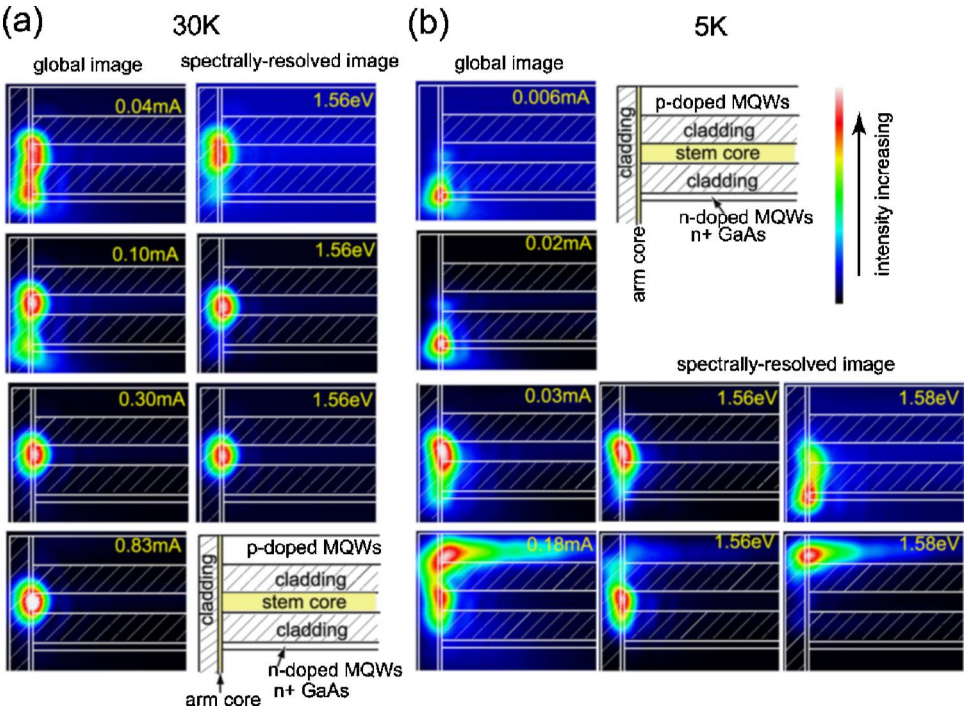

FIG. 6. (Color online) Images of EL emission patterns of uncoated T-wire-laser diode at (a) 30 K and (b) 5 K with increasing current injection. Injection current is denoted on each global image and bandpass photon energy is denoted on each spectrally resolved image. Inset shows the schematic structure of the sample. White lines superimposed on each image denote the sample structure; hatching shows T-shaped optical waveguide surrounded by three $Al_{0.5}Ga_{0.5}As$ cladding layers.

linearly for small injection currents. The slopes became larger from 5 to 30 K, peaked at 30 K, and became smaller from 30 to 80 K.

Figure 5(c) plots the threshold currents (I_{th}) and the external differential quantum efficiency (η_d) of the laser emission obtained from the slopes of $I-L$ curves above the thresholds as functions of temperature. The threshold current under cw operation increased from 0.27 to 0.73 mA, while the external differential quantum efficiency decreased from 12% to 8% when the cryostat temperature was increased from 30 to 70 K. The quantitative laser-performance values are analyzed in Sec. IV below.

E. Temperature and current-dependent EL images

Figure 6 shows microscopic EL images of a laser diode without HR coatings at various injection currents at (a) 30 K and (b) 5 K. The injection current is denoted on each global image and the bandpass photon energy is denoted on each spectrally resolved image. The contour colors in these images correspond to the normalized EL emission intensity shown in the color bar. The inset shows a schematic of the sample structure. White lines are also superimposed on each image to denote the sample structure to guide the reader's eyes with a spatial uncertainty of about 0.2 μm, where the hatching shows three $Al_{0.5}Ga_{0.5}As$ cladding layers surrounding the T-shaped optical waveguide.

The common feature of the EL images at both temperatures is that no emission was observed from stem wells at any of the current injection levels investigated here. This again demonstrates that carriers were completely blocked by the high-band-gap cladding layers and were not injected into the stem wells, as expected in this current-injection scheme.

In Fig. 6(a) for 30 K, at a low current of 0.04 mA, emission was observed from both the T-wire active region and the arm well that intersected the *n*-doped MQW layer (*n*-intersection). This suggests that some electrons were trapped at a potential well formed at the *n*-intersection, and others were injected into T-wires. The corresponding spectrum shows two peaks at 1.560 and 1.581 eV. The insertion of a 1.560 eV bandpass filter enabled us to see that the emission at 1.560 eV was from the T-wire region, which is consistent with the PL spectra in Fig. 1(b). As the current was increased, the emission intensity in the T-wire region increased and it dominated the image at currents above 0.30 mA. This indicates that, under an applied bias current near to and above 0.30 mA, almost all carriers were efficiently injected into the T-wire region and recombined there. Similar EL images showing efficient current injection and confinement were observed up to 100 K.

However, EL images at (b) 5 K were very different from those at 30 K. For a low injection current from 0.006 to 0.02 mA, EL from the *n*-intersection dominates the image, indicating most electrons were trapped in *n*-intersection at low bias current. Then, at a current of 0.03 mA, EL from the T-wire region became stronger and dominated the image, while weak EL from the *n*-intersection was still visible. This is similar to the case for 0.10 mA at 30 K, i.e., some electrons were still trapped in the *n*-intersection while others were injected into the T-wire active region. When the current was increased to 0.18 mA, the image is distinguished by the strong EL from the *p*-doped MQW layer, which indicates that many electrons passed through the T-wire region and recombined with the majority holes in *p*-type MQWs. This is probably because holes in the *p*-type MQWs are mostly frozen and cannot move as freely as electrons at very low temperatures. Thus, a high bias voltage or electric field is needed to make a current flow, which is in agreement with the high series resistance at 5 K. The significant consumption of electrons in the *p*-doped layer resulted in an insufficient carrier population for inversion in the T-wire active region. No las-

ing can be achieved at 5 K. Similar EL emission from *p*-doped layer was observed at several temperatures below 30 K.

IV. DISCUSSION

Efficient carrier injection into the T-wires at 30 K and inefficient injection at 5 K were visualized by the EL images in Fig. 6. These are consistent with the differences in laser-diode characteristics at 30 and 5 K observed in Figs. 3–5, which are a low lasing threshold, high differential quantum efficiency, and typical diode $I-V$ characteristics at 30 K, in contrast to no lasing, slow turn-on behavior of EL intensity, and high series resistance in $I-V$ characteristics at 5 K.

For more quantitative analysis on the performances of the HR-coated laser, which had a 50 nm (300 nm) thick Au coating on the 70 nm thick SiO_2 dielectric film at the front (rear) facet, we estimated the probabilities of reflection $R_1(R_2)$, transmission $T_1(T_2)$, and absorption $A_1(A_2)$ as 96.8%(98.1%), 1.0%(0%), and 2.2%(1.9%), respectively, by using the material parameters in Ref. 25. Thanks to these HR mirrors, the mirror loss $\alpha_m=(\ln R_1R_2)/2L=0.52$ cm^{-1} was very small in the 500 μm long laser diodes. Therefore, the threshold currents in the present experiment were predominantly determined by transparency currents.

The lowest threshold current of 0.27 mA at 30 K for 20 periods of 500 μm long T-wires represents 14 μA per 500 μm long single wire. The prediction by Yariv[3] on the ultralow threshold current of 2–3 μA in a single-quantum-wire laser is based on 1D transparency current of 0.6 μA estimated for cavity length $L=100$ μm, temperature $T=300$ K, and carrier lifetime $\tau=4$ ns, where the transparency current is proportional to $T^{1/2}L/\tau$. In our present experiment for the case of $T=30$ K, $L=500$ μm, and $\tau=0.4$ ns, an estimated transparency current is about 10 μA. The threshold-current value of 14 μA per single T-wire obtained in our experiment is comparable to this theoretical transparency current.

A formula[26] for the external differential quantum efficiency (η_d) of a typical laser without mirror absorption ($A_1=A_2=0$) is given by $\eta_d=\eta_i[\alpha_m/(\alpha_m+\alpha_i)]$, where η_i is the internal quantum efficiency, α_i is the internal absorption loss inside the cavity, and α_m is the mirror loss. If we make a simple insertion of $R_{1(2)}=1-T_{1(2)}-A_{1(2)}$ for finite $A_{1(2)}$ and approximation for $1-R_{1(2)}\ll 1$, the right-hand term of the formula is transformed to $\eta_i[(T_1+T_2+A_1+A_2)/(T_1+T_2+A_1+A_2+2\alpha_iL)]$. Therein, however, the A_1+A_2 term in the numerator shows the yield of photons absorbed in the mirrors, and only the T_1+T_2 term in the numerator shows the yield of output photons. Therefore, the external differential quantum efficiency η_d of our laser device with absorptions A_1 and A_2 in Au-coated mirrors is expressed as $\eta_d=\eta_i$, $\eta_d=\eta_i[(T_1+T_2)/(T_1+T_2+A_1+A_2+2\alpha_iL)]$. If we assume internal quantum efficiency $\eta_i=1$ on the basis of the high injection efficiency at 30 K seen in Fig. 6(a), then the measured differential quantum efficiency $\eta_d=12\%$ at 30 K and the above-calculated mirror parameters predict a very small internal loss $\alpha_i=0.32$ cm^{-1} or $\alpha_iL=0.02$. In this structure, free-carrier absorption and scattering are minimized because there are no dopants in the waveguide, and because all hetero-interfaces are formed by MBE growth and cleavage and have very high flatness with atomic-layer precision. This is the most likely reason for the very small value of the estimated internal loss.

If we make an alternative calculation assuming the ideal condition with $\eta_i=1$ and $\alpha_i=0$, we can estimate the maximum η_d with the same HR-Au-coated cavity to be 20%. Thus, the measured external differential quantum efficiency of 12% is a very high value, close to the maximum value possible using Au HR mirrors.

In the above estimations of the internal loss α_i and the maximum η_d, errors come mainly from calculated values of T_1, T_2, A_1, and A_2. Indeed, the thin metal evaporation of 50 and 300 nm thick Au on the 70 nm thick SiO_2 deposition may not form ideally uniform and smooth thin layers assumed in the calculation, which makes estimation of errors hardly possible. For more reliable estimation of the internal loss α_i, dielectric HR coatings with negligible mirror absorption or measurements of cavity-length dependence should be necessary, though they are technically not possible for now. The dielectric HR coatings, in addition, should improve the differential efficiency of T-wire lasers significantly.

We finally note the two main factors contributing to the low threshold current and high quantum efficiency for the single-mode lasing in the present T-wire-laser diodes. One is the excellent structural and morphological quality and the other is the efficient current injection. The narrow PL linewidth indicated a uniform morphology of the T-wire active region. The absence of EL from the stem wells indicated that the nondoped $Al_{0.5}Ga_{0.5}As$ cladding layers suppressed carrier injection into the stem wells, which otherwise would have increased the threshold current due to the large volume of the stem MQW. The small confinement energy of 16 meV prevents lasing of the device at high temperatures. At very low temperatures lasing cannot be achieved at present possibly due to hole freezing in the C-doped *p*-type MQW. To obtain enough hole mobility even at 5 K, modulation doping of the MQW will be helpful. That should lead to lasing from the T-wire active region at lower threshold currents and further basic laser-performance study over a wider temperature range should be possible, which will be useful for systematically comparing experimental data with theories.

V. CONCLUSION

In conclusion, we fabricated high-quality quantum-wire-laser diodes based on 20-period 14×6 nm T-wires by the CEO method with MBE and measured their micro-PL spectra, quantitative laser performances, and micro-EL images. We found that at 30–70 K, the forward-bias current injected from the parallel *p*- and *n*-type MQW layers was very well confined in the thin overgrown arm-well channel and injected into the T-wires efficiently, which leads to single-mode lasing. A low threshold current of 0.27 mA and a reasonably high differential quantum efficiency of 12% for single-mode lasing were achieved at 30 K from 500 μm long 20-period T-wire-laser diodes with HR Au

coating on both cavity facets. At temperatures below 30 K, on the other hand, no lasing was observed due to inefficient carrier injection into the active region.

ACKNOWLEDGMENT

This work was partly supported by a Grant-in-Aid from the Ministry of Education, Science, Sports, and Culture of Japan.

[1]Y. Arakawa and H. Sakaki, Appl. Phys. Lett. **40**, 939 (1982).
[2]M. Asada, Y. Miyamoto, and Y. Suematsu, Jpn. J. Appl. Phys., Part 1 **24**, L95 (1985); IEEE J. Quantum Electron. **QE-22**, 1915 (1986).
[3]A. Yariv, Appl. Phys. Lett. **53**, 1033 (1988).
[4]E. Kapon, D. M. Hwang, and R. Bhat, Phys. Rev. Lett. **63**, 430 (1989); S. Simhony, E. Kapon, E. Colas, D. M. Huang, N. G. Stoffel, and P. Worland, Appl. Phys. Lett. **59**, 2225 (1991).
[5]W. Wegscheider, L. N. Pfeiffer, M. M. Dignam, A. Pinczuk, K. W. West, S. L. McCall, and R. Hull, Phys. Rev. Lett. **71**, 4071 (1993).
[6]W. Wegscheider, L. Pfeiffer, K. West, and R. E. Leibenguth, Appl. Phys. Lett. **65**, 2510 (1994).
[7]S. Tiwari, G. D. Pettit, K. R. Milkove, F. Legoues, R. J. Davis, and J. M. Woodall, Appl. Phys. Lett. **64**, 3536 (1994).
[8]S. Hara, J. Motohisa, and T. Fukui, Electron. Lett. **34**, 894 (1998).
[9]Y. Hayamizu, M. Yoshita, S. Watanabe, H. Akiyama, L. N. Pfeiffer, and K. W. West, Appl. Phys. Lett. **81**, 4937 (2002).
[10]T. G. Kim and M. Ogura, Jpn. J. Appl. Phys., Part 1 **42**, 4162 (2003).
[11]H. Hino, A. Shigenobu, K. Ohmori, T. Kitada, S. Shimomura, and S. Hiyamizu, J. Vac. Sci. Technol. B **23**, 2526 (2005).
[12]H. Yagi, K. Miura, Y. Nishimoto, D. Plumwongrot, K. Ohira, T. Maruyama, and S. Arai, Appl. Phys. Lett. **87**, 223120 (2005).
[13]B. Zhao, T. R. Chen, L. E. Eng, Y. H. Zhuang, A. Shakouri, and A. Yariv, Appl. Phys. Lett. **65**, 1805 (1994).
[14]S. H. Groves, J. N. Walpole, and L. J. Missaggia, Appl. Phys. Lett. **61**, 255 (1992).
[15]L. N. Pfeiffer, K. W. West, H. L. Stormer, J. P. Eisenstein, K. W. Baldwin, D. Gershoni, and J. Spector, Appl. Phys. Lett. **56**, 1697 (1990).
[16]A. R. Goni, L. N. Pfeiffer, K. W. West, A. Pinczuk, H. U. Baranger, and H. L. Stormer, Appl. Phys. Lett. **61**, 1956 (1992).
[17]W. Langbein, H. Gislason, and J. M. Hvam, Phys. Rev. B **54**, 14595 (1996).
[18]J. Hasen, L. N. Pfeiffer, A. Pinczuk, S. He, K. W. West, and B. S. Dennis, Nature **390**, 54 (1997).
[19]T. Someya, H. Akiyama, and H. Sakaki, Phys. Rev. Lett. **74**, 3664 (1995); Phys. Rev. Lett. **76**, 2965 (1996); H. Akiyama, T. Someya, and H. Sakaki, Phys. Rev. B **53**, R16160 (1996); H. Akiyama, T. Someya, M. Yoshita, T. Sasaki, and H. Sakaki, *ibid.* **57**, 3765 (1998); H. Akiyama, J. Phys.: Condens. Matter **10**, 3095 (1998).
[20]H. Akiyama, L. N. Pfeiffer, M. Yoshita, A. Pinczuk, P. B. Littlewood, K. W. West, M. J. Matthews, and J. Wynn, Phys. Rev. B **67**, 041302 (2003); H. Akiyama, M. Yoshita, L. N. Pfeiffer, and K. W. West, J. Phys.: Condens. Matter **16**, S3549 (2004).
[21]M. Yoshita, H. Akiyama, L. N. Pfeiffer, and K. W. West, Jpn. J. Appl. Phys., Part 1 **40**, L252 (2001); Appl. Phys. Lett. **81**, 49 (2002).
[22]M. Yoshita, H. Akiyama, T. Someya, and H. Sakaki, J. Appl. Phys. **83**, 3777 (1998).
[23]K. D. Choquette, W. W. Chow, M. H. Crawford, K. M. Geib, and R. P. Schneider, Jr., Appl. Phys. Lett. **68**, 3689 (1996).
[24]N. Le Thomas, N. T. Pekekanos, A. Hatzopoulos, and E. Aperathitis, Appl. Phys. Lett. **81**, 1582 (2002).
[25]K.-H. Hellwege and J. L. Olsen, "Metals: Electronic Transport Phenomena," in *Landolt-Bornstein Numerical Data and Relationships in Science and Technology, New Series* (Springer, Berlin, 1985), Group III, Vol. 15b.
[26]L. A. Coldren and S. W. Corzine, *Diode Lasers and Photonic Integrated Circuits* (Wiley, New York, 1995), p. 42.

Temperature-dependent current injection and lasing in T-shaped quantum-wire laser diodes with perpendicular *p*- and *n*-doping layers

Makoto Okano,[a] Shu-man Liu, Toshiyuki Ihara, Hirotake Itoh, Masahiro Yoshita,[b] and Hidefumi Akiyama[b]
Institute for Solid State Physics, University of Tokyo, and CREST, JST, 5-1-5 Kashiwanoha, Kashiwa, Chiba 277-8581, Japan

Loren N. Pfeiffer, Kenneth West, and Oana Malis
Bell Laboratories, Lucent Technologies, 600 Mountain Avenue, Murray Hill, New Jersey 07974

(Received 10 January 2007; accepted 22 January 2007; published online 1 March 2007)

The authors measured the temperature dependence of the lasing properties of current-injection T-shaped GaAs/AlGaAs quantum-wire (T-wire) lasers with perpendicular *p*- and *n*-doping layers. The T-wire lasers with high-reflectivity coatings on both cleaved facets achieved continuous-wave single-mode operation between 5 and 110 K. The lowest threshold current was 2.1 mA at 100 K. The temperature dependences of differential quantum efficiency and threshold current were attributed mainly to that of current-injection efficiency. © *2007 American Institute of Physics*. [DOI: 10.1063/1.2709521]

The physics and device performances of semiconductor lasers based on one-dimensional quantum wires have attracted intensive interest for a few decades.[1–5] For applied physics study, cleaved-edge-overgrowth[6,7] T-shaped quantum-wire (T-wire) lasers[8–10] have unique advantages such as high controllability, high uniformity, and high crystal quality free from damage, impurity, or defects. The T-wire lasers have particular flexibility in doping and current injection. In fact, an interesting unique injection scheme into T wires via T-shaped perpendicular *p*- and *n*-doping layers was demonstrated, where carriers were injected via two intersecting modulation-doped quantum wells in *p* and *n* types.[9] This scheme achieved current-injection multimode lasing with a threshold of 0.4–0.8 mA at 4.2 K in 15-arrayed 7 nm $\times$7 nm T-wire lasers, though key characteristics such as quantitative optical power, efficiency, and lasing at higher temperatures have not been reported.[9]

In this work, we report the temperature dependence of quantitative characteristics in a current injection T-wire laser based on the same current-injection scheme as in the previous study.[9] To achieve lasing over a wide temperature range, we chose to use a 15-arrayed 14 nm$\times$6 nm T-wire laser with deeper confinement than the previous structure.[9] We observed single-mode lasing between 5 and 110 K, which is the highest lasing temperature reported for T-wire lasers. Optimum differential quantum efficiency (0.9%) and threshold current (2.1 mA) were obtained at 100 K. The optimized performance at the elevated temperature suggests that *p*- and *n*-type carrier injection is not centered but displaced from the T-wire active region.

Figure 1 shows the schematic structure of the current-injection T-wire laser with 15 T wires formed at the T-shaped intersections of 15-period (001) $Al_{0.07}Ga_{0.93}As$ multiple quantum wells (MQWs) denoted as stem wells and a (110) GaAs quantum well denoted as an arm well. The thicknesses of stem and arm wells are 14 and 6 nm, respectively. In the first molecular beam epitaxy growth on a (001) nondoped GaAs substrate, we successively formed a 0.3 μm GaAs buffer layer, a 1.5 μm $Al_{0.50}Ga_{0.50}As$ side cladding layer, a 15-period $Al_{0.07}Ga_{0.93}As/Al_{0.35}Ga_{0.65}As$ MQW structure with barrier and quantum well thicknesses of 58 and 14 nm, a 1.5 μm $Al_{0.50}Ga_{0.50}As$ side cladding layer, a cap layer of 1.5 μm $Al_{0.3}Ga_{0.7}As$, and 10 nm GaAs. All layers were undoped except for the $Al_{0.35}Ga_{0.65}As$ barrier. Carbon was delta doped (2×10^{11} cm^{-2}) at a 10 nm off-center position with respect to each barrier to compensate for segregation. On an *in situ* cleaved (110) surface of the wafer, we overgrew a 6 nm GaAs quantum well (undoped) followed by a 10 nm $Al_{0.50}Ga_{0.50}As$ barrier (undoped), a 40 nm $Al_{0.14}Ga_{0.86}As$ setback layer, a delta doping of Si (4×10^{11} cm^{-2}), a 120 nm lightly doped $Al_{0.14}Ga_{0.86}As$ layer, a 180 nm lightly doped $Al_{0.50}Ga_{0.50}As$ upper cladding layer, a 700 nm heavily doped $Al_{0.50}Ga_{0.50}As$ upper cladding layer, and a 10 nm heavily

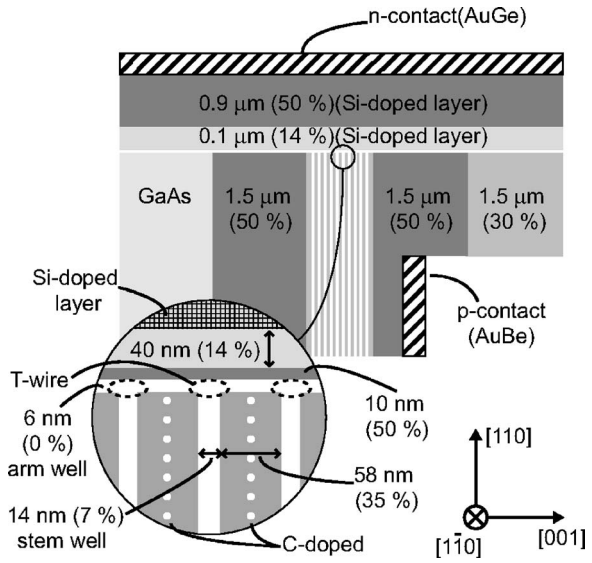

FIG. 1. Schematic structure of current-injection T-wire lasers. T wires are formed at the intersections of two quantum wells, as shown in the magnified drawing. Percentages in parentheses represent Al content x of $Al_xGa_{1-x}As$.

[a]Electronic mail: m-okano@issp.u-tokyo.ac.jp
[b]Also at Bell Laboratories, Lucent Technologies, 600 Mountain Avenue, Murray Hill, NJ 07974.

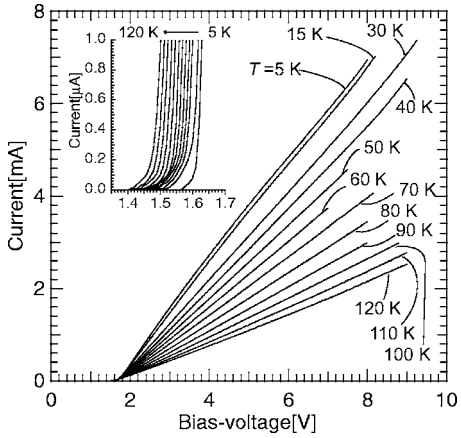

FIG. 2. Current vs bias-voltage characteristics of a T-wire laser at various temperatures between 5 and 120 K. The inset shows an enlarged view of the vicinity of the threshold voltages. Leakage currents were less than 10 nA at all the temperatures.

doped GaAs cap layer. The doping levels of Si in the lightly and heavily doped layers were 4×10^{17} and 2×10^{18} cm^{-3}, respectively.

To make contact with the *p*-doped MQW, parts of the side cladding layer on the cap side and the cap layer were etched away using H_2SO_4 solution, as shown in Fig. 1. After etching, *p*- and *n*-type metals (200 nm $Au_{0.82}Be_{0.18}$/100 nm Au and 100 nm $Au_{0.73}Ge_{0.27}$/50 nm Au) for electrodes were evaporated, as shown in Fig. 1. The distance between the T wires and the *p*-type electrode was about 500 μm. After the evaporation, the sample was annealed in Ar atmosphere in a furnace at 450 °C for 30 min to make Ohmic contacts. The sample was then cleaved to form an optical cavity bounded by mirrors perpendicular to the axis of the T wires. The cavity length was 500 μm. The cavity facets were coated with Au layers for high reflectivity after the deposition of 70 nm SiO_2 by plasma-assisted chemical vapor deposition for insulation. The thicknesses of Au layers were 50 nm on the detected side and 300 nm on the other side. The reflectivity *R* values were about 0.97 and 0.98. The T-wire laser diode was mounted on the cold finger in a He-flow-type cryostat. The laser diode was driven by a dc-voltage/current source and measured during continuous-wave operation. For the measurement of lasing characteristics, the light emission spectrum from the laser diode was detected with a cooled charge-coupled-device detector via a monochromator, and optical power from the laser was detected with a Si photodiode.

The temperature dependence of the current-voltage characteristics (*I-V* curve) from 5 to 120 K is shown in Fig. 2. The inset, which is a magnified view of the region around the threshold voltage (V_{th}), indicates that V_{th} was 1.4–1.56 eV in this measurement temperature range, and that the leakage current below V_{th} was less than 10 nA. The trend of the decrease in V_{th} with increasing temperature corresponds approximately to the temperature dependence of the band gap of GaAs. Above V_{th}, as the temperature increased, the resistance of the sample increased. The changes in resistance are consistent with the temperature-dependent changes in the mobility of holes in the stem wells, measured on the same original wafer by using the van der Pauw method. This obviously shows that the stem wells are the main source of series resistance.

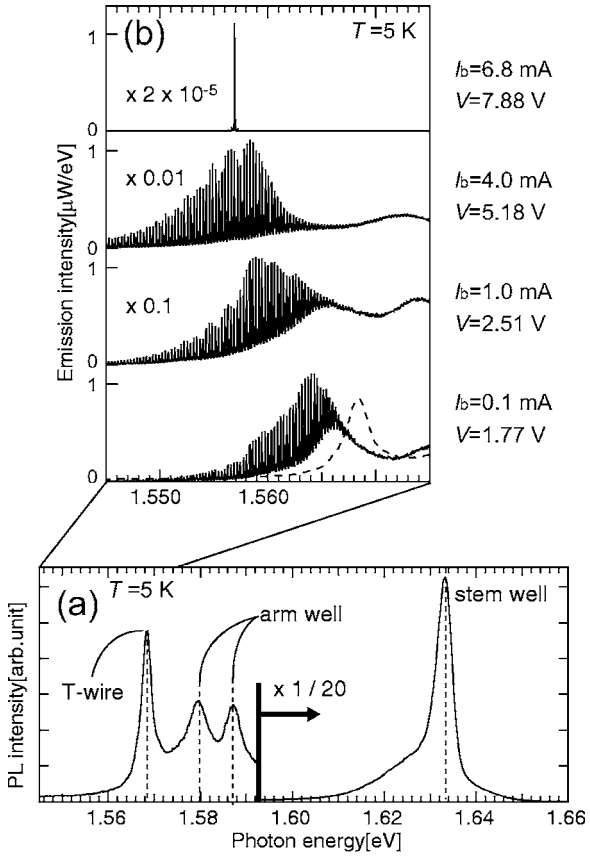

FIG. 3. (a) Photoluminescence spectrum at 5 K, where emissions from the T wires, the arm wells, and the stem wells were observed. (b) Electroluminescence spectra of a T-wire laser from the cavity edge for various bias currents at 5 K. Continuous-wave single-mode lasing above I_{th}=6.5 mA was observed at 1.557 eV. The dashed line in the bottom panel shows the T-wire peak in the photoluminescence spectrum at 5 K shown in (a).

A photoluminescence (PL) spectrum versus photon energy at 5 K is shown in Fig. 3(a). This spectrum has four emission peaks at 1.633, 1.587, 1.580, and 1.568 eV. These emissions were assigned by micro-PL measurements to the stem wells, the arm well on the side cladding layer, the arm well on the cap layer, and the T wires, respectively. Figure 3(b) shows electroluminescence (EL) spectra from the cavity edge versus photon energy at 5 K for various values of bias current (I_b). Fabry-Pérot oscillation can be observed in these spectra. In the bottom EL spectrum in Fig. 3(b) (I_b =0.1 mA), the emission peak at 1.564 eV was assigned to the *T* wires by separate EL imaging measurements; it is slightly redshifted from the PL peak of the T wires (dashed line). With increasing bias current, the emission peak from T wire showed an increasing gradual redshift. This redshift was most likely caused by band gap renormalization and by the quantum confined Stark effect. Above threshold current I_{th} =6.5 mA, EL of the T wires turned into single-mode lasing (top spectrum at I_b=6.8 mA). At other temperatures, the evolution characteristics of the T-wire emission with increasing current were almost the same.

The temperature dependence of the optical power versus bias current (*L-I* curve) between 5 and 120 K is shown in Fig. 4(a). The inset shows some curves at high temperatures between I_b=2.0 and 4.0 mA. At 100 K, we observed the lowest threshold current I_{th}=2.1 mA. The slope of each *L-I* curve above the threshold current shows differential quantum efficiency η_d of photons in laser emission versus electrons in

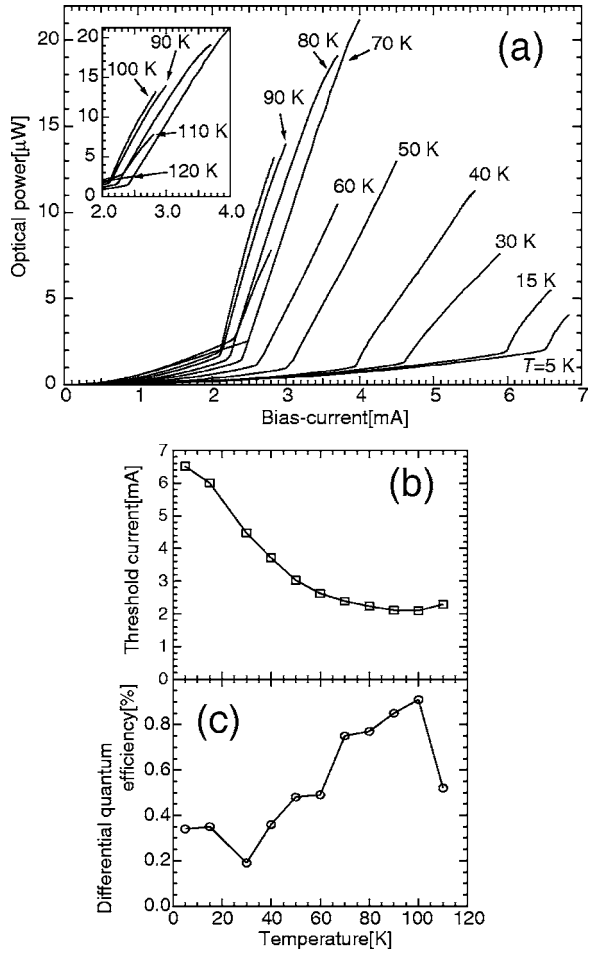

FIG. 4. Optical power vs current characteristics at various temperatures. The inset shows several curves at 90–120 K near the threshold currents. At 120 K, the sample did not show lasing. (b) Threshold current and (c) differential quantum efficiency plotted against temperature.

injection current. As the temperature increased from 5 to 100 K, the differential quantum efficiency η_d became larger and the threshold current I_{th} became lower. Figures 4(b) and 4(c) show the temperature dependences of I_{th} and η_d, respectively; they were derived from the *L-I* curves in Fig. 4(a). These plots show that η_d and I_{th} improved with increasing temperature up to 100 K. The optimum values of η_d and I_{th} achieved at 100 K were 0.9% and 2.1 mA, respectively. Lasing still occurred at 110 K though η_d and I_{th} were degraded. Note that this experiment demonstrates the highest operating temperature among all current-injection T-wire lasers.[9,11] The sample stopped lasing at 120 K, which is similar to the operating-temperature limit of nondoped T-wire lasers in separate optical pumping studies.

In current-injection T-wire lasers of a different type with parallel *p*- and *n*-doping layers and 20 T wires, the best values of η_d=12% and I_{th}=0.3 mA were achieved, though the highest operating temperature was 70 K.[11] Therefore, the present observed values of η_d=0.9% and I_{th}=2.1 mA are much worse than the best reported values. This is most likely because the current-injection efficiency η_{in}, i.e., the ratio of current injected into T wires to total current, was not optimized but was low. In fact, emission was observed not only from the T wires at the center of the waveguide core but also from the arm well on the side cladding and cap layers in separate EL imaging measurements, which indicates that electron-hole pair formation and recombination occurred widely, spreading over the arm well. This suggests that the active region of the T wire is not at the center of the *p-n* junction but instead close to the *p*-type region. Since these T-wire lasers with perpendicular *p*- and *n*-doping layers have unique T-shaped *p-n* junctions, further optimization of the structure to adjust the T-wire active region to the *p-n* junction center is a new and essential task. The observed temperature dependence in Fig. 4, or improved η_d and I_{th} with increased temperature up to 100 K, is also explained by current-injection efficiency. Some electron-hole pairs formed in the arm well displaced from the T wires can reach the active region and contribute to the emission of T wires due to enhanced diffusion of electron-hole pairs as the temperature increases.[12]

In summary, we have demonstrated continuous-wave single-mode lasing at 5–110 K in current-injection T-wire lasers with perpendicular *p*- and *n*-doping layers. The lasers showed a threshold current of 2.1 mA and differential quantum efficiency of 0.9% optimized at 100 K. The temperature dependences of differential quantum efficiency and threshold current were attributed mainly to the temperature dependence of current-injection efficiency.

This work was partly supported by a Grant-in-Aid from the Ministry of Education, Culture, Sports, Science, and Technology, Japan.

[1]Y. Arakawa and H. Sakaki, Appl. Phys. Lett. **40**, 939 (1982).
[2]M. Asada, Y. Miyamoto, and Y. Suematsu, Jpn. J. Appl. Phys., Part 2 **24**, L95 (1985).
[3]E. Kapon, D. M. Hwang, and R. Bhat, Phys. Rev. Lett. **63**, 430 (1989).
[4]S. Tiwari, G. D. Pettit, K. R. Milkove, F. Legoues, R. J. Davis, and J. M. Woodall, Appl. Phys. Lett. **64**, 3536 (1994).
[5]H. Yagi, T. Sano, K. Ohira, D. Plumwongrot, T. Maruyama, A. Haque, S. Tamura, and S. Arai, Jpn. J. Appl. Phys., Part 1 **43**, 3401 (2004).
[6]L. N. Pfeiffer, K. W. West, H. L. Stormer, J. P. Eisenstein, K. W. Baldwin, D. Gershoni, and J. Specter, Appl. Phys. Lett. **56**, 1697 (1990).
[7]M. Yoshita, H. Akiyama, L. N. Pfeiffer, and K. W. West, Jpn. J. Appl. Phys., Part 2 **40**, L252 (2001); Appl. Phys. Lett. **81**, 49 (2002).
[8]W. Wegscheider, L. Pfeiffer, M. Diagnam, A. Pinczuk, K. West, S. McCall, and R. Hull, Phys. Rev. Lett. **71**, 4071 (1993).
[9]W. Wegscheider, L. Pfeiffer, K. West, and R. E. Leibenguth, Appl. Phys. Lett. **65**, 2510 (1994).
[10]Y. Hayamizu, M. Yoshita, S. Watanabe, H. Akiyama, L. Pfeiffer, and K. West, Appl. Phys. Lett. **81**, 4937 (2002).
[11]S. M. Liu, M. Yoshita, M. Okano, H. Akiyama, L. N. Pfeiffeir, K. W. West, and K. W. Baldwin (unpublished).
[12]H. Hillmer, A. Forchel, S. Hansmann, M. Morohashi, E. Lopez, H. P. Meier, and K. Ploog, Phys. Rev. B **39**, 10901 (1989).

IOP PUBLISHING JOURNAL OF PHYSICS: CONDENSED MATTER

J. Phys.: Condens. Matter **19** (2007) 295217 (11pp) doi:10.1088/0953-8984/19/29/295217

T-shaped GaAs quantum-wire lasers and the exciton Mott transition

M Yoshita[1,2], S M Liu[1,2], M Okano[1,2], Y Hayamizu[1,2], H Akiyama[1,2], L N Pfeiffer[3] and K W West[3]

[1] Institute for Solid State Physics (ISSP), University of Tokyo, 5-1-5 Kashiwanoha, Kashiwa, Chiba 277-8581, Japan
[2] CREST, JST, 5-1-5 Kashiwanoha, Kashiwa, Chiba 277-8581, Japan
[3] Bell Laboratories, Alcatel-Lucent, Murray Hill, NJ 07974, USA

Received 17 April 2007
Published 11 June 2007
Online at stacks.iop.org/JPhysCM/19/295217

Abstract

T-shaped GaAs quantum-wire (T-wire) lasers fabricated by the cleaved-edge overgrowth method with molecular beam epitaxy on the interface improved by a growth-interrupt high-temperature anneal are measured to study the laser device physics and fundamental many-body physics in clean one-dimensional (1D) systems. A current-injection T-wire laser that has 20 periods of T-wires in the active region and a 0.5 mm long cavity with high-reflection coatings shows a low threshold current of 0.27 mA at 30 K. The origin of the laser gain above the lasing threshold is studied with the high-quality T-wire lasers by means of optical pumping. The lasing energy is about 5 meV below the photoluminescence (PL) peak of free excitons, and is on the electron–hole (e–h) plasma PL band at a high e–h carrier density. The observed energy shift excludes the laser gain due to free excitons, and it suggests a contribution from the e–h plasma instead. A systematic micro-PL study reveals that the PL evolves with the e–h density from a sharp exciton peak, via a biexciton peak, to an e–h-plasma PL band. The data demonstrate an important role of biexcitons in the exciton Mott transition. Comparison with microscopic theories points out some problems in the picture of the exciton Mott transition.

1. Introduction

Quantum-wire lasers have been studied intensively to examine the improved device performance due to a one-dimensional (1D) density of states at the lowest energy [1–3] and also to understand the fundamental physics of electron–hole (e–h) systems in one dimension [4–7].

A quantum-wire laser was first achieved by Kapon and co-workers [8] in 1989. They fabricated GaAs V-groove wires with 9 nm × 80–100 nm sizes by metal-organic chemical vapour deposition (MOCVD), and measured continuous-wave (cw) room-temperature lasing

with about 50 mA threshold current, though lasing occurred only at higher subbands in multi-mode wires. In 1994, Tiwari and co-workers [9] fabricated quantum-wire lasers with 3-stacked InGaAs V-groove wires with 10 nm × 35 nm sizes by molecular beam epitaxy (MBE). They measured a low threshold current of 0.19 mA at room temperatures. As the current was increased, lasing was switched to higher subbands. In the same year, Wegscheider and co-workers [10] fabricated current-injection T-shaped quantum-wire (T-wire) lasers with 15 periods of GaAs T-wires with 7 nm × 7 nm sizes by a cleaved-edge overgrowth method with MBE [11]. They measured 0.4–0.7 mA threshold currents for multi-mode cw lasing in the T-wire ground states at 4 K. In 2003, Yagi and co-workers [12] fabricated 1.5 μm wavelength etching–regrowth quantum-wire lasers consisting of an 80 nm spaced array of 5-stacked 7 nm × 23 nm InGaAsP/InP rectangular wires using well-controlled systematic methods with electron-beam lithography, dry and wet etching, and MOCVD growth and regrowth. They measured room-temperature cw lasing with a threshold of 142 mA, and operating time longer than 20 000 h. In 2005, they [13] also fabricated etching–regrowth distributed-feedback quantum-wire lasers consisting of a 240 nm spaced array of 5-stacked 9 nm × 24 nm InGaAsP/InP rectangular wires. They measured cw 1.5 μm wavelength lasing with low thresholds of 2.7 mA at room temperature and 1.2 mA at 180 K.

In spite of these developments in fabrications and device characterizations, the physics of quantum-wire lasers is still not established. The device physics of quantum-wire lasers for example threshold current density per wire, transparency current density per wire, and maximum gain as a function of the injection current has not been clarified. Experimentally, these quantities have not been evaluated separately from extrinsic problems in samples. Theoretical quantitative analyses on these key characteristics beyond free-electron theories [1, 2] have not been reported.

The fundamental physics of quantum-wire lasers and quantum wires includes many problems [14–17], and has been controversial. In 1993, Wegscheider and co-workers [4] for the first time demonstrated ground-state lasing in a T-wire laser via optical pumping, and found that the lasing energy was at the peak of excitonic spontaneous emission, and was nearly independent of pump levels. This suggested the absence of band-gap renormalization and an enhanced stability of 1D excitons, so the origin of gain was ascribed to excitons. This argument induced debates on the possibilities of excitonic gain [4, 18, 19]. Furthermore, discussion on the stability of excitons at high densities and apparent absence of band-gap renormalization [20] stimulated interests in the so-called exciton Mott transition in these systems.

In this paper, we investigate the quantum-wire-laser physics and the exciton Mott transition in our high-quality GaAs T-wire lasers with improved interface smoothness by a growth-interrupt high-temperature anneal [21–24]. A current-injection T-wire laser that has 20 periods of 14 nm × 6 nm T-wires and a 0.5 mm long cavity with high-reflection coatings shows a low threshold current at 30 K of 0.27 mA, namely 0.014 mA per wire or 0.27 mA cm^{-1} per wire. The origin of the laser gain is studied with an undoped single T-wire laser by means of optical pumping. The gain is ascribed not to free excitons, or localized excitons, but to the e–h plasma at a high-density regime above the threshold. A systematic micro-photoluminescence (PL) study reveals that the PL evolves with the e–h density from a sharp exciton peak, via a biexciton peak, to an e–h-plasma PL band. The data demonstrate the important role of biexcitons in the exciton Mott transition.

2. Current-injection T-shaped quantum-wire laser

A current-injection T-wire laser [25] with 20 T-wires at the right-angle T-shaped intersections of 20 periods of 14 nm $Al_{0.07}Ga_{0.93}As$ multiple quantum wells (stem wells) and a 6 nm GaAs

quantum well (arm well) was fabricated via the cleaved-edge overgrowth method with MBE by a growth-interrupt *in situ* annealing technique [21–24]. On a (001)-oriented n^+-GaAs substrate, we successively grew an n-type GaAs buffer layer, 20 periods of 6 nm n-type GaAs/9 nm $Al_{0.35}Ga_{0.65}As$ multiple quantum wells, a 1.5 μm $(GaAs)_4(AlAs)_4$ digital-alloy lower cladding layer, 20 periods of 14 nm $Al_{0.07}Ga_{0.93}As$/44 nm $Al_{0.35}Ga_{0.65}As$ stem wells, a 1.5 μm $(GaAs)_4(AlAs)_4$ digital-alloy upper cladding layer, 100 periods of 6 nm p-type GaAs/9 nm $Al_{0.35}Ga_{0.65}As$ multiple quantum wells, and a 10 nm p-type GaAs cap layer. Si and C were used as n-type and p-type dopants, respectively, with the nominal doping level of 1×10^{18} cm^{-3}. The cleaved-edge overgrowth was then performed on its *in situ* cleaved (110) edge to form a 6 nm GaAs arm well, a 11 nm $Al_{0.5}Ga_{0.5}As$ barrier layer, a 171 nm $Al_{0.1}Ga_{0.9}As$ layer, a 1.0 μm $(GaAs)_6(AlAs)_6$ digital-alloy cladding layer, and a 10 nm GaAs cap layer.

After the MBE growth, the upper (001) layers were partially etched away so as to minimize leakage current. AuBe/Au and Ni/Ge/Au/Ni/Au were used for the p-type and n-type ohmic contacts, respectively. After evaporation of these metal films, the wafer was annealed at 450 °C for 30 min to make ohmic contacts. The p-type and n-type doped multiple-quantum-well contact layers are electrically isolated by the two undoped cladding layers and are connected only via the arm well. Under a forward bias, both electrons and holes are injected into the arm well from the n-type and p-type doped layers, and then travel to the T-wire active region via the arm well. The injection current path is thus confined in the thin arm well during laser operation.

Laser bars of cavity length of 500 μm were cut from the wafer by cleavage with the cleaved facets perpendicular to the axis of the T-wires. After deposition of a 70 nm SiO_2 insulating layer with plasma-assisted CVD, the cavity facets were high-reflection (HR) coated by a 50 nm Au layer on the front and a 300 nm one on the rear.

Figure 1 shows the light output power characteristics from the front cavity facet of the T-wire laser as a function of the bias current at 30 K, together with the output spectra at four different bias points below and above threshold. The threshold current (I_{th}) of the laser device is 0.27 mA, and the mean differential quantum efficiency η_d is 12% at 30 K. The optical spectrum is modulated by Fabry–Pérot oscillations below the threshold current and turns into a single lasing mode at 1.554 eV after the current reaches the threshold. The energy shift of lasing as the current increases to 1.5 mA is as small as 1.2 meV, showing the stability of the lasing energy from our T-wire lasers. No emission or lasing from the stem wells has been observed at all injection currents investigated, indicating high injection efficiency into the T-wires. Single-mode lasing has been similarly observed at the cryostat temperatures between 30 and 70 K.

The I_{th} of 0.27 mA at 30 K for the 20 wires corresponds to a very low current of 0.014 mA per single wire, or current density of 0.27 mA cm^{-1} per single wire. If we assume that all injected electrons and holes form e–h pairs in the wires and use a separately measured carrier lifetime of 0.4 ns, the threshold carrier density is estimated to be 7×10^5 cm^{-1} per single wire. This estimated value agrees well with our separate experimental results on optically pumped T-wire lasers. Many-body e–h states corresponding to the carrier density of 7×10^5 cm^{-1} per single wire are discussed later in this paper.

In general, one of the problems in quantum-wire lasers is a small optical confinement factor, or Γ factor, which reduces modal gain. In fact, our present T-wire laser is estimated to have small Γ factor of about 4×10^{-3}. To assist lasing with small modal gain due to small Γ factor, HR coating to the optical-cavity facets to lower mirror loss is useful. However, if the mirror loss is too low compared with internal loss, the differential quantum efficiency will be degraded. Therefore, minimization of the internal loss is important in quantum-wire lasers. In the present sample, we obtained high differential quantum efficiency η_d of 12% with HR coatings thanks to the very small internal loss α_i in the T-wire waveguide, estimated to be 0.32 cm^{-1} [25].

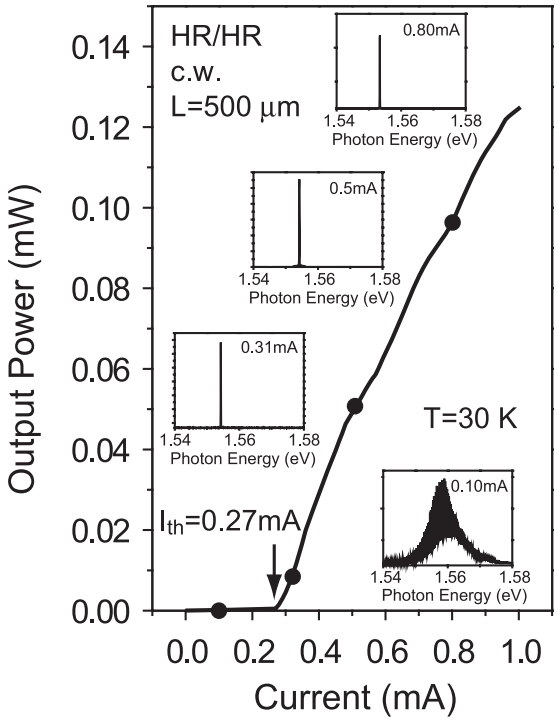

Figure 1. Light output power versus bias current characteristics and emission spectra at four different bias currents for a 20 period 14 nm × 6 nm T-wire laser diode with a 500 μm long cavity between high-reflection (HR) coated facet mirrors under cw operation at 30 K. The threshold current $I_{\rm th}$ is 0.27 mA, or 0.014 mA per single wire, and the differential quantum efficiency $\eta_{\rm d}$ is about 12% [25].

We comment finally on other current-injection T-wire-laser samples. Besides the present sample, we have studied various current-injection laser samples, which have almost the same T-wire-laser structures except for n-type and p-type doping profiles for different injection schemes [25]. They show very different temperature dependence for threshold currents, meaning that the threshold currents are rather strongly affected by transport properties in other regions than by optical properties of the wire region [26]. This suggests that basic studies on quantum-wire lasers should be made not only via current injection, but also via optical pumping [27–34], which we discuss in the next section.

3. Gain in T-shaped quantum-wire lasers

For studying the fundamental physics of quantum-wire lasers and quantum wires, undoped laser samples pumped optically are useful, because optical pumping allows versatile geometries for optical excitations and detections [27–34].

Here, we study an intrinsic single T-wire laser containing only one 14 nm × 6 nm T-wire in the active region of an undoped optical waveguide. The single T-wire laser [30] was fabricated by the cleaved-edge overgrowth method with MBE with a growth-interrupt *in situ* annealing technique [21–24], where a single wire was formed at a T-intersection of a single 14 nm (001) $Al_{0.07}Ga_{0.93}As$ stem well and a 6 nm (110) GaAs arm well. The cavity length of the lasers was 500 μm, and their cavity-mirror facets were coated by 120 nm and 300 nm thick Au films to

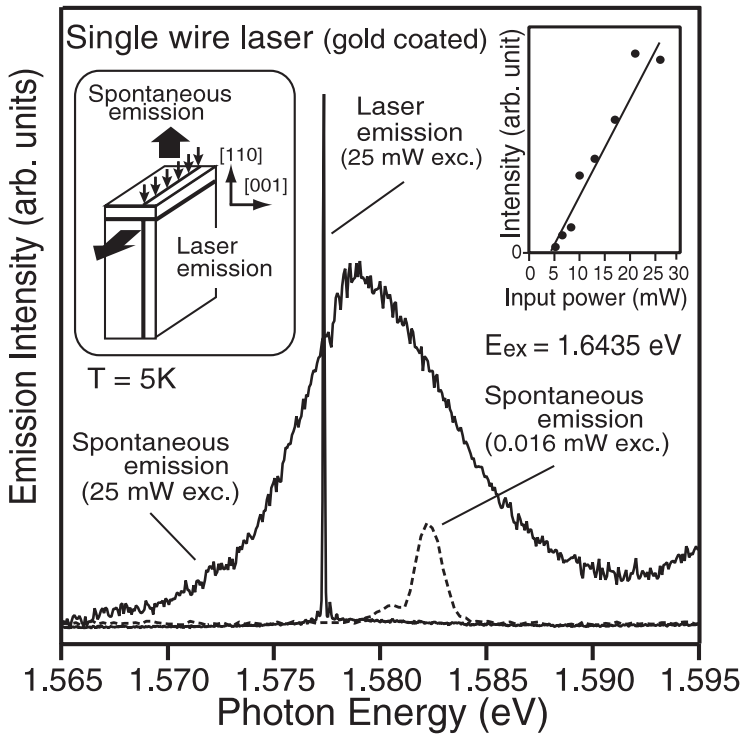

Figure 2. The solid curves show PL and laser-emission spectra of the single-wire laser with gold-coated mirrors at an excitation power of 25 mW, which is above the lasing threshold. The dashed curve shows the PL spectrum at an excitation power of 0.016 mW, which is considerably below the lasing threshold. The left inset shows a schematic diagram of the measurement setup. The right inset shows the excitation-power dependence of laser-emission intensities.

realize high reflection of about 94%. The structures and fabrication methods of the sample are described in detail in our previous reports [30].

Figure 2 shows the laser-emission and PL spectra of the single-wire laser at 5 K under optical pumping at $E_{ex} = 1.6435$ eV. The laser-emission intensities, which depend on the excitation power, indicate a threshold power of 5 mW (right inset). Solid curves show PL and laser-emission spectra of the T-wire at an excitation power of 25 mW, well above the lasing threshold. The laser emission is strongly polarized parallel to the arm well and shows single-mode lasing [30]. The dashed curve shows a PL spectrum at a very low excitation power of 0.016 mW, where the main peak at 1.582 eV and a tiny peak at a lower energy correspond to free and localized excitons, respectively [31, 33]. The lasing energy is about 5 meV below the PL peak of free excitons, and does not overlap with the peaks of free or localized excitons, which proves that lasing does not originate in free or localized excitons in the present sample. On the other hand, the PL spectrum for 25 mW excitation shows a broad PL peak which we ascribe to an e–h plasma discussed later in detail. The lasing energy is on this broad PL peak. Therefore, a gain for lasing well above the threshold was produced by the e–h plasma, though the gain mechanism near the threshold remains unsolved.

4. The exciton Mott transition in T-shaped quantum wires

Figure 3(a) shows PL spectra of a single T-wire at various excitation powers (P_{ex}) at 5 K measured by a micro-PL spectrograph method [31]. While the excitation powers are very low,

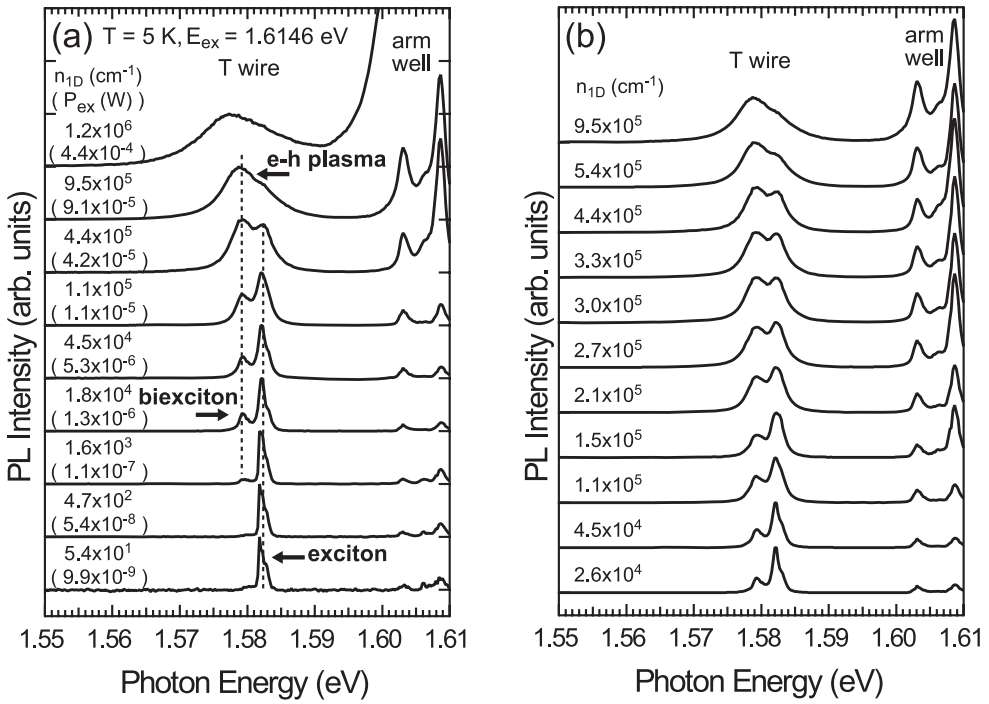

Figure 3. (a) Normalized micro-PL spectra of the single T-wire measured with the spectrograph method for various excitation powers (P_{ex}) at 5 K. Estimated 1D e–h pair densities n_{1D} are also shown. Two dashed vertical parallel lines are drawn to guide the eyes. (b) Normalized micro-PL spectra similar to (a) measured with fine steps of n_{1D} showing PL spectral change from excitons to biexcitons [31].

only a single PL peak due to 1D excitons of the wire is observed at 1.582 eV. As the excitation power is increased, a biexciton PL peak appears 2.8 meV below the exciton PL peak, and it increases its intensity superlinearly, keeping its width and its energy position. The biexciton peak overtakes the exciton peak as its width broadens, as shown more in detail in figure 3(b). Then, the biexciton PL peak changes to a broad PL peak of an e–h plasma, when the exciton PL peak fades into its high-energy tail. The PL peaks show almost no shift until this carrier density region. The plasma peak finally shows a slight red-shift and an asymmetric shape. Simultaneously, PL peaks from the arm well observed at 1.603 and 1.608 eV increase their intensities steeply.

The total PL intensity of the wire (filled squares), which is the sum of PL due to excitons and biexcitons or an e–h plasma, is plotted together with the PL intensity of the arm well (open triangles) in figure 4. The total PL intensity of the wire becomes saturated at an excitation power of about 2×10^{-4} W, while the PL intensity of the arm well still increases. This indicates that the electronic states in the wire are filled and that the Fermi filling of the arm well has started. This shows the formation of a degenerate e–h plasma in the wire, and supports the above assignment. The saturation density of e–h pairs in the wire, estimated from the 21 meV energy separation between the ground states of the wire and the arm well, is 1.2×10^6 cm^{-1}. By assuming that the PL intensity is proportional to the e–h pair density n_{1D} in the wire, we estimated n_{1D} for each PL spectrum, and show it in figure 3.

The e–h density range of superlinear increase in the biexciton PL intensity keeping its width corresponds to 4×10^3 to 1×10^5 cm^{-1}. The corresponding mean distances r_s between

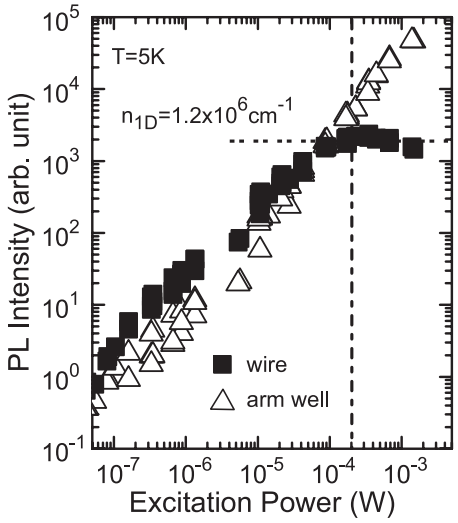

Figure 4. (a) Integrated intensities of PL from the wire (closed squares) and the arm well (open triangles) as a function of the excitation power. The PL intensity of the wire was saturated above the excitation power of 0.2 mW. The estimated saturation e–h pair density is 1.2×10^6 cm^{-1} [31].

carriers are $200a_B^*$ and $8a_B^*$, respectively, where $a_B^*(= 12.7\,\text{nm})$ is the Bohr radius of bulk GaAs. The estimated densities are reasonable values for the formation of a biexciton gas. Between 1×10^5 and 6×10^5 cm^{-1}, the width of the biexciton PL peak increases from 2 to 5 meV with the e–h density, as well as the width of the exciton PL peak. In this density region, the two PL peaks of excitons and biexcitons are well fitted by Lorentzians, which means that homogeneous broadening dominates the PL widths. These suggest increased interactions or overlaps among dense excitons and biexcitons. The e–h density when the biexciton peak overtakes the exciton peak is about 3×10^5 cm^{-1} ($r_s = 2.6a_B^*$). The e–h density when the exciton PL peak quenches is about 6×10^5 cm^{-1} ($r_s = 1.3a_B^*$). It is above 6×10^5 cm^{-1} where the PL peak of the wire is ascribed to the e–h plasma. Note that the biexciton PL changed continuously to the e–h plasma PL, and its peak position showed only small red-shift, less than 2 meV.

Figure 5 shows plots of energies and widths of the PL peaks in figure 3 as functions of the e–h pair density n_{1D} in the wire. The peak energies of excitons at 5 K are marked with filled circles, and their half-maximum widths with vertical bars. Filled diamonds show the peak energies of biexcitons or an e–h plasma at 5 K, and vertical bars show their widths. The relative size of the two symbols at each density n_{1D} approximately represents the relative intensity ratio of PL peaks. The origin and the scale of the plotted energies E is the measured onset energy E_{g0}^* of 1D continuum-state absorption and the measured energy difference E_b^* between the onset and the ground-state excitons, respectively, obtained in the low e–h density limit via PL excitation (PLE) spectra [33–35] and absorption spectra [32]. They are $E_{g0}^* = 1.593$ eV and $E_b^* = 11.4$ meV at 5 K. Since the excited exciton states due to higher Rydberg states and higher hole-subbands exist at the 1D continuum band edge [34, 35], the measured onset energy E_{g0}^* and the measured energy difference E_b^* are smaller than the expected 1D band edge $E_{g0} = 1.596$ eV and the exciton binding energy $E_b = 14$ meV, respectively, but are close to and represent them ($E_{g0}^* \sim E_{g0}$ and $E_b^* \sim E_b$). The plots clearly demonstrate the above-mentioned features observed between the e–h densities of 1×10^5 and 1×10^6 cm^{-1}, which are the constancy of PL peaks of excitons and biexcitons, the gradual switching of the exciton

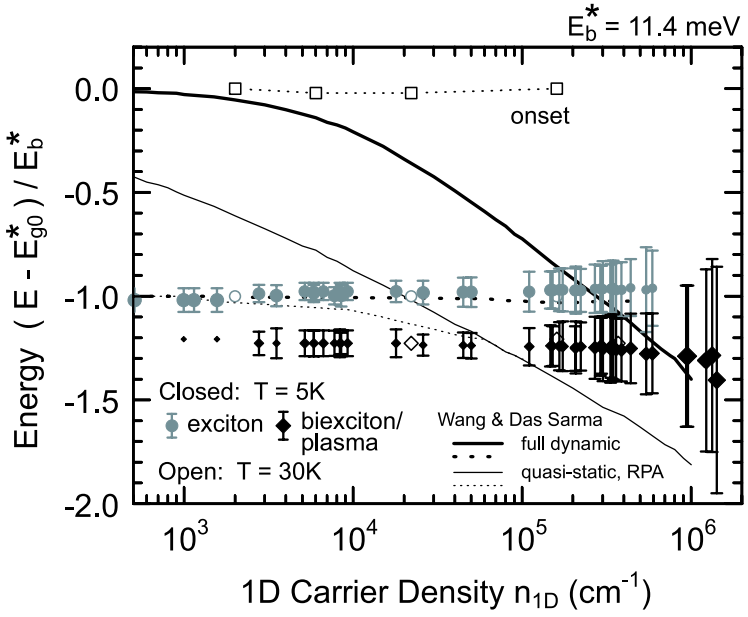

Figure 5. PL peak energies at 5 K (filled symbols) and 30 K (open symbols) for various 1D e–h carrier density n_{1D} for excitons (circles), biexcitons/e–h plasma (diamonds), and continuum band-edge onset (squares) [31]. Each vertical bar shows a half-maximum width of each PL peak. The origin and scale of the plotted energies E are the measured band-edge onset energy E^*_{g0} and the measured energy difference E^*_b between the onset and the ground-state excitons, respectively. Theoretical curves from [17] are also plotted for excitons (dashed curves) and the band edge (solid curves) calculated with dynamical (thick curves) and static (thin curves) screening functions.

PL to the biexciton PL, and the gradual change of the biexciton PL to the e–h plasma PL with broadening.

Also plotted in figure 5 by open circles, diamonds, and squares are PL energies of excitons, biexcitons/e–h plasma, and the onset of 1D continuum states, respectively, measured at 30 K. The PL energies of excitons and biexcitons/e–h plasma at 30 K are similar to those at 5 K. A difference is that PL from the onset of the 1D continuum states is observable at 30 K. Note that the onset show no shift as long as it is visible for densities up to about 2×10^5 cm^{-1}.

5. Discussions

In section 2, we estimated the threshold carrier density of 7×10^5 cm^{-1} in the current-injection T-wire laser. In section 3, we observed that the PL from the single T-wire laser emitted perpendicularly to the waveguide under optical pumping above the lasing threshold showed a broad PL peak from an e–h plasma. These results are consistent with the result that the broad PL originates from an e–h plasma for high e–h densities above 6×10^5 cm^{-1}, found in the systematic PL study in section 4. This confirms that the gain for lasing well above the threshold is produced by an e–h plasma in the quantum wire. To fully understand lasing mechanisms in quantum-wire lasers, we need to understand the data in figure 5 in relation to the exciton Mott transition.

Many theories [14–17] developing various approximation methods have been reported on the optical responses of 1D e–h systems at various densities and on the problem of the

exciton Mott transition. As shown in figure 5, we compare our experimental data with some calculated curves using dynamical (thick curves) and static (thin curves) screening functions for the ground-state exciton (dashed curves) and the band edge (solid curves) from one of the most recent papers [17]. The theoretical curves for the exciton energy, particularly the curve using the dynamical screening function, agree well with the experimental data, reproducing the very small peak shift of the wire exciton PL.

On the other hand, a significant difference is found for the band-edge shifts. Theoretical curves show very large band-edge shifts comparable to E_b for densities of 1×10^5 cm^{-1} ($r_s = 100$ nm) or 1×10^4 cm^{-1} ($r_s = 1$ μm). Experimental data have shown almost no shift of the band edge up to 2×10^5 cm^{-1}. We believe that this point is crucially important because of the following issues.

Firstly, the very small peak shift of the wire exciton PL against carrier density has often been interpreted as an exact cancellation between the shrinkage of the band gap (band-gap renormalization) and the reduction of the exciton binding energy. However, the absence of the band-edge shift up to 2×10^5 cm^{-1} demonstrates that such an explanation does not work, at least below 2×10^5 cm^{-1}.

Moreover, the exciton Mott transition is often pictured as quenching of the exciton binding energy, and hence the exciton bound states, as a result of level crossing between the rather constant exciton energy and the red-shifted renormalized band edge. However, we found that the red-shift of the band edge is absent up to 2×10^5 cm^{-1}, while broadening of PL from excitons, biexcitons, and the band edge starts near 1×10^5 cm^{-1}, and quenching of the exciton PL occurs at 6×10^5 cm^{-1}. This suggests that the prevailing picture of the exciton Mott transition is questionable.

Note that all the theories [14–17] neglected effects of biexcitons, or biexciton correlations. In experiment, the exciton–plasma crossover occurs via biexcitons. We strongly hope that a theory of the Mott transition including biexcitons is developed and compared with our experimental data.

Recently, high-density 1D e–h systems correlated through long-range Coulomb interactions were studied theoretically by using the Tomonaga–Luttinger model [36]. Therein the authors report significance of biexciton correlations in Coulomb-interacting 1D e–h systems, which was not taken into account in the previous theories. They showed that at absolute zero temperature, the system is an insulator even in the high e–h density regime, and that it has a strong instability towards biexciton crystallization. They also showed that, even at a finite temperature, the biexciton correlation dominates the other correlation effects and that the system has the character of a biexciton liquid. Hence, the 1D e–h plasma with Coulomb interactions should have strong biexciton correlations. Our experimental result that the e–h plasma emission appeared gradually at the energy position of the biexciton emission, indicating the importance of the biexciton correlations, is consistent with this theoretical result.

6. Conclusions

A current-injection T-wire laser that has 20 periods of 14 nm $\times$ 6 nm T-wires and a 0.5 mm long cavity with high-reflection coatings shows a low threshold current at 30 K of 0.27 mA, namely 0.014 mA per wire or 0.27 mA cm^{-1} per wire. The estimated threshold carrier density is 7×10^5 cm^{-1} per single wire. An optical pumping study for an undoped single T-wire laser clearly demonstrates that the gain for lasing is ascribed not to free excitons, or localized excitons, but to the e–h plasma in a high-density regime above the threshold. A systematic micro-PL study reveals that the PL evolves with the e–h density from a sharp exciton peak, via a biexciton peak, to an e–h-plasma PL band. The data demonstrate the important role

of biexcitons in the exciton Mott transition. Comparison with microscopic theories raises a question for the arguments based on the renormalized band-edge shift before the Mott transition.

Acknowledgments

We thank Professor T Ogawa, Professor K Asano, Dr P Huai, and Dr Y Tomio of Osaka University, Professor C Z Ning of NASA, and Professor H Sakaki of the University of Tokyo for valuable discussions. We acknowledge the financial support from MEXT, Japan.

References

[1] Arakawa Y and Sakaki H 1982 *Appl. Phys. Lett.* **40** 939
[2] Asada M, Miyamoto Y and Suematsu Y 1985 *Japan. J. Appl. Phys.* **24** L95
[3] Kapon E 1998 *Semiconductor Lasers I: Fundamentals* ed E Kapon (San Diego, CA: Academic) p 291
[4] Wegscheider W, Pfeiffer L N, Dignam M M, Pinczuk A, West K W, McCall S L and Hull R 1993 *Phys. Rev. Lett.* **71** 4071
[5] Ogawa T 2004 *J. Phys.: Condens. Matter* **16** S3567
Ogawa T and Takagahara T 1991 *Phys. Rev.* B **43** 14325
Ogawa T and Takagahara T 1991 *Phys. Rev.* B **44** 8138
[6] Akiyama H 1998 *J. Phys.: Condens. Matter* **10** 3095
Someya T, Akiyama H and Sakaki H 1996 *Phys. Rev. Lett.* **76** 2965
Someya T, Akiyama H and Sakaki H 1995 *Phys. Rev. Lett.* **74** 3664
Akiyama H, Someya T and Sakaki H 1996 *Phys. Rev.* B **53** R16160
[7] Akiyama H, Yoshita M, Pfeiffer L N and West K W 2004 *J. Phys.: Condens. Matter* **16** S3549
[8] Kapon E, Hwang D M and Bhat R 1989 *Phys. Rev. Lett.* **63** 430
[9] Tiwari S, Pettit G D, Milkove K R, Legoues F, Davis R J and Woodall J M 1994 *Appl. Phys. Lett.* **64** 3536
[10] Wegscheider W, Pfeiffer L, West K and Leibenguth R E 1994 *Appl. Phys. Lett.* **65** 2510
[11] Pfeiffer L N, West K W, Stormer H L, Eisenstein J P, Baldwin K W, Gershoni D and Spector J 1990 *Appl. Phys. Lett.* **56** 1697
[12] Yagi H, Sano T, Ohira K, Maruyama T, Haque A and Arai S 2003 *Japan. J. Appl. Phys.* 2 **42** L748
[13] Yagi H, Miura K, Nishimoto Y, Plumwongrot D, Ohira K, Maruyama T and Arai S 2005 *Appl. Phys. Lett.* **87** 223120
[14] Benner S and Haug H 1991 *Europhys. Lett.* **16** 579
[15] Rossi F and Molinari E 1996 *Phys. Rev. Lett.* **76** 3642
Rossi F and Molinari E 1996 *Phys. Rev.* B **53** 16462
[16] Tassone F and Piermarocchi C 1999 *Phys. Rev. Lett.* **82** 843
Piermarocchi C and Tassone F 2001 *Phys. Rev.* B **63** 245308
[17] Das Sarma S and Wang D W 2000 *Phys. Rev. Lett.* **84** 2010
Wang D W and Das Sarma S 2001 *Phys. Rev.* B **64** 195313
[18] Sirigu L, Oberli D Y, Degiorgi L, Rudra A and Kapon E 2000 *Phys. Rev.* B **61** R10575
[19] Rubio J, Pfeiffer L, Szymanska M H, Pinczuk A, He S, Baranger H U, Littlewood P B, West K W and Dennis B S 2001 *Solid State Commun.* **120** 423
[20] Ambigapathy R, Bar-Joseph I, Oberli D Y, Haacke S, Brasil M J, Reinhardt F, Kapon E and Deveaud B 1997 *Phys. Rev. Lett.* **78** 3579
[21] Yoshita M, Akiyama H, Pfeiffer L N and West K W 2001 *Japan. J. Appl. Phys.* 2 **40** L252
[22] Yoshita M, Akiyama H, Pfeiffer L N and West K W 2002 *Appl. Phys. Lett.* **81** 49
Yoshita M, Oh J W, Akiyama H, Pfeiffer L N and West K W 2003 *J. Cryst. Growth.* **251** 62
[23] Oh J W, Yoshita M, Akiyama H, Pfeiffer L N and West K W 2003 *Appl. Phys. Lett.* **82** 1709
Oh J W, Yoshita M, Hayamizu Y, Akiyama H, Pfeiffer L N and West K W 2004 *J. Appl. Phys.* **96** 6370
[24] Ishii A, Aisaka T, Oh J W, Yoshita M and Akiyama H 2003 *Appl. Phys. Lett.* **83** 4187
Ishii A, Aisaka T, Oh J W, Yoshita M, Akiyama H, Pfeiffer L N and West K W 2004 *Thin Solid Films* **464/465** 38
[25] Liu S M, Yoshita M, Okano M, Ihara T, Itoh H, Akiyama H, Pfeiffer L N, West K W and Baldwin K W 2007 *Japan. J. Appl. Phys.* 2 **46** L330
Okano M, Liu S M, Ihara T, Itoh H, Yoshita M, Akiyama H, Pfeiffer L N, West K and Malis O 2007 *Appl. Phys. Lett.* **90** 091108

[26] Kapon E, private communications
[27] Akiyama H, Pfeiffer L N, Yoshita M, Pinczuk A, Littlewood P B, West K W, Matthews M J and Wynn J 2003 *Phys. Rev.* B **67** 041302
[28] Takahashi Y, Watanabe S, Yoshita M, Itoh H, Hayamizu Y, Akiyama H, Pfeiffer L N and West K W 2003 *Appl. Phys. Lett.* **83** 4089
[29] Akiyama H, Pfeiffer L N, Pinczuk A, West K W and Yoshita M 2002 *Solid State Commun.* **122** 169
[30] Hayamizu Y, Yoshita M, Watanabe S, Akiyama H, Pfeiffer L N and West K W 2002 *Appl. Phys. Lett.* **81** 4937
[31] Yoshita M, Hayamizu Y, Akiyama H, Pfeiffer L N and West K W 2006 *Phys. Rev.* B **74** 165332
[32] Takahashi Y, Hayamizu Y, Itoh H, Yoshita M, Akiyama H, Pfeiffer L N and West K W 2005 *Appl. Phys. Lett.* **86** 243101
Takahashi Y, Hayamizu Y, Itoh H, Yoshita M, Akiyama H, Pfeiffer L N and West K W 2005 *Appl. Phys. Lett.* **87** 223119
[33] Akiyama H, Yoshita M, Pfeiffer L N, West K W and Pinczuk A 2003 *Appl. Phys. Lett.* **82** 379
[34] Itoh H, Hayamizu Y, Yoshita M, Akiyama H, Pfeiffer L N, West K W, Szymanska M H and Littlewood P B 2003 *Appl. Phys. Lett.* **83** 2043
[35] Szymanska M H, Littlewood P B and Needs R J 2001 *Phys. Rev.* B **63** 205317
[36] Asano K and Ogawa T 2005 *J. Lumin.* **112** 200

Exciton-plasma crossover with electron-hole density in T-shaped quantum wires studied by the photoluminescence spectrograph method

Masahiro Yoshita, Yuhei Hayamizu, and Hidefumi Akiyama*
Institute for Solid State Physics, University of Tokyo, and CREST, JST, 5-1-5 Kashiwanoha, Kashiwa, Chiba 277-8581, Japan

Loren N. Pfeiffer and Ken W. West
Bell Laboratories, Lucent Technologies, 600 Mountain Avenue, Murray Hill, New Jersey 07974, USA
(Received 14 June 2006; revised manuscript received 5 September 2006; published 27 October 2006)

We investigated the evolution of photoluminescence (PL) spectra with the electron-hole (*e-h*) pair density in a single T-shaped quantum wire of high quality grown by a cleaved-edge overgrowth method with molecular-beam epitaxy. By using a spectrograph imaging method for the PL measurements, we obtained PL spectra free from carrier migration effects for the one-dimensional (1D) *e-h* system in the T wire for a wide range of *e-h* pair densities from 5×10^{1} to 1.2×10^{6} cm^{-1}. In the low *e-h* pair density region below 4×10^{3} cm^{-1}, PL only from 1D excitons in the wire was observed. At a pair density of 4×10^{3} cm^{-1}, a new peak characteristic of biexcitons with a binding energy of 2.8 meV appeared below the exciton peak. At a pair density of 1×10^{5} cm^{-1}, the biexciton peak started broadening without a peak energy shift and completely changed to an *e-h* plasma at 6×10^{5} cm^{-1}. The transition from the dilute exciton gas to the *e-h* plasma is, therefore, a gradual crossover via biexcitons, which indicates the importance of biexcitonic effects in 1D *e-h* systems. Moreover, we found that during the continuous exciton-plasma crossover, the band edge of 1D excitons showed no significant energy shift at an *e-h* pair density as high as 2×10^{5} cm^{-1}, where the biexciton PL peak had already started broadening in linewidth and changing to the degenerate *e-h* plasma peak. The level crossing between the band edge and the exciton was not observed experimentally.

DOI: 10.1103/PhysRevB.74.165332 PACS number(s): 78.67.Lt, 73.21.Hb, 71.35.−y, 78.55.Cr

I. INTRODUCTION

Many-body effects in optically excited semiconductors, which play essential roles in the crossover from an exciton gas at low electron-hole (*e-h*) pair densities to a dense *e-h* state (e.g., an *e-h* plasma) at high densities, have attracted much attention and have been actively studied experimentally and theoretically.[1,2] Recently, intensive interest has been focused on one-dimensional (1D) *e-h* systems in semiconductor quantum wires, where Coulomb interactions become more important.[3–16] In three-dimensional (3D) *e-h* systems, it is accepted that the exciton-plasma transition with the carrier density is well described by a familiar picture of exciton Mott transition. In this picture, the binding energy of excitons decreases with carrier density due to screening, and the Mott transition to the *e-h* plasma occurs at the critical density n_c (the Mott density) where the exciton binding energy is reduced to zero and the energy position of the band edge coincides with that of the excitons.[17] However, in 1D *e-h* systems, the validity of the exciton Mott transition picture is still questionable because the screening effect, which is a key factor in this picture, becomes much weaker in lower-dimensional systems.[18–20] Indeed, a many-body theory shows that optical spectra for quasi-1D systems calculated for various carrier densities with and without screening effects are almost identical,[21] indicating that the screening effects are less important in the exciton-plasma crossover in quasi-1D systems.[1] Furthermore, it is known that any weak attractive potential forms at least one bound state in 1D. The 1D exciton Mott transition picture includes these crucial problems.

Experimental studies[9,10] on many-body effects for semiconductor quantum wires reported that photoluminescence (PL) peak positions of excitons in the quantum wires are almost independent of the *e-h* pair densities up to a very high carrier density of 3×10^{6} cm^{-1}. Recent many-body theories explain this constancy of the exciton peak positions qualitatively as an exact cancellation between the reduction in the exciton binding energy and the shrinkage of the band gap due to band-gap renormalization.[7] However, quantitative comparisons of experimental data with theories have not been achieved yet. Moreover, the crucial energy shift of the band edge and the reduction of the exciton binding energy have not been directly measured. To solve these problems and establish a picture for the 1D exciton-plasma crossover, quantitative systematic experiments are necessary.

In practical experiments on low-dimensional systems formed in heterostructures, interface roughness and the resulting localization of the electronic states are crucial issues.[22,23] If structural roughness is large, carriers are localized and zero-dimensional (0D) states are formed. Indeed, localized states formed in thin two-dimensional (2D) quantum wells with large interface roughness have been used to study 0D quantum-dot features[24–26] as those realized in self-assembled InAs quantum dots.[27] In such systems, 0D states show sharp PL peaks with radiative-relaxation widths due to 0D excitons, biexcitons, and other neutral exciton complexes, which do not shift with carrier densities as a result of 3D confinement. Detailed PL studies on previous T-shaped quantum wires (T wires) formed by a cleaved-edge overgrowth method have revealed 0D-like localized electronic states in the T wires.[23,28] Therefore, for investigations of the intrinsic 1D problems in the exciton-plasma crossover at low temperatures, it is important to minimize structural roughness in order to get small inhomogeneous PL linewidth and localization energy, at least smaller than the many-body Coulomb interaction energies such as exciton and biexciton binding energies.

Recently, the structural uniformity of T wires has been significantly improved. In our 20-period multiple T-wire laser samples, the 1D-exciton ground state and 1D continuum states were spectrally separated,[29,30] and PL peaks of excitons, biexcitons, and an *e-h* plasma were found as well as laser emissions.[16] Further improvements in structural uniformity and spectral sharpness were achieved in single T-wire laser samples, where we observed single-mode lasing[31,32] and sharp strong exciton photoabsorption in a waveguide-transmission measurement.[33]

In this paper, we describe our first quantitative PL studies on the single T wire with the current-best quality, whose inhomogeneous broadening is smaller than the relevant Coulomb interaction energies under investigation. In particular, we studied the evolution of PL shape, energy, and intensity during the crossover from dilute 1D excitons to a dense *e-h* plasma as a function of well-characterized *e-h* density.

In high-quality quantum wires with reduced interface roughness, the migration of carriers (electrons, holes, and excitons) is enhanced. In micro-PL experiments, this enhanced carrier migration causes spatial gradation of carrier densities in the wire, which leads to the obtained PL spectra of the wire becoming average spectra from various *e-h* density regions. To reduce this averaging effect in the spectra, in this work we used a spectrograph imaging method for micro-PL measurements and derived PL spectra of the wire free from the carrier migration. In addition, we estimated carrier densities in the wire at each excitation power by comparing PL intensities to that obtained at the saturated carrier density in the wire. These improvements in experiments enable quantitative discussion of the spectral evolution of PL from the wire with the carrier density.

This paper is organized as follows. In the next section, we describe the single T-wire sample structure and micro-PL experimental setup combined with the spectrograph method. In Sec. III A, we characterize the spatial uniformity and quality of the single T wire by scanning micro-PL spectroscopy. Then, in Sec. III B, we report spectrograph PL imaging experiments for the single T wire at various excitation powers. We demonstrate spectrograph PL images that are strongly dependent on the excitation power and show significant carrier migration in the wire. In Secs. III C–III E, we derive intrinsic PL spectra from the spectrograph images for various *e-h* densities. We focus on PL from the ground state of 1D excitons and from the 1D continuum states in the wire and discuss their spectral evolution as a function of the 1D carrier density. Finally, in Sec. IV, we discuss problems of the exciton Mott picture in the 1D *e-h* system of the wire by comparing the obtained experimental results with theoretical predictions based on the exciton Mott transition picture.

II. EXPERIMENT

A. Sample preparation

A single T wire was fabricated by the cleaved-edge overgrowth method with molecular beam epitaxy[34,35] with a growth-interrupt *in situ* annealing technique.[36,37] As schematically illustrated in Fig. 1(a), the single T wire consisted of a 14-nm-thick $Al_{0.07}Ga_{0.93}As$ quantum well (QW) (stem well) grown on a (001) substrate and an intersecting 6-nm-thick GaAs QW (arm well) overgrown on a cleaved (110) edge of the stem well. We improved the interface flatness of the arm well by performing growth-interrupt *in situ* annealing at a substrate temperature of 600 °C for 10 min on the arm-well upper surface.[36,37] The sample structure and fabrication procedures are reported in detail in separate papers.[31,32]

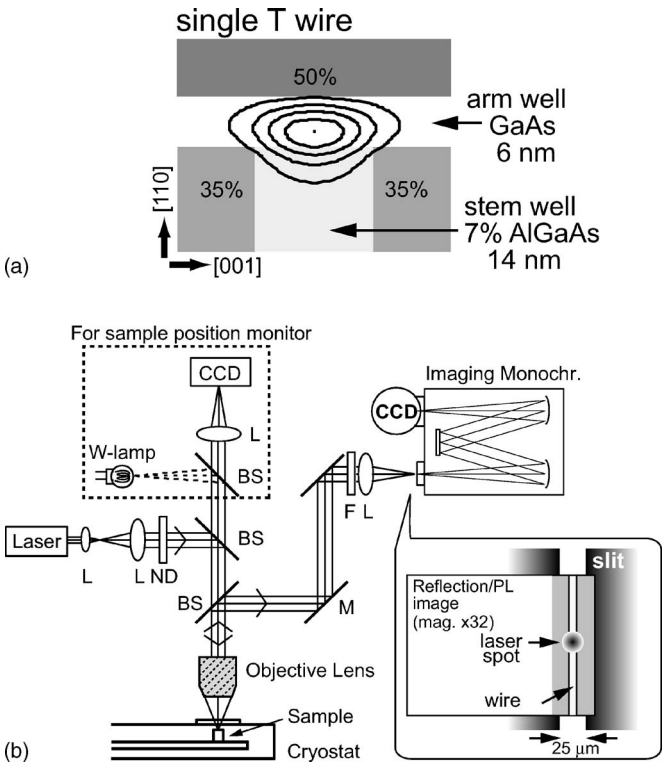

FIG. 1. (a) Schematic of a single T-wire structure. Percentages show aluminum content x in $Al_xGa_{1-x}As$ layers. (b) Microphotoluminescence (micro-PL) setup used for PL spectrograph experiments. PL from the sample was collected by an objective lens and imaged on the entrance slit of the imaging monochromator by aligning the wire parallel to the slit. The PL image dispersed by the monochromator was detected by a liquid-nitrogen-cooled charge-coupled device (CCD) detector.

B. Micro-PL experiments combined with spectrograph imaging method

The micro-PL setup used in this study is schematically shown in Fig. 1(b). For photoexcitation, light from a titanium-sapphire laser was focused, via an objective lens with a numerical aperture (NA) of 0.5, to an almost-diffraction-limited spot with a diameter of 0.8 μm on the sample surface.[38] For PL detection, we used a spectrographic technique with an imaging monochromator and a liquid-nitrogen-cooled charge-coupled-device (CCD) camera with 1024×256 pixels. PL from the sample was collected by the objective lens and projected onto the entrance slit of the monochromator via an imaging lens. Then, the PL images were dispersed in wavelength by the monochromator and detected by the CCD camera.

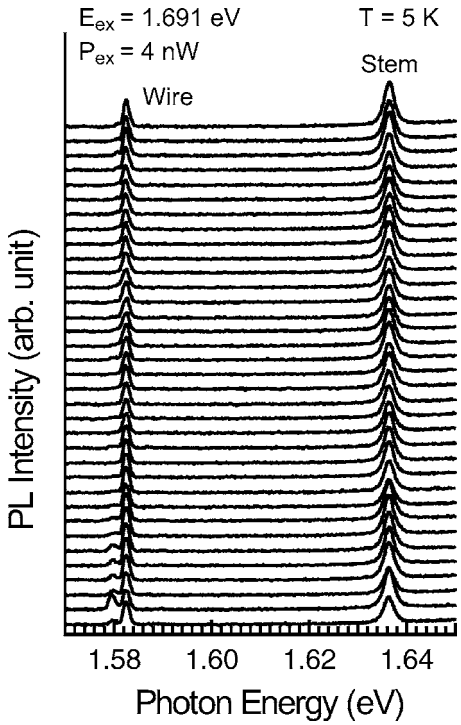

FIG. 2. Spatially resolved PL spectra of the T wire at 5 K under point excitation scanned along the wire in steps of 0.5 μm.

In the experiments, we projected the PL images on the slit with the wire direction aligned parallel to the slit, as illustrated in Fig. 1(b), so that the spatial distribution of PL and hence the spatial distribution of photo-excited carriers in the wire could be observed directly. In addition, by extracting a specific row of the dispersed PL image detected by the CCD camera, we obtained a spatially resolved PL spectrum of the wire at the corresponding sample position. In particular, the PL spectrum extracted at the excitation position of the laser corresponds to the spectrum obtained in the confocal microspectroscopy experiments.

The spatial resolution of the spectrograph image along the wire direction was about 0.8 μm on the sample, which is determined by the NA (=0.5) of the objective lens, the magnification factor ($\times$32) of the micro-PL detection system, and the pixel size (24 μm$\times$24 μm) of the CCD camera. The spatial resolution across the wire direction was also determined by these values in the micro-PL detection system mentioned above and by the slit width of the monochromator. In this study, the slit width was set to 25 μm, which limited the detection area to about 0.8 μm on the sample across the wire direction and gave a spectral resolution of 0.1 nm.

III. RESULTS

A. Spatial uniformity of the T wire

Figure 2 shows spatially resolved PL spectra of the single T wire at 5 K obtained by scanning the 0.8-μm-diameter excitation spot along the wire in steps of 0.5 μm over a distance of 15 μm. The photon energy of the excitation laser was 1.691 eV and the excitation power was as low as 4 nW on the sample surface. PL peaks observed around 1.582 and 1.636 eV are ascribed to the wire and the stem well, respectively, on the basis of a separate PL imaging experiment.[32] PL from the arm well was not observed due to the fast flow of carriers from the arm well to the wire.

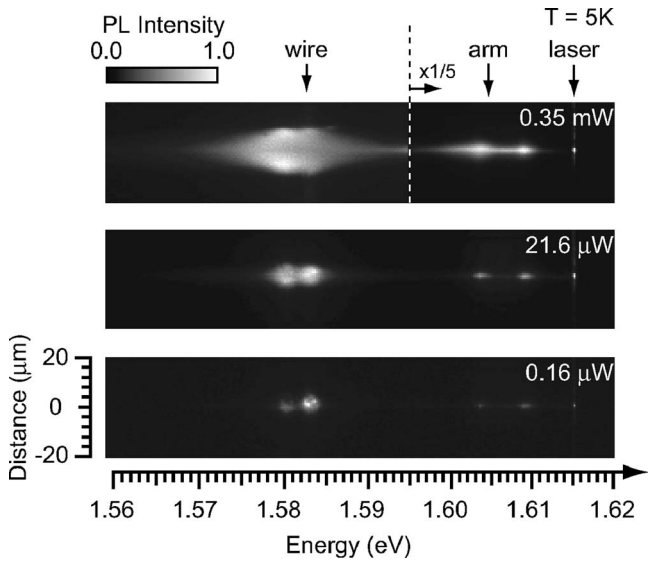

FIG. 3. Spectrograph PL images of the T wire at three different excitation powers at 5 K. Tiny spots seen at 1.6146 eV are reflection images of the excitation laser.

The dominant PL peak from the wire at 1.582 eV had a narrow linewidth of 1.3 meV and uniform peak intensity and energy. This peak has been ascribed to the ground state of the 1D excitons in the wire with a small Stokes shift of less than 0.3 meV.[29,30,33] Tiny PL peaks locally observed at 1.580 eV are from 1D excitons in the wire formed in the arm-well monolayer-island regions.[37] However, as seen in Fig. 2, these monolayer fluctuations are rare in the constituent arm well and a continuous sequence of wire PL spectra was obtained, which demonstrates that the spatially uniform 1D exciton states were formed over a region at least 10 μm in length in the wire. Scanning PL experiments over the entire sample have confirmed that the whole 500-μm-long wire has features very similar to Fig. 2.

B. Spectrograph images of PL from the T wire

Spectrograph images of PL from the single T wire observed at three different excitation powers (0.16 μW, 21.6 μW, and 0.35 mW) are shown in Fig. 3. The excitation position was selected at the center of the spatially uniform PL region in Fig. 2. The photon energy of the excitation laser was 1.6146 eV. This excitation created *e-h* pairs in the T wire and the arm well, but not in the stem well. The horizontal and vertical axes of the images represent photon energy and spatial distance from the excitation position on the sample, respectively. Tiny spots seen at 1.6146 eV are reflection images of the excitation laser spot. Their image sizes along the wire direction are almost 1 pixel of the CCD, which ensures that the spot size of the excitation laser was 0.8 μm or less on the sample surface.

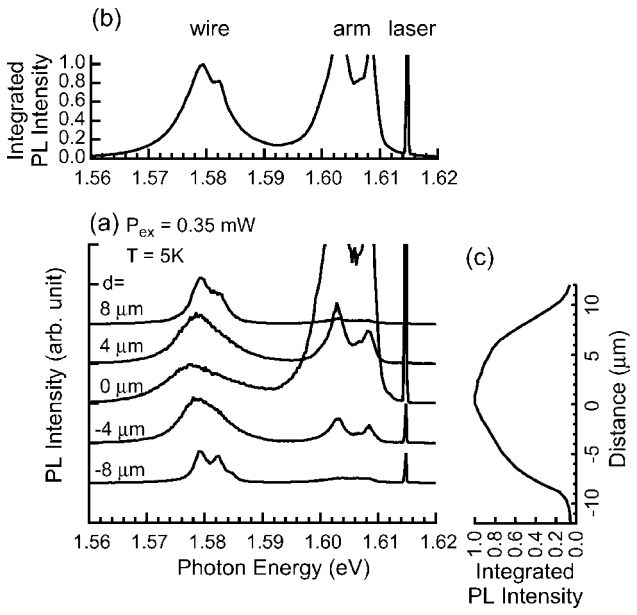

FIG. 4. (a) PL spectra of the wire at different positions, derived from the 0.35-mW spectrograph PL image in Fig. 3. (b) PL spectrum integrated over all the rows of the 0.35-mW spectrograph image in Fig. 3 along the wire direction. (c) Intensity profile of the wire PL along the wire direction, obtained by summing the PL intensities of the wire between 780 and 790 nm.

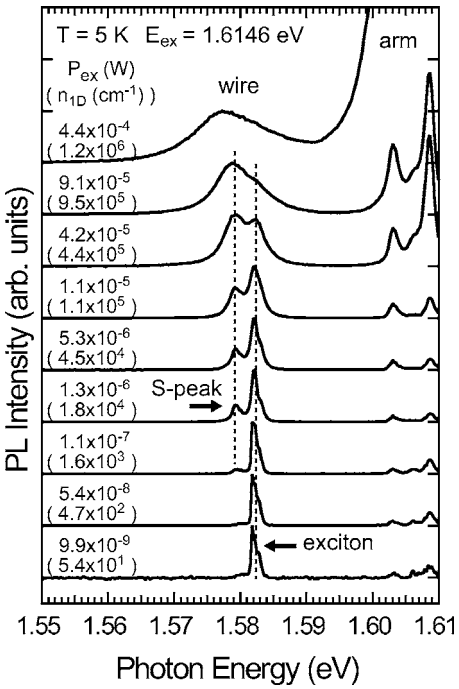

FIG. 5. Normalized PL spectra of the T wire for various excitation powers (P_{ex}) at 5 K. Numbers in parentheses are estimated 1D *e-h* pair densities (n_{1D}). The low-energy side peak that appeared below the wire exciton peak is labeled as the S-peak. Two dashed vertical parallel lines are drawn to guide the eyes. PL peaks observed above 1.60 eV were from the arm wells.

In Fig. 3, the PL images strongly depend on the excitation power. The PLs of the wire and the arm well were observed from regions widely spread along the wire direction from the excitation position. In particular, at the highest excitation power of 0.35 mW, strong PL was observed even at positions 10 μm away from the excitation position, which indicates the existence of significant carrier migration in the wire. In addition, the spectral linewidth of the wire PL increased as the excitation power was increased.

Figure 4(a) shows PL spectra at every 4-μm step from the excitation position (d=0 μm), extracted from the spectrograph image for 0.35-mW excitation power in Fig. 3. For comparison, the PL spectrum integrated over all the rows of the spectrograph image along the wire direction is shown in Fig. 4(b). The PL spectra of the wire strongly depended on the detection position because of significant carrier migration in the wire. The spectrum at the excitation position (d=0 μm) has a broad single-peak structure, while those at the positions far from the excitation spot ($d=\pm 8$ μm) have a double peak structure. Figure 4(c) shows the PL intensity profile along the wire, obtained by summing the PL intensities of the wire between 780 and 790 nm. This intensity profile indicates that the photogenerated carriers were spatially extended over a distance of 10 μm along the wire direction, and relatively strong PL was observed at positions 5 μm from the laser excitation position. As a consequence, the integrated PL spectrum shown in Fig. 4(b), which corresponds to the spectrum obtained in a conventional micro-PL measurement without using the spectrograph technique or confocal microspectroscopy, does not represent an intrinsic PL spectrum of the wire at a defined carrier density but shows only a mixed PL spectrum of the wire under a larger spatial distribution of carriers. Therefore, we extracted PL spectra at the excitation position from the spectrograph images to eliminate the influence of carrier migration along the wire direction on the PL spectra and compared them at various excitation powers. Since the carrier migration length was larger than the spatial resolution and the laser spot size of 0.8 μm, the carrier-distribution effects were negligible in the extracted PL spectra.

C. Excitation-power dependence of PL spectra and evaluation of the *e-h* density

Figure 5 shows PL spectra of the T wire at the center position of the excitation spot for various excitation powers (P_{ex}) at 5 K, derived from the spectrograph images. At excitation powers less than 0.1 μW, only a single PL peak due to 1D excitons of the wire was observed at 1.582 eV. As the excitation power was increased from 0.1 μW to around 10 μW, a new PL peak (labeled the S-peak) appeared 2.8 meV below the exciton PL peak and increased in intensity rapidly. Above 10 μW the S-peak dominated the PL of the wire as its linewidth broadened. Above 50 μW the exciton peak faded into the high-energy tail of the S-peak. The dominant S-peak finally showed a redshift and an asymmetric shape. Simultaneously, PL peaks from the arm well observed at 1.603 and 1.608 eV strongly increased in intensity.

Integrated area intensities (the sum of the exciton- and S-peak intensities) of the wire PL spectra and those of the arm-well PL spectra are plotted in Fig. 6. The PL intensity of

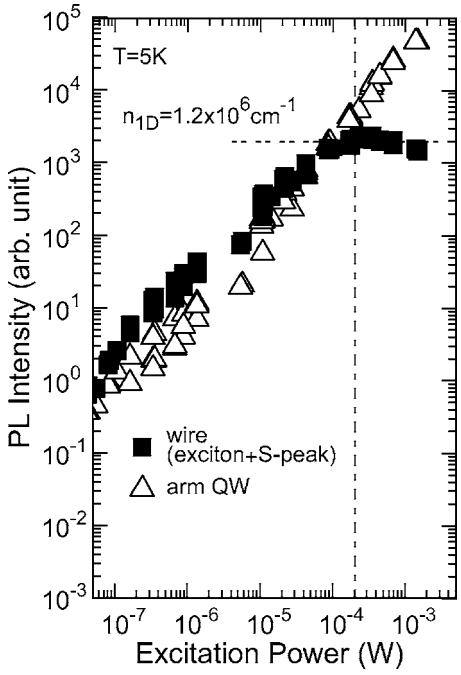

FIG. 6. Integrated intensities of PL from the wire (closed squares) and the arm well (open triangles) as a function of the excitation power. The PL intensity of the wire was saturated above the excitation power of 0.2 mW.

the wire became saturated at an excitation power of about 0.2 mW while that of the arm well still increased. This indicates that the electronic states in the wire were completely filled and the Fermi filling of the arm well had started.

The saturation density of the *e-h* pairs in the wire, estimated from the 21-meV energy separation between the ground states of the wire and the arm well in this T-wire sample, was 1.2×10^6 cm^{-1}. By assuming that the PL intensity is proportional to the *e-h* pair density (n_{1D}) in the wire, we estimated n_{1D} for each PL spectrum, which is shown in parentheses under the P_{ex} in Fig. 5. In the following sections, we use the estimated 1D *e-h* pair density n_{1D} to discuss the spectral evolution quantitatively.

D. PL of excitons, biexcitons, and an *e-h* plasma in the T wire

Figure 7(a) shows the PL intensities of the wire and the arm well plotted as a function of the estimated 1D *e-h* pair densities n_{1D}. PL intensities of the exciton and the S-peak constituting the wire PL are also shown. The PL intensity of the wire was saturated at n_{1D} of 1.2×10^6 cm^{-1} while that of the arm well increased.

At carrier densities below 4×10^3 cm^{-1}, only the PL peak from excitons in the wire had a measurable intensity. Above 4×10^3 cm^{-1}, however, the S-peak appeared and increased in intensity steeply [Fig. 7(a)]. Log-log plots of the integrated intensity of the S-peak against that of the exciton peak are shown in Fig. 7(b). The S-peak intensity increased superlinearly against the exciton peak intensity, and the slope gradually approached 2. Peak energy positions and linewidths (FWHM) of these two peaks are shown as a function of n_{1D} in the upper and lower panels of Fig. 8, respectively. The

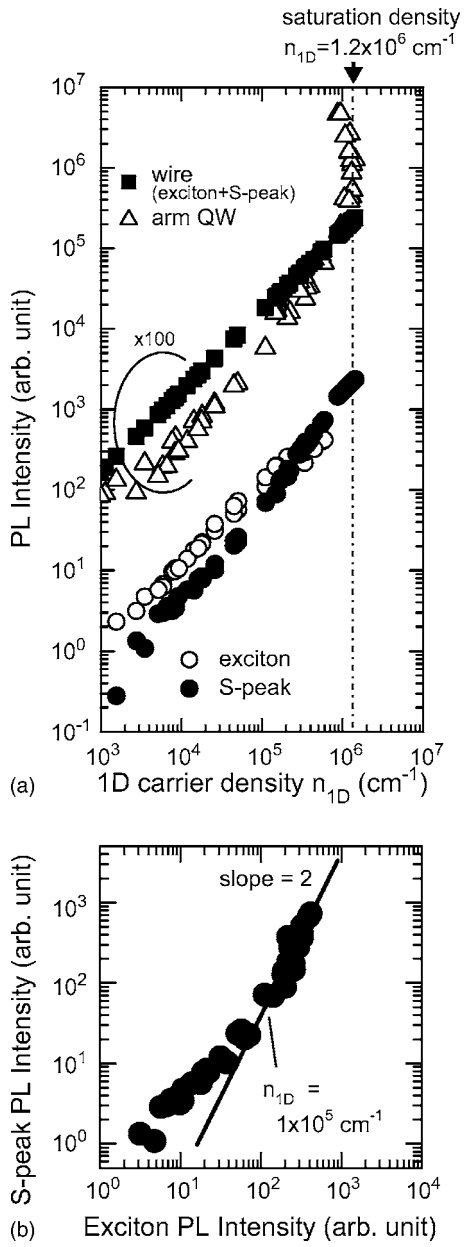

FIG. 7. (a) Integrated intensities of PL from the wire (closed squares) and the arm well (open triangles) plotted as a function of the estimated 1D carrier density n_{1D}. PL intensities of the exciton (open circles) and S-peak (closed circles) constituting the wire PL are also shown. (b) Log-log plots of the integrated PL intensity of the S-peak against that of the exciton peak.

energy position and the linewidth of the S-peak and the exciton peak were almost unchanged in the 1D *e-h* pair densities between 4×10^3 cm^{-1} and about 1×10^5 cm^{-1} (Fig. 8). In addition, these two peaks come from the same position in the wire at the excitation spot. Therefore, we ascribe the S-peak in this density region to a dilute gas of biexcitons. The corresponding mean distances r_s between carriers are $200a_B^*$ and $8a_B^*$, respectively, where a_B^* (=12.7 nm) is the Bohr radius of bulk GaAs. These values are reasonable for the formation of biexcitons. The biexciton binding energy estimated from the PL spectra was 2.8 meV, which is in

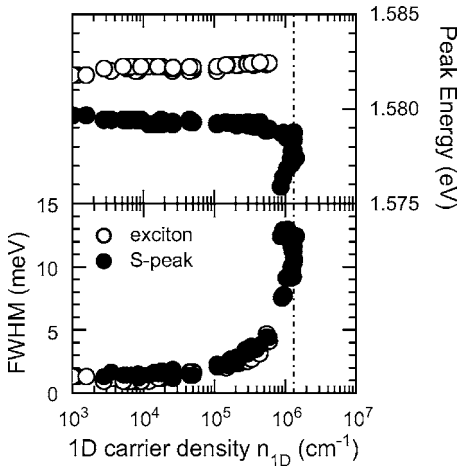

FIG. 8. Energy positions and widths of the exciton peak and S-peak in the wire PL spectra shown in Fig. 5 as a function of the 1D carrier density n_{1D}.

agreement with our previous result for multiple T wires.[16]

In the high density region above n_{1D} of 1×10^5 cm^{-1}, the linewidth of the S-peak increased significantly from 2 to 12 meV with the excitation power (bottom panel of Fig. 8). The linewidth of the exciton peak also increased with the excitation power, but its intensity was saturated at 6×10^5 cm^{-1} and then rapidly decreased (Fig. 5). In this density region, each PL peak is well fitted by a Lorentzian function, which means that homogeneous broadening dominates the PL linewidths. As the carrier density was further increased above 6×10^5 up to 1.2×10^6 cm^{-1}, the S-peak gradually became asymmetric in shape and dominated the wire PL.

The corresponding mean distance r_s is from $8a_B^*$ at 1×10^5 cm^{-1} to $0.7a_B^*$ at 1.2×10^6 cm^{-1}. In such a high density region, excitons start overlapping with each other and the interactions between them increase with the *e-h* pair density. Indeed, the exciton PL peak and the S-peak rapidly increased in linewidth, indicating significant increases in many-body interaction effects among carriers in the wire. On the basis of the lower density picture, our interpretation is that above 1×10^5 cm^{-1}, interacting excitonic and biexcitonic states are formed and their interaction strength increases, and at 6×10^5 cm^{-1} the interacting states completely change to the 1D *e-h* plasma. Saturation of the wire PL at higher excitation powers in Fig. 6 indicates Fermi filling of the wire electronic states, and supports the formation of degenerate *e-h* plasma in the wire. Note that the 1D *e-h* plasma peak appears at the energy position of the biexciton peak and shows small peak shifts of no more than 1 meV.

At higher excitation powers, above 0.2 mW, where the intensity and the linewidth of the wire PL were saturated, the peak position of the wire showed a redshift up to 4 meV from the peak position of biexcitons (Fig. 8). The reason for this peak shift after complete Fermi filling of the wire states is not clear at present, but could be due to interactions with the increasing number of carriers in the arm well.

E. PL of 1D-exciton band edge

The excitation power dependence of the PL spectra from the wire at 30 K is shown in Fig. 9. For low excitation powers at 30 K, we observed not only strong PL from the ground state of 1D excitons at 1.582 eV (labeled *ground*) but also a small PL peak at 1.589 eV (labeled *excited*) and a continuous PL band with an onset at 1.593 eV (labeled *onset*). The new small peak is due to an excited state of the excitons and the continuous band is due to higher excited states of the excitons and 1D continuum states. These assignments were previously achieved by detailed PLE and absorption measurements and numerical calculations.[29,30,33]

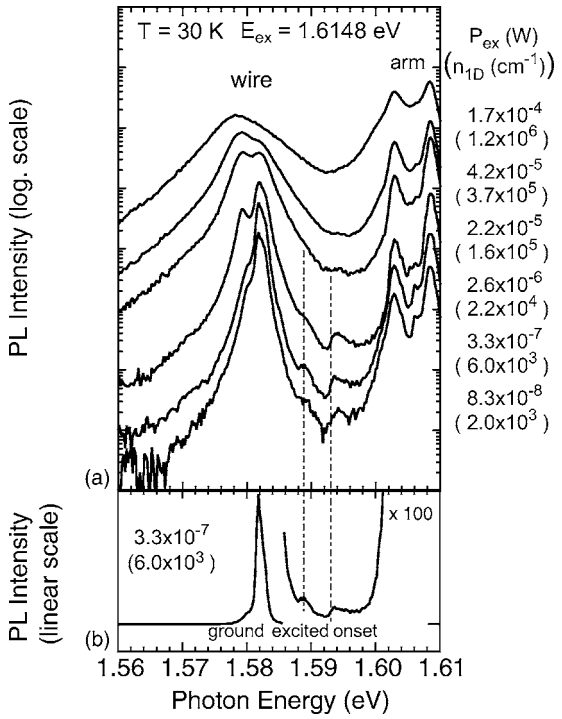

FIG. 9. (a) Excitation power dependence of PL spectra from the T wire at 30 K on a log scale. The PL spectrum at P_{ex} of 3.3×10^{-7} W is also given on a linear scale at the bottom.

In the PL spectra for higher excitation powers, it is remarkable that the *excited*-exciton peaks and the *onset* of the continuum states show no shift from their initial positions. This is still the case when the pair density is as high as 2×10^5 cm^{-1} ($r_s=4a_B^*$), where the linewidth of the S-peak has already started broadening. This is crucially important and could be a key criterion in the comparison with theory, which we discuss later. At the highest pair density, 1.2×10^6 cm^{-1} ($r_s=0.7a_B^*$), these excited-state features become smeared and buried in the tail of the broad plasma PL. However, they stay at the same energies as long as they are visible. This suggests that dense carriers contribute more effectively to scattering that broadens energy levels than to screening and self-energy change that reduce exciton binding energy in the quantum wire.

Energy positions of the PL peaks (exciton, S-peak, and exciton *excited* states) and the continuum-state *onset* observed at 5 K and 30 K are summarized all together in Fig. 10 as a function of the 1D *e-h* pair density n_{1D}. The origin of the vertical axis is the measured continuum-state *onset* energy (E_{g0}^*) in the low *e-h* density limit. The measured energy difference between the peak (or *onset*) energy

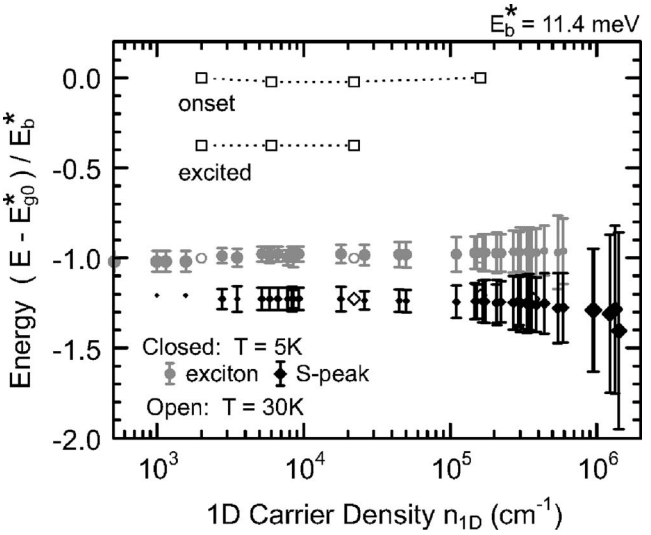

FIG. 10. Energy positions of the PL peaks (exciton, S-peak, and exciton *excited* states) and the continuum-state *onset* observed at 5 K (closed symbols) and 30 K (open symbols) as a function of the 1D *e-h* pair density n_{1D} in the wire. The origin of the vertical axis is the measured continuum-state *onset* energy (E_{g0}^*) in the low *e-h* density limit. The energy difference between the measured peak (or *onset*) energy (E) at each density n_{1D} and the continuum-state *onset* energy (E_{g0}^*) normalized with the measured energy difference (E_b^* =11.4 meV) between the ground-state exciton and the continuum-state *onset* in the low *e-h* density limit is plotted. Relative size of the two symbols for the exciton and S-peak at 5 K approximately represents relative intensity ratio of PL peaks at each density n_{1D}. Vertical bars represent FWHMs of PL peaks.

(E) at each density n_{1D} and the continuum-state *onset* energy (E_{g0}^*) normalized with the measured energy difference (E_b^*=11.4 meV) between the ground-state exciton and the continuum-state *onset* in the low *e-h* density limit is plotted.[39] Relative size of the two symbols for the exciton (closed circles) and S-peak (closed diamonds) at 5 K at each density n_{1D} approximately represents relative intensity ratio of PL peaks. Vertical bars represent FWHMs of PL peaks. As seen in Fig. 10, the broad plasma PL observed at high pair densities above 6×10^5 cm^{-1} does not continuously connect to the PL of the continuum band-edge *onset* observed as ionized states of excitons in the low density limit. Instead, it continuously begins at the energy position of biexcitons observed as S-peak in the intermediate density region. Hence, the level crossing between the continuum band edge and the exciton expected in the exciton Mott transition was not observed. In addition, at the *e-h* pair density of 2×10^5 cm^{-1}, PL of the continuum band edge seemed to coexist with that of the plasma as seen in Fig. 9.

IV. DISCUSSION

We first comment on the inhomogeneous broadening caused by interface roughness in the T-wire structure. In the low *e-h* density region, we observed a single and spatially uniform PL peak with a linewidth of 1.3 meV. This value is much larger than the probable homogeneous broadening of 1D excitons of the order of 0.1 meV. This finite linewidth of 1.3 meV and the finite Stokes shift of 0.3 meV most likely come from the thickness fluctuation of the stem well.[40] Therefore, the PL obtained in the low carrier density region was not from a single quantum state of a 1D exciton but from an ensemble of 1D exciton states. However, at high *e-h* densities, above n_{1D} of 1×10^5 cm^{-1}, the PL peak became broader than the inhomogeneous broadening, which indicates that the homogeneous broadening due to many-body interactions between carriers dominates the PL linewidth, and inhomogeneous broadening plays only a minor role. Therefore, at the intermediate and high densities above n_{1D} of 1×10^5 cm^{-1} of interest to us, many-body effects inherent in 1D *e-h* systems predominantly appeared in the spectra.

In discussing many-body effects of 1D *e-h* systems in quantum wires, we should take into account the finite lateral size of the quantum wires. As shown in Fig. 1, the T wire consists of two QWs (stem and arm wells) with finite well widths, which means that the *e-h* system formed in the T wire is not a pure 1D *e-h* system but a quasi-1D system. However, the quasi-1D *e-h* system with strong carrier confinement whose lateral size is similar or smaller than the Bohr radius of excitons, can theoretically be treated as a pure 1D system with a modified (and screened) Coulomb potential.[7,41] This is true for the T wire in this study. We should also consider the carrier-induced effects from higher-dimensional structures (stem and arm wells in the T wire) closely surrounding quantum wires. In this experiment, the excitation light created *e-h* pairs in the arm well and the wire but not in the stem. At low excitation powers and a low temperature, most of the photo-generated carriers in the arm well flow into the T wire and hence the carrier population in the arm well is negligible. However, at high excitation powers such that the arm-well states are filled with carriers, quasi-1D screened Coulomb potentials for the carriers in the T wire might be modified by 2D carriers existing in the arm well. Indeed, at higher excitation powers, above 0.2 mW where the wire states are almost filled and the Fermi filling has started in the arm well, the wire PL peak shows large redshift of the peak position and broadening of the linewidth. Since the 1D *e-h* pair densities around and below the exciton Mott density we focus on in this work is well below the saturation density of 1.2×10^6 cm^{-1}, discussions on the 1D exciton-plasma crossover in the T wire based on the theoretical predictions for 1D *e-h* systems are appropriate.

Several theoretical papers have investigated 1D *e-h* systems during the crossover from a dilute exciton gas to a dense *e-h* plasma at low temperatures.[3–7] Calculations by Rossi and Molinari showed that *e-h* Coulomb correlation removes the 1D band-edge singularity in the optical response of an *e-h* plasma and theoretically showed the constancy of the excitonic peak position in optical spectra during the exciton-plasma crossover.[3] Tassone and Piermarocchi investigated strong *e-h* Coulomb correlation effects on scattering, which are relevant even at a high *e-h* density and demonstrated gradual broadening of the excitonic peak during the exciton-plasma crossover.[5] Das Sarma and Wang made self-consistent Green's-function calculations including dynamical screening in comparison with more simplified theoretical

models.[7] Optical spectra obtained as a function of the *e-h* density showed that the critical density separating the exciton and plasma regimes was about 3×10^5 cm^{-1}. These calculated features agree well with our present observation of the exciton-plasma crossover, but there are some important differences.

First, the papers by Das Sarma and Wang give plots of the calculated 1D continuum band edge and exciton energies for various *e-h* densities, which demonstrate redshifts of the band-edge energy, no shift of the exciton energy, and hence a reduction of the exciton binding energy. As a result, the constancy of the excitonic peak energy was explained as a cancellation between the band gap shrinkage and the reduced exciton binding energy. The critical density where the exciton binding energy becomes zero and the exciton level crosses the 1D continuum band edge is interpreted as the Mott density, or the critical density of the exciton Mott transition. This picture is very popular and has been also mentioned in the other papers. However, such a plot does not agree with our present observation summarized in Fig. 10. In our experiments, the 1D continuum band edge was not shifted, at least in the range up to 2×10^5 cm^{-1}, while the calculation predicts a redshift of 15 meV or more at this density.[7] Furthermore, our experiment found no shift of the 1D continuum band edge as far as it was visible. There is no experimental evidence for level crossing between excitons and the 1D continuum band edge. Therefore, our experiment does not give any well-defined critical density or critical point for the exciton Mott transition. These discrepancies at least suggest the need to reconsider the prevailing picture of the exciton Mott transition in 1D *e-h* systems.

Second, all the above theories neglected the spins of electrons and holes, and hence neglected biexcitons. However, our present experiment shows that spins, or biexciton effects, are very important. In fact, the plasma PL band was continuously formed from the biexciton PL peak as a result of increased intensity and broadened width. The energy of the plasma PL stayed centered at the peak of biexciton PL.

The importance of the biexciton correlations in dense 1D *e-h* systems has been shown by Asano and Ogawa.[42] They theoretically studied dense 1D *e-h* systems correlated through long-range Coulomb interactions by using the Tomonaga-Luttinger model. In that paper, they found that at absolute zero temperature, the system is an insulator even in the high *e-h* density regime and exhibits strong instability toward the biexciton crystallization. They also predicted that, even at a finite temperature, the biexciton correlation would dominate the other correlation effects and that the system would have the character of a biexciton liquid. In short, the 1D *e-h* plasma with Coulomb interactions should have strong biexciton correlations. Our experimental result that the *e-h* plasma emission appeared gradually at the energy position of the biexciton emission, indicating the importance of the biexciton correlations, is consistent with this theoretical result. This theory assumes a mathematical model of a 1D *e-h* system. The inclusion of spins, or biexciton effects, in many-body theories during the exciton-plasma crossover in realistic 1D *e-h* systems is a very important subject of future study.

Finally, we comment on the biexciton binding energy of the T wire, E_b^{xx}. The value that we obtained was 2.8 meV, which is larger than values previously reported for other kinds of quantum wires.[14,15] The exciton binding energy E_b of this T wire was 14 meV, as characterized in our previous paper.[30] Thus, the ratio of the biexciton binding energy to the exciton binding energy (E_b^{xx}/E_b) was 0.2. An earlier theoretical work without the inclusion of excitonic polarization and deformation effects predicted E_b^{xx}/E_b of about 0.1 for a quantum wire of similar size.[43] However, recent calculations using quantum Monte Carlo methods report E_b^{xx} of 2–3 meV and E_b^{xx}/E_b close to 0.2 for quantum wires,[44] which is consistent with our result. Langbein *et al.* also reported the experimentally obtained biexciton binding energy for a T wire.[45] They obtained E_b^{xx} of 2 meV for a T wire that was 24 nm$\times$6.6 nm in size and surrounded by $Al_{0.3}Ga_{0.7}As$ barriers with E_b of 12 meV. Since our T wire was smaller and surrounded by higher-Al-content barriers, the larger biexciton binding energy that we obtained is reasonable. Reasons for the difference in biexciton binding energies between V and T wires may relate to differences in localization[46] and/or confinement structures such as lateral confinement width and strength.

V. CONCLUSION

We investigated PL spectral evolution with the *e-h* density in a single T-shaped quantum wire with the current-best quality by means of micro-PL spectroscopy. By using the spectrograph imaging method for the micro-PL experiments, we obtained carrier-density-dependent PL spectra for the 1D *e-h* system in the T wire for a wide range of *e-h* pair densities from 5×10^1 to 1.2×10^6 cm^{-1}.

The PL spectra from the wire reveal that the transition from excitons to an *e-h* plasma is a gradual crossover via biexcitons in the 1D *e-h* system. In the low *e-h* density region, PL from only excitons was observed. At a pair density of 4×10^3 cm^{-1}, the PL was characteristic of biexcitons shifted below the exciton peak by the 2.8-meV biexciton binding. At a pair density of 1×10^5 cm^{-1}, the biexciton peak broadened without an energy shift and completely changed to an *e-h* plasma at a density of 6×10^5 cm^{-1}. The gradual appearance of the *e-h* plasma peak from the biexciton peak indicates the importance of biexcitonic correlations in 1D *e-h* systems. Moreover, during the continuous exciton-plasma crossover, the 1D continuum band edge showed no significant energy shift at a density as high as 2×10^5 cm^{-1}, where the biexciton PL peak had already started broadening in linewidth and changing to a degenerate *e-h* plasma peak. Experimental evidence for the level crossing between the continuum band edge and the exciton does not exist, which doubts the existence of an abrupt metal-insulator phase transition, or exciton Mott transition, in the 1D *e-h* system.

ACKNOWLEDGMENTS

We thank T. Ogawa, K. Asano, and P. Huai (Osaka University) for valuable discussions and suggestions. This work was partly supported by a Grant-in-Aid from the Ministry of Education, Culture, Sports, Science and Technology, Japan.

*Also at Bell Laboratories, Lucent Technologies.

[1] H. Haug and S. W. Koch, *Quantum Theory of the Optical and Electronics Properties of Semiconductors*, 4th ed. (World Scientific, Singapore, 2004).

[2] C. F. Klingshirn, *Semiconductor Optics* (Springer-Verlag, Berlin, 1997).

[3] F. Rossi and E. Molinari, Phys. Rev. Lett. **76**, 3642 (1996).

[4] E. H. Hwang and S. Das Sarma, Phys. Rev. B **58**, R1738 (1998).

[5] F. Tassone and C. Piermarocchi, Phys. Rev. Lett. **82**, 843 (1999).

[6] C. Piermarocchi, R. Ambigapathy, D. Y. Oberli, E. Kapon, B. Deveaud, and F. Tassone, Solid State Commun. **112**, 433 (1999).

[7] S. Das Sarma and D. W. Wang, Phys. Rev. Lett. **84**, 2010 (2000); D. W. Wang and S. Das Sarma, Phys. Rev. B **64**, 195313 (2001).

[8] R. Cingolani, R. Rinaldi, M. Ferrara, G. C. La Rocca, H. Lage, D. Heitmann, K. Ploog, and H. Kalt, Phys. Rev. B **48**, 14331 (1993).

[9] W. Wegscheider, L. N. Pfeiffer, M. M. Dignam, A. Pinczuk, K. W. West, S. L. McCall, and R. Hull, Phys. Rev. Lett. **71**, 4071 (1993).

[10] R. Ambigapathy, I. Bar-Joseph, D. Y. Oberli, S. Haacke, M. J. Brasil, F. Reinhardt, E. Kapon, and B. Deveaud, Phys. Rev. Lett. **78**, 3579 (1997).

[11] F. Vouilloz, D. Y. Oberli, F. Lelarge, B. Dwir, and E. Kapon, Solid State Commun. **108**, 945 (1998).

[12] J. Rubio, L. Pfeiffer, M. H. Szymanska, A. Pinczuk, S. He, H. U. Baranger, P. B. Littlewood, K. W. West, and B. S. Dennis, Solid State Commun. **120**, 423 (2001).

[13] A. Crottini, J. L. Staehli, B. Deveaud, X. L. Wang, and M. Ogura, Phys. Rev. B **63**, 121313(R) (2001).

[14] A. Crottini, J. L. Staehli, B. Deveaud, X. L. Wang, and M. Ogura, Solid State Commun. **121**, 401 (2002).

[15] T. Guillet, R. Grousson, V. Voliotis, M. Menant, X. L. Wang, and M. Ogura, Phys. Rev. B **67**, 235324 (2003).

[16] H. Akiyama, L. N. Pfeiffer, M. Yoshita, A. Pinczuk, P. B. Littlewood, K. W. West, M. J. Matthews, and J. Wynn, Phys. Rev. B **67**, 041302(R) (2003).

[17] H. Haug and S. Schmitt-Rink, Prog. Quantum Electron. **9**, 3 (1984); S. Schmitt-Rink, D. S. Chemla, and D. A. B. Miller, Adv. Phys. **38**, 89 (1989); R. Cingolani and K. Ploog, *ibid.* **40**, 535 (1991).

[18] F. Stern, Phys. Rev. Lett. **18**, 546 (1967).

[19] J. Lee and H. N. Spector, J. Appl. Phys. **57**, 366 (1985).

[20] J. A. Reyes and M. del Castillo-Mussot, Phys. Rev. B **57**, 9869 (1998).

[21] S. Benner and H. Haug, Europhys. Lett. **16**, 579 (1991).

[22] H. F. Hess, E. Betzig, T. D. Harris, L. N. Pfeiffer, and K. W. West, Science **264**, 1740 (1994).

[23] J. Hasen, L. N. Pfeiffer, A. Pinczuk, S. He, K. W. West, and B. S. Dennis, Nature (London) **390**, 54 (1997).

[24] A. Zrenner, L. V. Butov, M. Hagn, G. Abstreiter, G. Böhm, and G. Weimann, Phys. Rev. Lett. **72**, 3382 (1994).

[25] K. Brunner, G. Abstreiter, G. Böhm, G. Tränkle, and G. Weimann, Phys. Rev. Lett. **73**, 1138 (1994).

[26] Q. Wu, R. D. Grober, D. Gammon, and D. S. Katzer, Phys. Rev. B **62**, 13022 (2000).

[27] E. Dekel, D. Gershoni, E. Ehrenfreund, D. Spektor, J. M. Garcia, and P. M. Petroff, Phys. Rev. Lett. **80**, 4991 (1998).

[28] M. Yoshita, N. Kondo, H. Sakaki, M. Baba, and H. Akiyama, Phys. Rev. B **63**, 075305 (2001).

[29] H. Akiyama, M. Yoshita, L. N. Pfeiffer, and K. W. West, Appl. Phys. Lett. **82**, 379 (2003).

[30] H. Itoh, Y. Hayamizu, M. Yoshita, H. Akiyama, L. N. Pfeiffer, K. W. West, M. H. Szymanska, and P. B. Littlewood, Appl. Phys. Lett. **83**, 2043 (2003).

[31] Y. Hayamizu, M. Yoshita, S. Watanabe, H. Akiyama, L. N. Pfeiffer, and K. W. West, Appl. Phys. Lett. **81**, 4937 (2002).

[32] M. Yoshita, Y. Hayamizu, H. Akiyama, L. N. Pfeiffer, and K. W. West, Physica E (Amsterdam) **21**, 230 (2004).

[33] Y. Takahashi, Y. Hayamizu, H. Itoh, M. Yoshita, H. Akiyama, L. N. Pfeiffer, and K. W. West, Appl. Phys. Lett. **86**, 243101 (2005).

[34] L. N. Pfeiffer, K. W. West, H. L. Störmer, J. P. Eisenstein, K. W. Baldwin, D. Gershoni, and J. Spector, Appl. Phys. Lett. **56**, 1697 (1990).

[35] A. R. Gõni, L. N. Pfeiffer, K. W. West, A. Pinczuk, H. U. Baranger, and H. L. Stormer, Appl. Phys. Lett. **61**, 1956 (1992).

[36] M. Yoshita, H. Akiyama, L. N. Pfeiffer, and K. W. West, Jpn. J. Appl. Phys., Part 2 **40**, L252 (2001).

[37] M. Yoshita, H. Akiyama, L. N. Pfeiffer, and K. W. West, Appl. Phys. Lett. **81**, 49 (2002).

[38] M. Yoshita, H. Akiyama, T. Someya, and H. Sakaki, J. Appl. Phys. **83**, 3777 (1998).

[39] Since the excited exciton states due to higher Rydberg states and higher hole-subbands exist at the 1D continuum band edge, the measured continuum *onset* energy E^*_{g0} and the measured energy difference E^*_b (=11.4 meV) are smaller than the expected 1D band-edge energy E_{g0} and the exciton binding energy E_b (=14 meV), respectively, but are close to and represent them ($E^*_{g0} \sim E_{g0}$ and $E^*_b \sim E_b$).

[40] One monolayer thickness difference in the (001) stem well causes an energy shift of 0.28 meV for the ground state of the T wire.

[41] T. Ogawa and T. Takagahara, Phys. Rev. B **43**, 14325 (1991); T. Ogawa and T. Takagahara, Phys. Rev. B **44**, 8138 (1991).

[42] K. Asano and T. Ogawa, J. Lumin. **112**, 200 (2005).

[43] L. Banyai, I. Galbraith, C. Ell, and H. Haug, Phys. Rev. B **36**, 6099 (1987).

[44] T. Tsuchiya, Int. J. Mod. Phys. B **15**, 3985 (2001).

[45] W. Langbein, H. Gislason, and J. M. Hvam, Phys. Rev. B **60**, 16667 (1999).

[46] A. Feltrin, F. Michelini, J. L. Staehli, B. Deveaud, V. Savona, J. Toquant, X. L. Wang, and M. Ogura, Phys. Rev. Lett. **95**, 177404 (2005).

Strong photoabsorption by a single-quantum wire in waveguide-transmission spectroscopy

Yasushi Takahashi,[a] Yuhei Hayamizu, Hirotake Itoh, Masahiro Yoshita,[b] and Hidefumi Akiyama[b]
Institute for Solid State Physics, University of Tokyo, and CREST, JST, 5-1-5 Kashiwanoha, Kashiwa, Chiba 277-8581, Japan

Loren N. Pfeiffer and Ken W. West
Bell Laboratories, Lucent Technologies, 600 Mountain Avenue, Murray Hill, New Jersey 07974

(Received 14 February 2005; accepted 9 May 2005; published online 6 June 2005)

We measured the absorption spectrum of a single T-shaped 14×6 nm lateral-sized quantum wire embedded in an optical waveguide using waveguide-transmission spectroscopy at 5 K. In spite of its small volume, the one-dimensional-exciton ground state shows a large absorption coefficient of 80 cm^{-1}, or a 98% absorption probability for a single pass of the 500 μm long waveguide. © *2005 American Institute of Physics*. [DOI: 10.1063/1.1947902]

In quantum wires, interband optical transitions are expected to have enhanced oscillator strength at the lowest-energy levels.[1] This enhancement originates from the inverse-square-root divergence of the one-dimensional (1D) joint density of states, and then from the enhanced excitonic effects in 1D systems. In fact, these two effects have been intensively studied in theories[2–5] and in experiments of photoluminescence (PL) and PL-excitation spectroscopy.[6,7]

In optical device applications,[8–11] however, small volume of wires, and hence a slight overlap between the quantum wires and the optical waveguide, should reduce modal absorption and gain in devices, which could be a critical drawback. Therefore, it is important to perform direct absorption measurements and characterize the absorption spectra quantitatively for quantum-wire devices. Until now, such data has never been reported.

In this letter, we report the absorption spectrum of a single T-shaped quantum wire (T-wire) at 5 K for light propagating along the T-wire. To measure the absorption spectrum, we employed waveguide-transmission spectroscopy using an appropriate interaction length.[12] Even though this is a good method for investigating the absorption of small-volume nanostructures, it requires uniformity of the nanostructures over the entire length. Because the T-wire is fabricated using the cleaved-edge overgrowth with molecular-beam epitaxy[13] and a newly developed growth-interrupt annealing technique,[14] it has unprecedented high uniformity,[15] and the absorption-coefficient peaks that correspond to the 1D-exciton ground state, excited state 1D-exciton, and 1D continuum states are clearly resolved and evaluated in the spectrum.

Figure 1 shows schematic views of the single T-wire sample and the waveguide-transmission experiment. A single T-wire is formed at the T-shaped intersection of an (001) $Al_{0.07}Ga_{0.93}As$ quantum well (stem well) and a (110) GaAs quantum well (arm well). The T-wire size is 14×6 nm. The contour lines show a constant probability for electrons confined in the T-wire ($|\psi|^2=0.2$–1.0). The T-wire is embedded in the core of the T-shaped optical waveguide (T-waveguide) that consists of 514 nm thick (001) layers and 127 nm thick (110) layers, surrounded by $Al_{0.5}Ga_{0.5}As$ cladding layers. A 500 μm long Fabry–Perot cavity is formed by the uncoated cleaved facets. Details about the fabrication processes and lasing properties of the single T-wire are reported elsewhere.[16]

The waveguiding modes are calculated using a finite element method for the T-waveguide model of a 514 nm thick (001) layer of $Al_{0.35}Ga_{0.65}As$ (refractive index $n=3.38$) and a 127 nm thick (110) layer of $Al_{0.1}Ga_{0.9}As$ ($n=3.56$) surrounded by $Al_{0.5}Ga_{0.5}As$ layers ($n=3.28$). The refractive indices, n for 1.580 eV at 5 K, used in the calculation are derived from the data for 300 K[17] at energy shifted by the band-gap-energy difference for the temperature. The lowest calculated waveguiding mode has a mode refractive index of $n=3.38$, and an optical confinement factor of $\Gamma=4.6\times10^{-4}$,

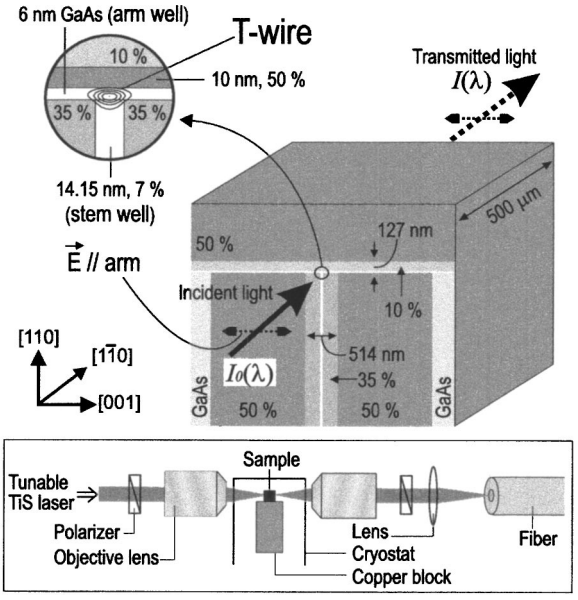

FIG. 1. Schematic views of the single T-wire sample (above) and the waveguide-transmission experiment (below). Percentage for each layer represents the Al content of $Al_xGa_{1-x}As$. The sample was attached to a copper block in the cryostat and cooled to 5 K.

[a]Electronic mail: taka8484@issp.u-tokyo.ac.jp
[b]Also a Visiting Scientist at Bell Laboratories, Lucent Technologies, 600 Mountain Ave., Murray Hill, NJ 07974.

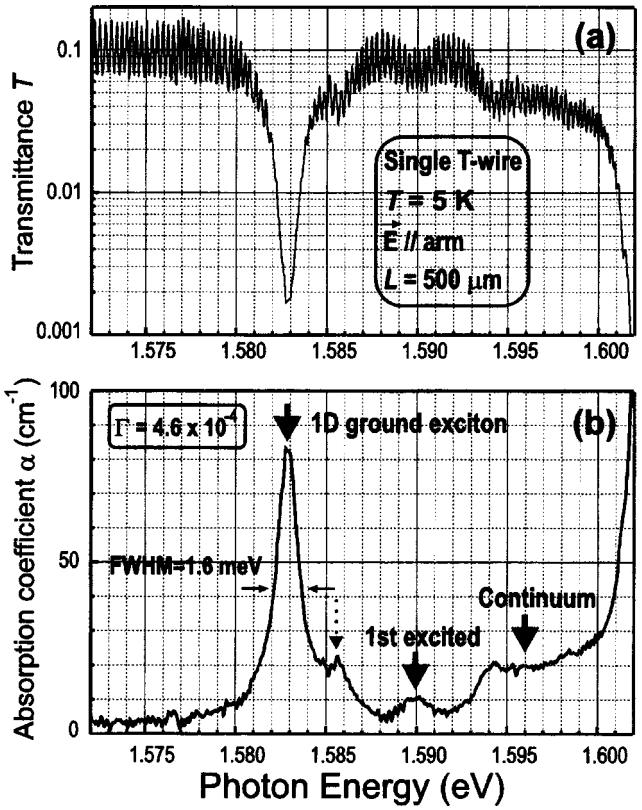

FIG. 2. (a) The transmittance spectrum $T(\lambda)$ of a single T-wire for light polarized parallel to the arm well at 5 K. (b) The absorption spectrum derived from the transmittance spectrum.

which is defined as the overlap portion of the 14×6 nm area of the T-wire. This Γ value is about two orders of magnitude smaller than that of ordinary multiple-quantum-well lasers.

A tunable continuous-wave titanium-sapphire (TiS) laser was used as the light source and divided into a 1% duty ratio. The laser beam was spatially filtered, focused by a 0.5-numerical-aperture objective lens to a spot with a diameter of about 1 μm on the cavity facet, and then coupled to the T-waveguide. The transmitted light from the other cavity facet was collimated using an objective lens and coupled using another lens to an optical fiber with a core diameter of 50 μm, in a confocal microscope configuration. This configuration enabled us to eliminate the stray light, which does not propagate through the T-waveguide. Furthermore, we checked the mode pattern of the transmitted light from the T-waveguide using the microscopic imaging method,[18] and confirmed a circular pattern that corresponded to the lowest mode for all wavelengths. The transmitted light intensity $I(\lambda)$ from T-waveguide was measured using a liquid-nitrogen-cooled charge coupled device detector with scanning wavelength λ of the TiS laser. After removing the sample and adjusting the focus of the lenses, we measured incident light intensity $I_0(\lambda)$ to obtain the transmittance spectrum $T(\lambda)=I(\lambda)/I_0(\lambda)$. Because the T-wire is optically inactive for polarization parallel to the stem well, the polarizations of incident and transmitted light were both set parallel to the arm well using two polarizers.

Figure 2(a) shows the transmittance spectrum $T(\lambda)$ for the single T-wire around the band gap at 5 K. We set $I_0(\lambda)$ to 200 nW or less to avoid absorption saturation, which occurs above 440 nW. The spectral resolution is 0.025 meV, as defined by the scanning steps of the laser wavelength. Strong attenuation is observed at 1.5828 eV and above 1.600 eV due to excitons in the T-wire and arm well, respectively. This will be explained later. In the other region, we observe clear Fabry–Perot oscillations.

The equation for the transmittance spectrum is given by

$$T(\lambda)=\frac{(1-R)^2 e^{-\alpha(\lambda)L}\eta}{\{1-e^{-\alpha(\lambda)L}R\}^2+4e^{-\alpha(\lambda)L}R\sin^2\delta(\lambda)}, \tag{1}$$

where R is the reflectance of 0.295 corresponding to $n=3.38$, L is the cavity length of 500 μm, $\alpha(\lambda)$ is the modal absorption coefficient, η is the coupling efficiency of the incident light to the T-waveguide, and $\delta(\lambda)$ $(=2\pi nL/\lambda)$ is the round-trip phase difference in the cavity, respectively. As will be proven later, analysis of the Fabry–Perot fringes enables estimation of the coupling efficiency η, and the obtained value is $\eta=0.24\pm 0.05$. The second term in the denominator can be ignored in large absorption coefficients.

In Eq. (1), $\sin^2\delta(\lambda)$ can be replaced with $1/2$ if we take the inversed average of $T(\lambda)$ over one oscillation period. Then, $\alpha(\lambda)$ can be derived from the equation without oscillation. Indeed, we took the inversed average of $T(\lambda)$ in Fig. 2(a) over an oscillation period of 0.285 meV, except for the strong-absorption regions without fringes, and derived $\alpha(\lambda)$ using $\eta=0.24$.

Figure 2(b) shows the absorption spectrum for the single T-wire at 5 K. It should be noted that the line shape of the absorption spectrum agrees well with that of the PL-excitation spectrum,[7] and we are able to observe the assigned structures of the 1D-exciton ground state, the excited state of the 1D exciton, and the 1D continuum states, as denoted in the figure. The absorption above 1.600 eV is due to the arm well. The absorption peak of 1D-exciton ground state has a full width at half maximum of 1.6 meV. The Stokes shift, that is the peak shift energy of PL and absorption peaks, is 0.4 meV or less.[6] These demonstrate the high uniformity of our quantum wire in the whole region. It is remarkable that both sides of the exciton peak drop sharply to the background level. The small additional peak at around 1.5856 eV (dashed arrow) is due to the T-wire that consists of a 1-monolayer-thinner arm well.[14]

The absolute values of the absorption coefficient shown in Fig. 2(b) are the key results of this experiment. In the low-energy region below the 1D-exciton ground state, there is a background absorption of 3.5 cm^{-1}. This is likely due to waveguide loss and it adds a flat background to the whole spectrum. The absorption maximum for the 1D-exciton ground state shows $\alpha=80$ cm^{-1}, when we subtract the waveguide loss. The area of absorption coefficient for the peak is evaluated to be 190 cm^{-1} meV. The value of $\alpha=80$ cm^{-1} gives $e^{-\alpha L}=0.018$, which means that 98% of the transmission light is absorbed by a single pass of the 500 μm long waveguide. This demonstrates a strong excitonic absorption of the single T-wire, in spite of the small optical confinement factor $\Gamma=4.6\times 10^{-4}$. The so-called material absorption α/Γ of the wire is calculated to be 17.4×10^4 cm^{-1}, which is 16 times larger than the bulk exciton absorption of 1.1×10^4 cm^{-1}.[19] On the other hand, the absorption coefficient of 1D continuum states is about 16 cm^{-1}. This is much smaller than that of the 1D-exciton ground state, and the inverse-square-root singularity at the band edge is absent, as predicted theoretically.[4]

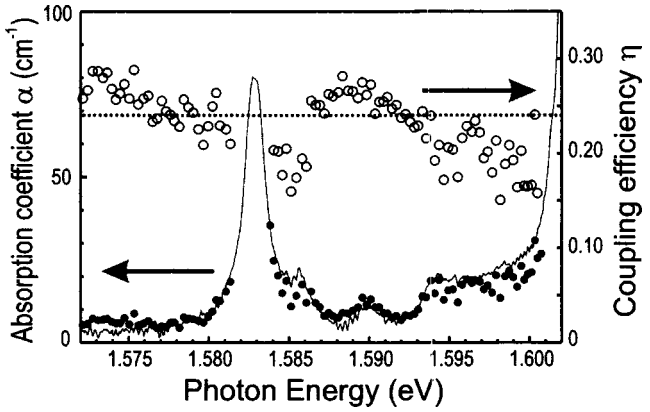

FIG. 3. A comparison of the absorption coefficient α derived using Hakki and Paoli's method (dots) with that shown in Fig. 2(b) (solid line). They correspond to the left longitudinal axis. Open circles with right longitudinal axis show the coupling efficiency η derived using Hakki and Paoli's method. The dotted horizontal line represents $\eta=0.24$.

For a 7×7 nm lateral-sized T-wire, Wang and Das Sarma calculated the material absorption coefficient of the 1D-exciton ground state at 10 K.[5] From the figure shown in their paper, the area of material absorption coefficient for the peak is estimated to be 6.2×10^2 cm^{-1} eV. If we embed a 7 $\times7$ nm T-wire into our T-waveguide, where Γ is 2.7×10^{-4}, the area of the modal absorption coefficient becomes 167 cm^{-1} meV. This shows good agreement with our experimental result.

We verify the accuracy of α and η, based on the Fabry–Perot-fringe analysis method by Hakki and Paoli.[20] In this analysis, α is derived from the ratio of transmittance maximum $T_{\max}$ and minimum $T_{\min}$ in each oscillation using $T_{\max}/T_{\min}=\{(1+e^{-\alpha L}R)/(1-e^{-\alpha L}R)\}^2$,[20] and η can then be derived from $T_{\max}$ or $T_{\min}$ in Eq. (1). The analysis tends to overestimate α if the spectral resolution is not high enough and to have large scattering or error in the region of strong absorption,[21] but it is useful for checking the internal consistency. In Fig. 3, the open circles (○) and dots (●) plot η and α, respectively, using this analysis. This allow us to achieve a coupling efficiency of $\eta=0.24\pm0.05$. In the figure, the absorption spectrum of Fig. 2(b) derived for the constant $\eta=0.24$ is shown using a solid curve. The two absorption shapes are similar and the difference or experimental error is at most 3 cm^{-1}.

In summary, we measured the absolute values of the absorption coefficients for single-quantum-wire device using waveguide-transmission spectroscopy. The single-quantum wire has a sharp, strong absorption peak at the energy of the 1D-exciton ground state for the light propagating along the wire, in spite of its small volume. This shows great promise for future applications of quantum wires to optical devices.

This work was partly supported by a Grant-in-Aid from the Ministry of Education, Culture, Sports, Science, and Technology, Japan.

[1] M. Asada, Y. Miyamoto, and Y. Suematsu, Jpn. J. Appl. Phys., Part 2, **24**, L95 (1985).
[2] R. Elliott and R. Loudon, J. Phys. Chem. Solids **8**, 382 (1959).
[3] S. Abe, J. Phys. Soc. Jpn. **58**, 62 (1989).
[4] T. Ogawa and T. Takagahara, Phys. Rev. B **44**, 8138 (1991).
[5] D. Wang and S. Das Sarma Phys. Rev. B **64**, 195313 (2001).
[6] H. Akiyama, M. Yoshita, L. Pfeiffer, K. West, and A. Pinczuk, Appl. Phys. Lett. **82**, 379 (2003).
[7] H. Itoh, Y. Hayamizu, M. Yoshita, H. Akiyama, L. Pfeiffer, K. West, M. Szymanska, and P. Littlewood, Appl. Phys. Lett. **83**, 2043 (2003).
[8] Y. Arakawa and H. Sakaki, Appl. Phys. Lett. **40**, 939 (1982).
[9] E. Kapon, D. Hwang, and R. Bhat, Phys. Rev. Lett. **63**, 430 (1989).
[10] W. Wegscheider, L. Pfeiffer, M. Dignam, A. Pinczuk, K. West, S. McCall, and R. Hull, Phys. Rev. Lett. **71**, 4071 (1993).
[11] H. Yagi, T. Sano, K. Ohira, T. Maruyama, A. Haque, and S. Arai, Jpn. J. Appl. Phys., Part 2 **42**, L748 (2003)
[12] J. Weiner, D. Chemla, D. Miller, H. Haus, A. Gossard, W. Wiegmann, and C. Burrus, Appl. Phys. Lett. **47**, 664 (1985); R. Grousson, V. Voliotis, P. Lavallard, M. Roblin, and R. Planel, Semicond. Sci. Technol. **8**, 1217 (1993)
[13] L. Pfeiffer, K. West, H. Störmer, J. Eisenstein, K. Baldwin, D. Gershoni, and J. Spector, Appl. Phys. Lett. **56**, 1697 (1990).
[14] M. Yoshita, H. Akiyama, L. Pfeiffer, and K. West, Appl. Phys. Lett. **81**, 49 (2002).
[15] M. Yoshita, Y. Hayamizu, H. Akiyama, L. Pfeiffer, and K. West, Physica E (Amsterdam) **21**, 230 (2004).
[16] Y. Hayamizu, M. Yoshita, S. Watanabe, H. Akiyama, L. Pfeiffer, and K. West, Appl. Phys. Lett. **81**, 4937 (2002).
[17] D. Aspnes, S. Kelso, R. Logan, and R. Bhat, J. Appl. Phys. **60**, 754 (1986).
[18] Y. Takahashi, S. Watanabe, M. Yoshita, H. Itoh, Y. Hayamizu, H. Akiyama, L. Pfeiffer, and K. West, Appl. Phys. Lett. **83**, 4089 (2003).
[19] M. D. Sturge, Phys. Rev. **127**, 768 (1962).
[20] B. Hakki and T. Paoli, J. Appl. Phys. **46**, 1299 (1974).
[21] V. Jordan, IEE Proc.: Optoelectron. **141**, 13 (1994).

Room-temperature excitonic absorption in quantum wires

Yasushi Takahashi,[a] Yuhei Hayamizu, Hirotake Itoh, Masahiro Yoshita,[b] and Hidefumi Akiyama[b]
Institute for Solid State Physics, University of Tokyo, and CREST, JST, 5-1-5 Kashiwanoha, Kashiwa, Chiba 277-8581, Japan

Loren N. Pfeiffer and Ken W. West
Bell Laboratories, Lucent Technologies, 600 Mountain Avenue, Murray Hill, New Jersey 07974

(Received 14 June 2005; accepted 29 September 2005; published online 23 November 2005)

We measured the absorption spectra of T-shaped quantum wires at room temperature using waveguide-transmission spectroscopy. A strong and narrow room-temperature one-dimensional-exciton absorption peak was observed, which indicates a peak modal absorption coefficient of 160 cm^{-1} per 20 wires with a Γ-factor of 4.3×10^{-3}, a width of 7.2 meV, and strong polarization anisotropy. © *2005 American Institute of Physics*. [DOI: 10.1063/1.2135872]

The optical properties of quantum wires have been intensively studied toward achieving novel device applications.[1,2] So far, most research has relied on emission measurements, such as photoluminescence (PL),[3] PL excitation (PLE),[3,4] and lasing,[5–8] and there have been no measurements of quantitative direct absorption on quantum wires. We recently measured the absorption spectrum of a single T-shaped quantum wire (T-wire) embedded in an optical waveguide using straightforward waveguide-transmission spectroscopy at 5 K, and found that the one-dimensional (1D)-exciton ground state has a large modal absorption coefficient of 80 cm^{-1}, despite the small lateral size of the T-wire, i.e., 14 nm$\times$6 nm.[9] The exciton peak exhibited thermal broadening at high temperatures, and room-temperature absorption was not measurable.

It is very important to measure room-temperature quantitative absorption in the investigation of the application of quantum wires to practical optical devices. However, the absorption spectra of quantum wires at room temperature have not been measured even with PLE.

In this letter, we report the absorption spectra of 20 T-wires embedded in an optical waveguide at 297 K and 5 K using waveguide-transmission spectroscopy. Because of the increased overlap between the wires and the optical waveguide compared with the previous single-wire device, the 20-wire device has a strong absorption peak at room temperature, demonstrating room-temperature 1D-exciton absorption. The 1D-exciton absorption peak has a maximum value of 160 cm^{-1} and a full width at half maximum (FWHM) of 7.2 meV. In addition, the absorption by the T-wires has strong polarization anisotropy.

Figure 1 is a schematic view of a 20-wire device fabricated by the cleaved-edge overgrowth method with molecular-beam epitaxy[10] and a growth-interrupt annealing technique.[11] The 20 T-wires are formed at the T-shaped intersections of 20 multiple (001) $Al_{0.07}Ga_{0.93}As$ quantum wells (stem wells) and a (110) GaAs quantum well (arm well). The T-wires are embedded in the core of the T-shaped optical waveguide (T-waveguide) with a lateral size of 1162 nm$\times$183 nm, surrounded by $Al_{0.5}Ga_{0.5}As$ cladding layers. The cavity length L is 512 μm, and cavity facets are uncoated. Details on sample fabrication and characterizations are discussed in separate papers.[4,12,13]

The upper columns in Table I summarize the structural parameters of the 20-wire device, in comparison with those of the single-wire device used in the previous low-temperature transmission study.[9] Each T-wire has the same structure of 14 nm (stem well) $\times$6 nm (arm well) formed with the same materials in both devices, while the T-waveguide structure is changed to optimize the optical confinement factor Γ for the lowest waveguide mode. We calculated Γ using a finite element method and obtained $\Gamma=4.3\times10^{-3}$ for the 20-wire device. This value is larger than that for the single-wire device by a factor of 9.3.

The experimental method for waveguide-transmission spectroscopy was described previously.[9] In the present experiment, we measured transmission spectra at 297 K and 5 K for two linear polarizations parallel to the arm well (denoted as arm polarization) and the stem well (stem polarization). Coupling efficiency η of incident light to the T-waveguide was 0.4 at both temperatures.

Figure 2 plots the absorption spectra for 20 wires at 297 K. The longitudinal axis represents the modal absorption coefficient α. The solid curve represents the absorption for arm polarization, and the dotted for stem polarization. As will be explained later in Fig. 4, the absorption peak at

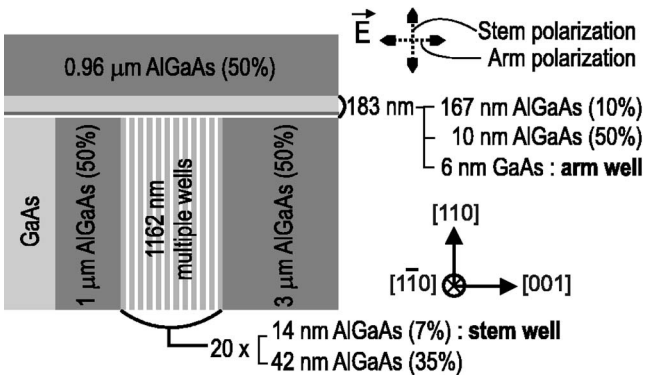

FIG. 1. Schematic view of 20-wire device, where 20 T-wires are embedded in T-waveguide. Cross section of each T-wire is 14 nm (stem well) $\times$6 nm (arm well). Percentages in parentheses represent Al content x of $Al_xGa_{1-x}As$.

[a]Electronic mail: taka8484@issp.u-tokyo.ac.jp
[b]Also at: Bell Laboratories, Lucent Technologies, 600 Mountain Ave., Murray Hill, NJ 07974.

TABLE I. Comparison of structures and measured data for 20-wire and single-wire devices. Listed absorption data are for arm polarization. Peak area is evaluated as product of peak value and FWHM. Ratio is evaluated for values (*a*) and (*b*).

Sample	20 wire		Single wire	Ratio
T-wire size (nm^2)	14×6		14×6	
Waveguide size (nm^2)	1162×183		514×127	
Confinement factor Γ	$4.3\times10^{-3(a)}$		$4.6\times10^{-4(b)}$	9.3
Temperature (K)	297	5	5	
Coupling efficiency (η)	0.40	0.40	0.24	
α for continuum (cm^{-1})		$150^{(a)}$	$16^{(b)}$	9.4
α for exciton peak (cm^{-1})	160		80	
FWHM (meV)	7.2	<2	1.6	
Peak area (cm^{-1} meV)	$1152^{(a)}$		$128^{(b)}$	9.0
Peak energy (eV)	1.4884	1.5808		

1.4884 eV for arm polarization is due to the 1D-exciton ground state.

The absolute value of the absorption coefficient, $\alpha = 160\ cm^{-1}$, for the 1D-exciton peak is one of the most important results in this letter. The value of $\alpha = 160\ cm^{-1}$ gives a very small transmission probability of $e^{-\alpha L} = 2.8\times10^{-4}$, when L is 512 μm. This demonstrates that the quantum wires in an optical waveguide have strong excitonic absorption for light propagating along the wires even at room temperature, despite the small optical confinement factor Γ, which is about one order of magnitude smaller than those of ordinary multiple-quantum-well devices.

The 1D-exciton peak at 1.4884 eV is indicated by the dotted vertical line in Fig. 2. This peak is overlapped by the absorption tail of the arm well at higher energy. Thus, the FWHM of the peak is estimated as 7.2 meV from a half-width of 3.6 meV of half-maximum on the lower-energy side.

The absorption spectrum for stem polarization has no peak structure. The difference in the absorption coefficient between the two polarizations is 145 cm^{-1} at 1.4884 eV, which corresponds to $e^{-\alpha L} = 6.0\times10^{-4}$. The stronger absorption for arm polarization indicates that the T-wires have a polarization dependence similar to the arm well.[14] This characteristic originates from the strong quantum confinement in the [110] direction.

These experimental results on 1D-excitonic absorption support the potential applications of quantum wires to various optical devices, such as modulators, switches, and amplifiers. The observed quantities are useful in the practical design of such optical devices.

Figure 3 plots the absorption spectra for the 20 wires at 5 K. The solid and dotted curves correspond to the absorption spectra for arm and stem polarizations. The spectral shape of the absorption for arm polarization agrees well with the results of our previous PLE study[4] and the absorption spectrum for a single-wire device,[9] which assigns each peak to the 1D-exciton ground state, the first excited state of the 1D exciton, and the 1D continuum states, as denoted in the figure. The increasing absorption above 1.598 eV is due to exciton in the arm well.

The polarization dependence for each absorption peak is clearly observed. The absorption of the 1D exciton and continuum states decreases drastically in stem polarization. The excited exciton, on the other hand, has a similar absorption value for both polarizations. This difference originates from the difference in the hole subbands contributing to optical transition.[4]

In this experimental setup, we were not able to measure absorption coefficients above 200 cm^{-1} because of the limited transmission light. Although the peak value of the 1D exciton for arm polarization is above the detection limit, the FWHM is estimated to be 2 meV or less from that in stem

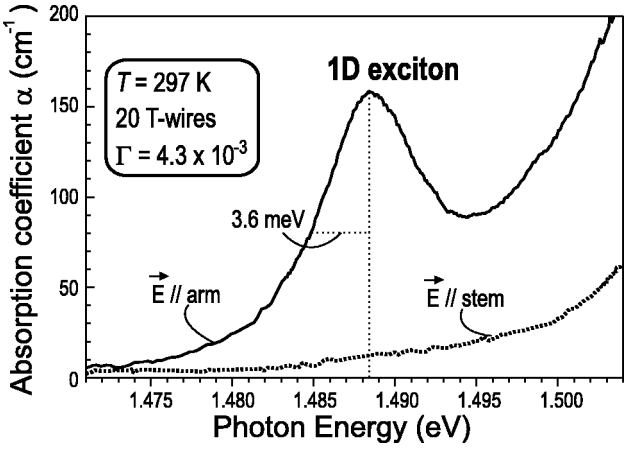

FIG. 2. Absorption spectra of 20 wires at 297 K. Solid curve and dotted curve represent absorption spectra for arm and stem polarizations, respectively. Room-temperature 1D-excitonic absorption is observed at 1.4884 eV.

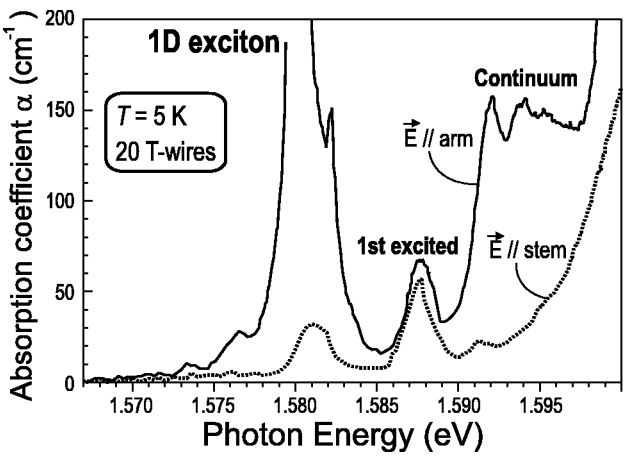

FIG. 3. Absorption spectra of 20 wires at 5 K. Solid curve and dotted curve show absorption spectrum for arm and stem polarizations, respectively.

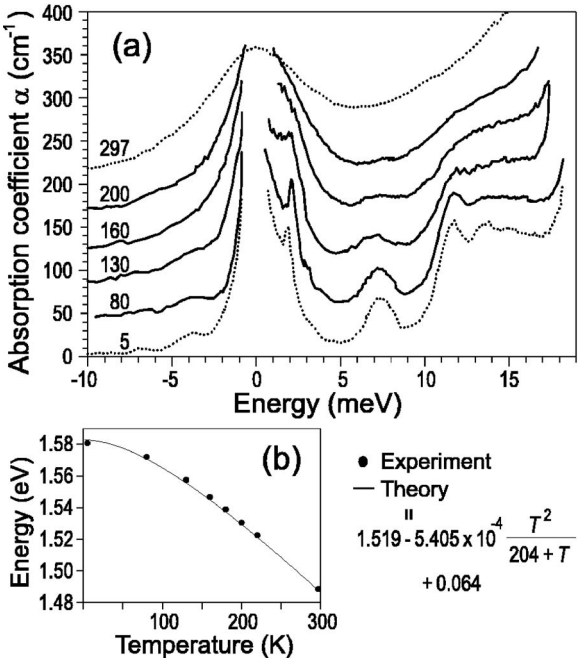

FIG. 4. (a) Absorption spectra of 20 wires for arm polarization at 5 K, 80 K, 130 K, 160 K, 200 K, and 297 K. Each curve is plotted with offset of 40 cm^{-1}. (b) Measured energies of the 1D-exciton peak (dots) and the calculated band-gap energy of GaAs plus 64 meV (solid curve) for various temperatures.

polarization or that of the excited exciton state. This indicates a small amount of inhomogeneous broadening, or high uniformity in the 20 T-wires throughout the whole region. Therefore, the 7.2 meV FWHM at 297 K for the 1D exciton represents the intrinsic homogeneous width of the 20 T-wires.

The solid curves in Fig. 4(a) show the absorption spectra for the arm polarization at intermediate temperatures and the dotted curves represent those of Figs. 2 and 3. The energy is measured from the lowest-energy peak. Figure 4(b) shows the absolute energies of the lowest peak between 5 K and 297 K.

As temperature increases, all of the peaks and the continuum edge become broad, and, at 297 K, the continuum edge is not visible. However, the 1D-exciton peak at 5 K changes continuously to the lowest peak at 297 K. Furthermore, an energy shift of the lowest peak [shown by dots (●) in Fig. 4(b)] fits well to the band-gap energy shift for bulk GaAs with wire quantization energy of 64 meV (solid curve).[15] These facts prove that the absorption peak at 297 K in Fig. 2 is due to the 1D-exciton ground state. It should be stressed that this experiment demonstrates room-temperature 1D-excitonic absorption, which has never been observed before.

The lower columns in Table I summarize the measured absorption data for a 20-wire device at 297 K and 5 K, and for a single-wire device at 5 K for arm polarization.[9]

The absorption coefficient of the continuum states for arm polarization at 5 K is about 150 cm^{-1}. This value is 9.4 times greater than that for the single-wire device, 16 cm^{-1}, whose ratio corresponds to that for optical confinement factor Γ. This demonstrates that the so-called material absorption coefficient defined by α/Γ is the same in both 20-wire and single-wire devices for 1D continuum states at 5 K.

The 1D-exciton peak area at 297 K is evaluated to be 1152 cm^{-1} meV from the product of its peak value, 160 cm^{-1}, and the FWHM, 7.2 meV. We are not able to compare it with that for the 20-wire device at 5 K, because the peak absorption at 5 K could not be measured. Instead, we compare it with the value of 128 cm^{-1} meV for a single-wire device at 5 K. The 1D-exciton peak area for the 20-wire device at 297 K is 9.0 times larger than that for a single-wire device at 5 K. Thus, the area of material absorption coefficient α/Γ is almost the same at both temperatures. This is reasonable because theories have predicted that the absorption area of the exciton peak should be preserved against changes in temperature.[15,16]

In summary, we observed room-temperature 1D excitonic absorption in 20 T-wires embedded in an optical waveguide using waveguide-transmission spectroscopy. The absorption peak has a maximum value of 160 cm^{-1} and a FWHM of 7.2 meV with strong polarization anisotropy, which support the application of quantum wires to practical optical devices.

This work was partly supported by a Grant-in-Aid from the Ministry of Education, Culture, Sports, Science, and Technology, Japan.

[1] Y. Arakawa and H. Sakaki, Appl. Phys. Lett. **40**, 939 (1982).
[2] M. Asada, Y. Miyamoto, and Y. Suematsu, Jpn. J. Appl. Phys., Part 2 **24**, L95 (1985).
[3] H. Akiyama, J. Phys.: Condens. Matter **10**, 3095 (1998), and references therein.
[4] H. Itoh, Y. Hayamizu, M. Yoshita, H. Akiyama, L. Pfeiffer, K. West, M. Szymanska, and P. Littlewood, Appl. Phys. Lett. **83**, 2043 (2003); H. Akiyama, M. Yoshita, L. N. Pfeiffer, A. Pinczuk, and K. W. West, *ibid.* **82**, 379 (2003).
[5] E. Kapon, D. Hwang, and R. Bhat, Phys. Rev. Lett. **63**, 430 (1989).
[6] W. Wegscheider, L. Pfeiffer, M. Dignam, A. Pinczuk, K. West, S. McCall, and R. Hull, Phys. Rev. Lett. **71**, 4071 (1993).
[7] Y. Hayamizu, M. Yoshita, S. Watanabe, H. Akiyama, L. Pfeiffer, and K. West, Appl. Phys. Lett. **81**, 4937 (2002).
[8] H. Yagi, T. Sano, K. Ohira, T. Maruyama, A. Haque, and S. Arai, Jpn. J. Appl. Phys., Part 2 **42**, L748 (2003).
[9] Y. Takahashi, Y. Hayamizu, H. Itoh, M. Yoshita, H. Akiyama, L. Pfeiffer, and K. West, Appl. Phys. Lett. **86**, 243101 (2005).
[10] L. Pfeiffer, K. West, H. Störmer, J. Eisenstein, K. Baldwin, D. Gershoni, and J. Spector, Appl. Phys. Lett. **56**, 1697 (1990).
[11] M. Yoshita, H. Akiyama, L. Pfeiffer, and K. West, Appl. Phys. Lett. **81**, 49 (2002).
[12] H. Akiyama, L. N. Pfeiffer, M. Yoshita, A. Pinczuk, P. B. Littlewood, K. W. West, M. J. Matthews, and J. Wynn, Phys. Rev. B **67**, 041302(R) (2003).
[13] Y. Takahashi, S. Watanabe, M. Yoshita, H. Itoh, Y. Hayamizu, H. Akiyama, L. Pfeiffer, and K. West, Appl. Phys. Lett. **83**, 4089 (2003).
[14] A. Yamaguchi, K. Nishi, and A. Usui, Jpn. J. Appl. Phys., Part 2 **33**, L912 (1994).
[15] W. W. Chow and S. W. Koch, *Semiconductor-Laser Fundamentals* (Springer, Berlin, 1999).
[16] H. Haug and S. W. Koch, *Qnantum Theory of the Optical and Electronic Properties of Semiconductors*, 4th ed. (World Scientific, Singapore, 2004).